Development of a Membrane Pack for Immersed Membrane Bioreactors

Report to the

Water Research Commission

by

V L Pillay and E P Jacobs

on behalf of

Durban Institute of Technology &

Institute of Polymer Science, University of Stellenbosch

WRC Report No. 1369/1/08

ISBN 978-1-77005-757-9

OCTOBER 2008

DISCLAIMER

This report has been reviewed by the Water Research Commission (WRC) and approved for publication. Approval does not signify that the contents necessarily reflect the views and policies of the WRC, nor does mention of trade names or commercial products constitute endorsement or recommendation for use.

Executive Summary

Background

An immersed membrane bioreactor (IMBR) incorporates membrane filtration technology in a bioreactor to provide a single unit for biological treatment and high quality effluent production.

IMBRs offer various advantages over the conventional activated sludge (CAS) process for waste water treatment, including compact process with small footprint; operation at elevated biomass concentrations ranging from 15 000 to 20 000 mg/L, as compared to approximately 4 000 mg/L for CAS; increased sludge age and reduced sludge production; provides a higher quality product, substantially free of pathogens. As a result, IMBRs have become very popular for onsite wastewater treatment, and are increasingly being applied for remediation of domestic wastewater as well as a wide range of industrial effluents.

IMBRs have major potential applications in South Africa, as well as other developing economies, particularly in terms of point of source treatment of domestic effluents, e.g. small communities, farms, hotels and tourist resorts. The final effluent here could be used directly for agriculture; could be used as "grey" water for flushing of toilets cleaning of grounds, etc.; or could be upgraded via reverse osmosis for recycling. If IMBRs are used as point of source treatment for industrial effluents, the product could be used as "grey" water, or could be upgraded for recycling back to the plant.

The international MBR market is dominated by two systems, viz. the hollow-fibre membrane Zeeweed® system and the flat-sheet membrane Kubota system. However, the economics of these systems put them beyond the reach of most of the smaller domestic effluent treatment applications, as mentioned above, or the smaller industrial effluent treatment applications. This project concerned the development of an inexpensive MBR technology for smaller scale applications that could fill the economic void left by the current commercial systems. The tasks of the project included:

(i) developing a membrane module, based on locally available membranes, that could be employed in MBRs,

(ii) investigating the factors that effect the hydraulic performance of MBRs, and hence developing a design for small scale MBRs,

(iii) investigate the development of a unique *hybrid* IMBR (HIMBR), where tubular silicone membrane aerators will be inserted between flat-sheet dewatering membranes to act as oxygenators and scourers.

Aims

The aims of the project were to:

(i) develop flat-sheet membrane casting procedures, cartridges and a manifolding system suitable for use in IMBRs.

(ii) develop an aerated hybrid immersed membrane bioreactor containing flat-sheet or capillary dewatering membranes, using air sparging and silicone rubber membranes for oxygenation.

(iii) develop fabrication protocol to produce narrow bore and thick-walled skinless capillary ultrafiltration membranes. The former could potentially be employed as the dewatering membranes in IMBRs, whilst the latter would have application in gradostat reactors.

AIM I: Development of a flat-sheet membrane module

Criteria

The criteria for a membrane module for dewatering in IMBR applications are:

(i) it should be simple and robust, and inexpensive in construction;

(ii) it should give a good permeate quality;

(iii) it should give a good flux that would be viable for MBR applications;

(iv) it should require easy and inexpensive cleaning strategies;

(v) for thermophilic operations, the module should be able to operate at temperatures up to 60°C;

(vi) it should preferablyutilise membranes that are readily available in South Africa, obviating the research and development costs to develop new membranes.

Project Outputs

Capillary (hollow-fibre) modules were compared with flat-sheet modules in terms of packing density, ease of fabrication, robustness and fouling. It was found that flat-sheet modules had various advantages over capillaries. The project subsequently focused on flat-sheet modules.

Two type of flat-sheet modules were developed and evaluated. The first utilised the "tubular" woven fibre microfiltration (WFMF) fabric, whilst the second utilised a standard flat-sheet fabric. A fabrication protocol was then developed for a flat-sheet module. In this project the module utilised the woven fibre microfiltration (WFMF) fabric developed by a local company, Gelvanor, and the module developed was approximately A4 in size.

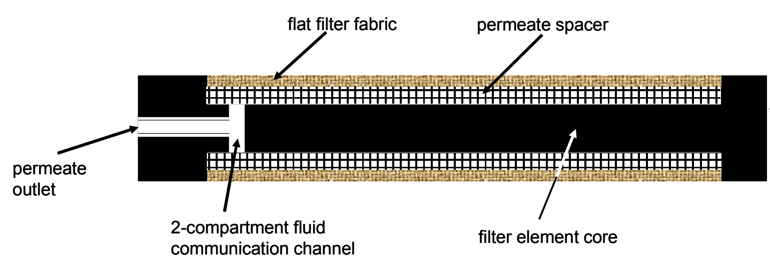

In evaluations on both mineral and biological suspensions, the module gave very good rejections of suspended solids, with permeate turbidities ranging from 0,2 NTU to 0,9 NTU. Cleaning of the membrane is very simple, with either simple scrubbing or soaking in a commercial bleach solution to remove foulants. It was also observed that on drying, the fouling layer peels away from the membrane and can be easily removed. This is a unique advantage to the membrane, since the leading commercial IMBR membranes are destroyed on drying.

The protocol for the module is fairly simple and does not require highly skilled technicians or specialist materials. The materials can be chosen to be resistant to temperatures up to 60°C, fulfilling the requirement for operation in thermophilic IMBRs.

The fabrication protocol may equally be applied to other flat-sheet membranes, including non-woven fabric membranes or polymeric membranes.

AIM II: Development of a design for IMBRs

<u>Criteria</u>

The criteria for a hydrodynamic design for IMBRs, include the following:

(i) there should be stable circulation of the biomass around the membranes;

(ii) the hydrodynamics of the flow across the membranes should ensure stable scouring of the entire membrane surface.

<u>Project Outputs</u>

Investigations indicated that the HIMBR concept, which incorporates silicone rubber membrane in-between the dewatering membranes, would not be feasible at this stage due to cost and fouling aspects. Hence the project focused on the development of a “standard” IMBR.

The effects of geometric and operating variables on fluid dynamics in IMBRs were investigated. It emerged that the fluid flow patterns across the membrane, and hence the rate of fouling, was substantially affected by air flowrate and the following geometric parameters:

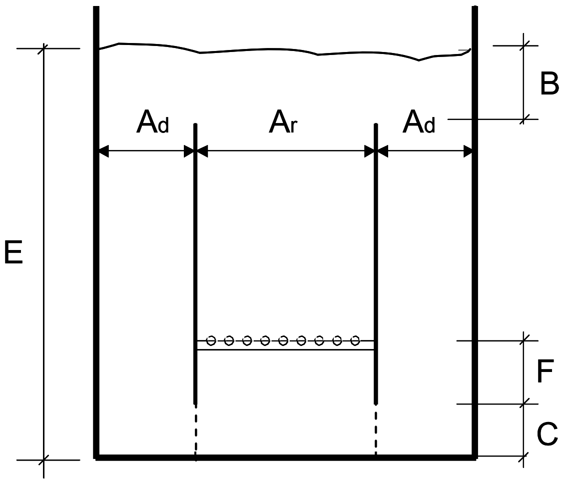

A_d	area of the down-comer section
A_r	area of the riser section
B	clearance height between the top of the membrane stack and the liquor level
C	bottom entry clearance for fluid recirculation
F	position of the air sparger relative to the top of the bottom entry clearance (liquor level)
E	total liquor head in reactor vessel

Typical hydrodynamic field patterns are shown below: (a) fast rising bubbles in the middle with stagnant bubbles, and consequent severe fouling, on the sides; (b) uniformly fast rising bubbles with overall low fouling; and (c) fast rising bubbles on the sides with stagnant bubbles, and consequent severe fouling, in the middle.

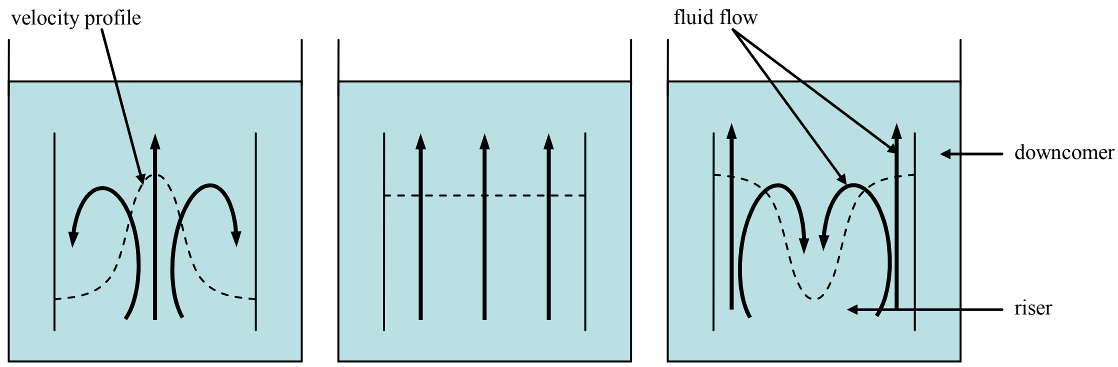

(a) (b) (c)

A model for the optimization of IMBR hydrodynamics was developed, based on an identification of the important geometric and operating variables that affect circulation and fouling, and on a factorial experimental optimization of these variables.

The model was implemented in the design and construction of a pilot plant IMBR, which was evaluated on both mineral suspensions and a biological suspension (activated sludge). Various views of the membrane pack are shown below:

Overview of membrane case

View from side, showing air inlet for gas spargers

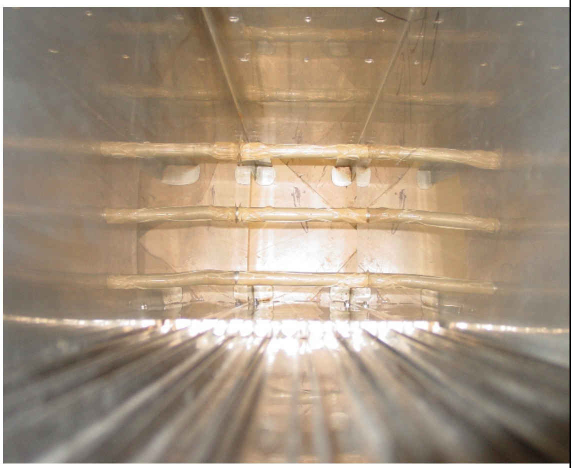

Top view, showing gas spargers

Permeate off-takes on panels

In both laboratory and on-site evaluations, smooth and stable circulation was obtained within the reactor, with no indication of the stagnant zones obtained in the preliminary experiments in this project. On examination of the membranes after each run, there were no signs of preferential fouling zones. It would thus seem that the proposed IMBR design meets the hydrodynamic criteria, i.e. to ensure stable circulation and uniform scouring of the membrane modules.

The IMBR showed the typical characteristics of commercial IMBRs in terms of critical flux, i.e. a critical flux exists which is a function of feed concentration and aeration intensity. Commercial IMBRs operate at critical fluxes of about 15 LMH to 25 LMH, for MLSS values between 12 g/L and 15 g/L. In the evaluation performed on the biological sludge, a critical flux of about 10 LMH to 15 LMH was achieved at a MLSS value of 9 g/L. However, the aeration intensity used here was substantially below that used in commercial IMBRs. Commercial flat-sheet IMBR systems use air-flow rates of 7 L/min to 10 L/min per membrane module. In this study the flowrates ranged from 0,3 L/min/module to 2,5 L/min/module, about 5% to 35% of the commercial units.

Overall, the evaluations indicated that the IMBR membrane module design produced by this project were technically adequate and competent for IMBR applications.

AIM III: Morphology of *Skinless* capillary ultrafiltration membranes

Objectives

The main objectives here were:

(i) to identify the production parameters that influence the structure and performance of skinless capillary ultrafiltration membranes;

(ii) to identify their effect on membrane structure and performance;

(iii) to identify regimes for the production of skinless membranes.

Project Outputs

The important production parameters were identified as dope extrusion rate (DER), bore fluid flowrate (BFFR) and spinning bath composition. Regimes have been identified where (undesirable) externally skinned membranes would form, and where (desirable) externally unskinned membranes would form. The qualitative effects of the production variables on membrane thickness, flux and rejections have been identified. This can be utilised to define regimes for producing unskinned membranes of the desired properties.

Recommendations

Flat-sheet module for IMBRs

There is a huge potential for flat-sheet alternatives to the Kubota membrane module in the rapidly growing IMBR and immersed filtration markets. The fabrication protocol developed in this project should be developed further towards producing a commercially competitive product. Amongst the issues to be addressed are:

(i) choosing less expensive materials;

(ii) increasing the size of the modules; and

(iii) industrialising the production protocol, using current mass-production fabrication techniques.

IMBR design

The evaluations trials performed here were merely to determine the technical adequacy of the project outputs. Substantially longer and more detailed trials need to be performed on biological suspensions in order to determine the long-term performance of the system and to obtain sufficient data for comparative evaluations with current commercial systems.

The current tendency is to divide the bioreactor into two zones, viz. a zone of fine bubble aeration for biological degradation, and a zone with coarse bubble aeration, where the dewatering membranes would be situated. Future trials should use this two-zone configuration. This would simplify and improve system hydrodynamics, since larger A_d/A_r ratios can be achieved in a two-zone system.

Fabrication protocol for skinless membranes

The membranes produced in this project were subjected only to short term evaluations. Longer term trials must be performed to unequivocally determine "recipes" for unskinned membranes of particular properties.

ACKNOWLEDGEMENTS

The Project Team gratefully acknowledges the inputs of the following people to the project:

(i) The Project Steering Committee, for their constructive criticism, valuable technical input and overall guidance:

Dr G Offringa	:	Water Research Commission (Chairman)
Prof SM Bradshaw	:	University of Stellenbosch
Prof CA Buckley	:	University of KwaZulu-Natal
Mr GH du Plessis	:	Sasol
Mr F Matfield	:	Sappi
Prof P Swart	:	University of Stellenbosch
Prof M Wentzel	:	University of Cape Town
Mr SA Pieterse	:	City of Cape Town

(ii) The Management of the Northern Waste Water Treatment Works, Durban, for facilitating the on-site trials at NWWTW

TABLE OF CONTENTS

LIST OF FIGURES

LIST OF TABLES

GLOSSARY

CAS	conventional activated sludge
COD	chemical oxygen demand
EMBR	extractive membrane bioreactor
HIMBR	hybrid immersed membrane bioreactor
IMBR	immersed membrane bioreactor
MABR	membrane aerated bioreactor
MBR	membrane bioreactor
MLSS	mixed liquor suspended solids
WFMF	woven fibre microfilter

1 INTRODUCTION

1.1 Background to the Project

A membrane bioreactor (MBR) incorporates membrane filtration technology in a bioreactor to provide a single unit for biological treatment and high quality effluent production. MBRs have become very popular for onsite wastewater treatment, because of their inherent compact design and intensified biological processing. MBRs therefore not only have a reduced footprint, but also have the ability to surpass control and quality standards of conventional wastewater treatment processes [Churchouse (1997), Husain and Côté (1999)].

Aerobic immersed membrane bioreactors (IMBRs) were first introduced some 15 years ago, and their application to wastewater treatment has increased rapidly over the past few years. The current commercial systems make use of either capillary or flat-sheet membrane cartridges to dewater the bioreactor. The membranes used in IMBRs are either ultrafiltration or microfiltration membranes with pore sizes that range from 100 000 kD cut-off to as large as 0,5 μm. IMBRs have a small footprint compared to conventional aerated bioreactors, are energy efficient and produce an excellent quality, low chemical oxygen demand (COD) final product. Log 4 plus removal rates of viruses and product turbidity in the order of 0,1 NTU have been reported.

Figure 1 compares the conventional activated sludge (CAS) process with an equivalent MBR process.

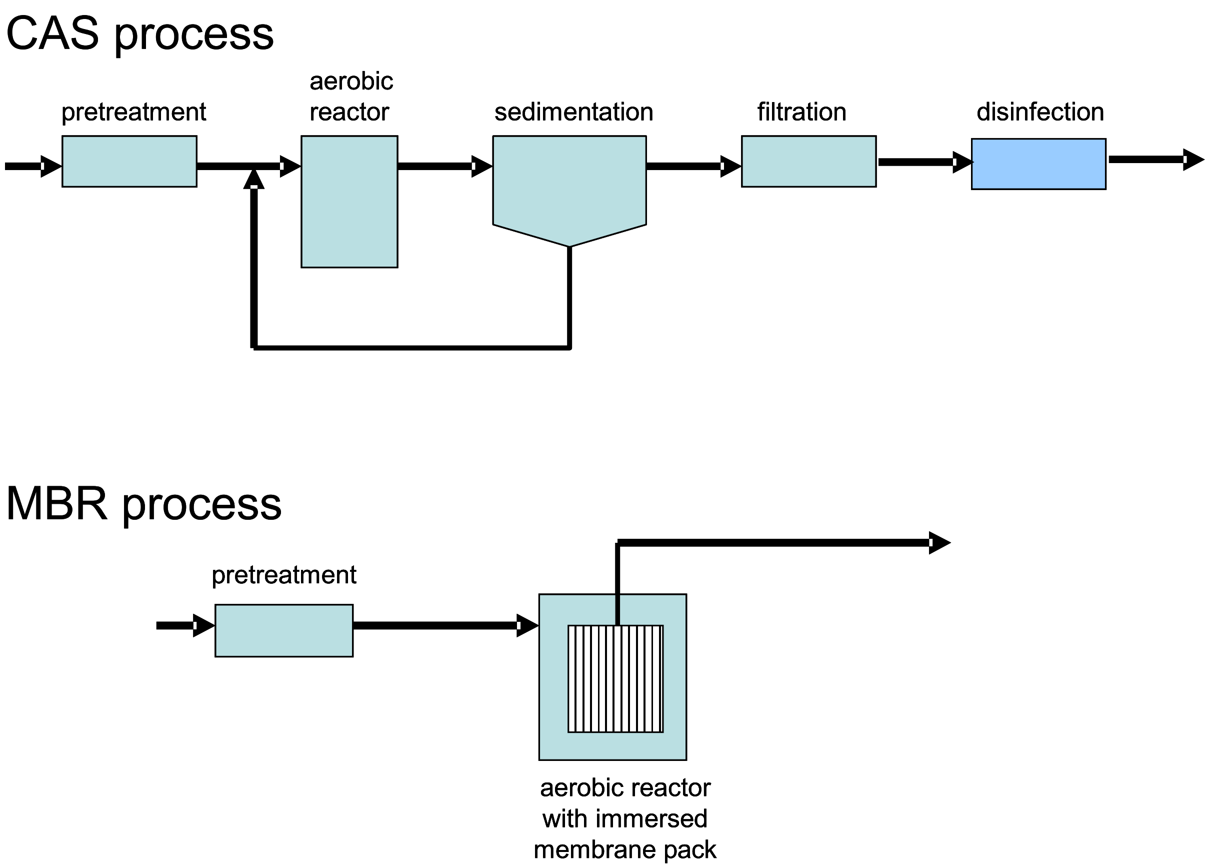

Figure 1. Comparison between the MBR and CAS processes

The advantages offered by MBRs over the CAS process include:

(i) *reduction in the number of process units*:- the filtration membranes in the MBR are responsible for the complete removal of solids from the treated water, thereby replacing the sedimentation step in the CAS process. Membrane filtration, given that the membranes contain relative small pores, can also replace CAS process tertiary treatment steps such as filtration and disinfection

(ii) *smaller footprint*:- since membranes can fulfill the function of sedimentation, filtration and disinfection, there is a considerable reduction in treatment area as consequence. The MBR process typically requires only about 50% of the land area of a CAS process for the same throughput

(iii) *decoupling of hydraulic retention time (HRT) and solids retention time (SRT)*:- the absolute solids separation in the MBR enables the hydraulic retention time to be decoupled from the sludge retention time. The mixed liquor suspended solids (MLSS) concentration can therefore be set to any desired value. MLSS concentration levels greater than 20 000 mg/L can easily be maintained by the membranes in an MBR, compared to the typical

MLSS concentration levels of 3 000 to 4 000 mg/L for CAS processes [Günder and Krauth (1998)]. With the higher achievable MLSS concentrations in MBRs, reactor volumes are even further reduced. There is no reason why MLSS concentrations in CAS processes cannot be increased, but the sedimentation tanks are limited by capital cost and surface area for high settling fluxes at high MLSS concentrations [Muller *et al.* (1995)].

(iv) *reduction in sludge production*, because of the much higher achievable MLSS levels. It is estimated that MBR processes produce only half as much sludge as the CAS process [Mayhew and Stephenson (1997)].

(v) *providing a higher quality, disinfected, product*:- it has been reported that a greater diversity exists in the consortia of microorganisms that are cultivated in a MBR compared with that which exists in conventional bioreactors. This is because the settling tank selector, common with conventional reactors, is replaced with an absolute membrane barrier which prevents planktonic and non-settling microorganisms from escaping the MBR. The presence of a greater amount of enzymes in MBRs has also been noted. This improves both the ability of MBRs to produce final effluents lower in COD and its capability to handle high organic shock loads. Since the final product is membrane-filtered, the amount of oxidation needed for final disinfection is reduced.

MBRs have been successfully applied to treat domestic effluents and a great variety of industrial effluents. The immersed filtration system is also being increasingly applied to potable water treatment.

In view of the advantages of MBRs over the CAS process, MBRs have major potential applications in South Africa, as well as other developing economies. These include:

(i) **point of source treatment of domestic effluents**, e.g. small communities, farms, hotels, tourist resorts. The final effluent here could be used directly for agriculture; could be used as second grade water for flushing of toilets cleaning of grounds, etc; or could be upgraded by means of reverse osmosis for recycling,

(ii) **point of source treatment of industrial effluents**. In these instances, the product from the MBRs could be used as second grade water, or could be upgraded for recycling back to the plant. In either instance, the load placed on local municipal waste water treatment works would be reduced.

The international MBR market is dominated by two systems, viz. the hollow-fibre membrane Zeeweed® system and the flat-sheet membrane Kubota system. Some of the larger SA industries have started evaluating these systems for effluent treatment. However, the economics of these systems puts them beyond the reach of most of the smaller domestic effluent treatment applications, as mentioned above, or the smaller industrial effluent treatment applications.

This project concerns the development of an inexpensive MBR technology for smaller scale applications that could fill the economic void left by the current commercial systems. The tasks of the project will include :

(i) investigating the factors that effect the hydraulic performance of MBRs, and hence developing a design for small scale MBRs

(ii) developing a membrane module, based on locally available membranes, that could be employed in MBRs

It is also planned that the project would result in the development of a unique *hybrid* MBR (HIMBR), which could have significant advantages over the current commercial ones. Membrane aeration bioreactors (MABRs) are a separate class of membrane bioreactors. In these systems, pure oxygen is provided to a biofilm immobilized on the outside of silicone rubber membranes in bubble-less fashion. Most literature on the subject indicate that the process is suited to treat wastewater that require high oxygen demand, treat volatile organic compounds, combined nitrification, denitrification and/or organic carbon oxidation in a single biofilm. Because the biofilm is attached to a membrane, much higher oxygen utilization rates and efficiencies can be achieved compared to conventional pure oxygen processes. The biofilm thickness is controlled through regular cleaning.

In the HIMBR proposed in this project, vertical plate-and-frame flat-sheet (ultrafiltration/microfiltration) cartridges (or horizontally mounted narrow-bore skinless capillary membranes) will provide for bioreactor dewatering (similar to conventional MBRs). These filter cartridges, as in the case of the Kubota system, will be aerated with air from below to provide oxygen to the bioreactor and scour the flat-sheet membranes to facilitate cleaning. However, completely different to the Kubota system, an array of narrow-bore silicone rubber membranes will be installed in-between the flat-sheet plates, in a transverse orientation to the stream of rising air. The silicon rubber capillary membranes will serve as a surface for biofilm attachment and development and will also provide a means for pure oxygen transport to the biofilm by diffusion (similar to the MABR). This is of specific interest when the bioreactor is operated in the thermophilic temperature range, where the equilibrium solubility concentration of oxygen is reduced.

Different microbial populations will exist in the floc contained in the bulk of the bioreactor and in the biofilm that develops on the silicone rubber membranes. It is envisaged that the greater diversity in microbial population will lead to better breakdown efficiencies of the hybrid reactor compared to that of the conventional MBRs and MABRs. Although little information is available on MBRs operating under thermophilic conditions, the system under development will be engineered right from the start to be able to operate at temperatures as high as 60^{o} C.

Cleaning of the dewatering membranes and control of biofilm thickness on the aeration membranes is of concern in immersed MBRs and MABRs respectively. Back-flushing with permeate was shown to be effective to control fouling of capillary membranes. Flat-sheet membranes cannot be back-flushed. Circulating sponge balls are a very effective technique to maintain tubular membrane surfaces clean by a rubbing action. This is where the secondary function of the silicon rubber membranes in the HIMBR comes into play. The silicon rubber membranes will be positioned such that the rising aeration air will agitate them in a random fashion and cause them to touch both each other as well as the flat-sheet membrane cartridges. In the HIMBR therefore, the respective thickness of the fouling layer on the dewatering membranes and the biofilm on the silicone rubber tubes will be controlled by both the scouring action of the rising aeration air and the mechanical rubbing action caused by the silicone rubber membranes.

1.2 Aims

(i) Develop flat-sheet membrane casting procedures, cartridges and a manifolding system suitable for use in IMBRs.

(ii) Develop an aerated hybrid immersed membrane bioreactor containing flat-sheet or capillary dewatering membranes, using air sparging and silicone rubber membranes for oxygenation.

(iii) Develop fabrication protocol to produce narrow bore and thick-walled skinless membranes for respective use in the HIMBR and the gradostat reactor.

1.3 Report Organisation

An overview of MBRs is presented in Section 2. Section 3 concerns the development of a membrane module for use in IMBRs. Section 4 concerns the development of a design for IMBRs. The geometric and operating variables that effect IMBR performance are investigated. A factorial experimental design is subsequently utilised to develop guidelines for optimal IMBR designs. An optimal design selected from the outcomes of Section 4 is subsequently evaluated on a model foulant (bentonite) and a real foulant (activated sludge) in Section 5. Section 6 concerns the development of fabrication protocols for skinless capillary ultrafiltration membranes. Section 7 concludes the report.

2. OVERVIEW OF MEMBRANE BIOREACTORS

2.1 Membrane bioreactor types

Three fundamentally different MBRs exist for the treatment of wastewater:- the solid-liquid separation MBR, the membrane aeration bioreactor MABR) and the extractive membrane bioreactor (EMBR).

The solid-liquid separation MBR, where the membranes replace the sedimentation step in conventional processes, is the most widely studied and full-scale applied MBR for wastewater treatment [Brindle and Stephenson, (1996)].

In MABRs the membranes serve as an interface between, usually, oxygen and an attached biofilm [Rothemund *et al*. (1994), Brindle *et al.* (1998)]. The attached biofilms receive bubbleless oxygen through the gas permeable membranes and substrates from the bulk fluid. Such systems have increased oxygen utilisation efficiencies [Brindle and Stephenson (1999)] and contain biofilms with a different population composition than biofilms growing on inert surfaces, since they receive oxygen and substrates from opposite directions [Semmens and Hanus (1999)].

As in MABRs, the membranes in EMBRs (usually silicon tubes) separate two distinct phases. The membranes separate the suspended biomass from an aggressive industrial effluent. Biomass growth is stimulated by providing nutrients, oxygen and regulating the bioreactor temperature at the optimum. The undesired components are removed from the effluent stream through the membranes into the bioreactor where it is biologically treated. The concentration driving force for the mass transfer of the pollutants is maintained by the biodegradation of the pollutants in the bio-medium phase. Even wastewater streams of extreme conditions will not harm the microorganisms, since they are not in direct contact with the hostile environment in the wastewater stream [Livingston (1994), Brindle and Stephenson (1996), Livingston *et al.* (1998)]. It is therefore unnecessary to pre-condition or dilute the wastewater stream.

2.2 MBRs in wastewater treatment

Although there is a growing interest in MABRs and EMBRs, these processes have been limited, so far, to pilot-scale operations. On the other hand, the world has seen an exponential growth in full-scale commercial solid-liquid separation MBRs over the last ten years. In the rest of this survey there will only be referred to solid-liquid separation MBRs, unless otherwise stated.

Today there are over 500 commercial MBRs in operation of which most are situated in Japan [Stephenson *et al.* (2000)], largely because of the Japanese government's Aqua Renaissance program '90 [Kimura (1991)] to invest in a water treatment technology for recycling purposes in tall rise buildings. Therefore, most of the Japanese MBRs are fairly small-scale and located inside buildings to treat in-building wastewater for purposes of recycling.

Not only have MBRs grown in number, but also in capacity [Churchouse and Wildgoose (1999)]. Originally MBRs were developed, as mentioned, for in-building water treatment, but the scale has been continuingly increased to even treat the domestic effluent of communities. Also, the applications of MBRs have diversified to treat a wide spectrum of wastewaters [Churchouse and Wildgoose (1999)].

Because of ever-increasing stringent regulations, conventional wastewater treatment plants and industries producing liquid waste are faced more and more with problems such as:

- no location to build or expand a conventional treatment plant because they are traditionally large, produce unpleasant odours, lower the aesthetical value of the environment or the existing plant layout prohibits it;
- final effluent does not comply with regulations to be discharged into a watercourse;
- systems require continued upgrading as water quality regulations become more stringent; and
- conventional sewage treatment produces large amounts of sludge.

MBRs have proved to be an answer for not just solving the above-mentioned problems, but also added, because of a consistently high-quality final effluent, a commercial value to the treated water with recycling possibilities [Jefferson *et al.*(1999), Mallon *et al* (1999)]. Table 1 explains the advantages of an MBR as opposed to a conventional biological treatment process [Mallon *et al.* (1999), Stephenson *et al.* (2000)].

Table 1: Advantages of a biological treatment process combined with membrane filtration

Disadvantages of conventional biological treatment processes	Effect of introducing membranes to the process
Sludge bulking	Consistent high quality treated water production, even when system is subjected to shock loadings
Slow reaction kinetics	Natural selection and total retention of microorganism population, rapid start up
Slow bacteria settling in clarifier	Bacteria kept in bioreactor
Tertiary treatment to remove viruses	Considerable removal of viruses and no tertiary treatment required
Inadequate microorganism-substrate contact time	Increased contact time
Sludge production	Reduced sludge production
Inconsistent treated water quality containing bacteria	Consistent high quality treated water production, containing no bacteria
Huge and difficult to expand	Small footprint and modular

2.3 Membrane Technology

2.3.1 Role of membranes in MBRs

Any material that displays a selective permeability for different substances, and thereby separating them, can be considered as a membrane. In the solid-liquid separation MBR the membrane serves to retain suspended material (microfiltration) and even dissolved macromolecular species (ultrafiltration) in the bio- medium phase and allow treated water to pass through. The treated water leaving the membrane is known as the permeate. A pressure difference, the trans-membrane pressure (TMP), across the membrane acts as the driving force for mass transfer of treated water. The ability to decouple solids retention time from hydraulic retention time enables the MBR to operate at any desired MLSS concentration and sludge age. The MLSS concentration and sludge age are the two parameters that determine the biological treatment capability of a biological treatment process and, since these two parameters can be set (by will) to much higher values in an MBR than in a conventional biological treatment process, makes the MBR a far more effective treatment process [Bouhabila *et al.* (1998), Gander *et al.* (2000)].

In an MABR the membrane's role is to transfer oxygen from the gas phase to the wastewater, whereas in the EMBR the membrane extracts pollutants from the wastewater to the bio-medium phase. In both these MBR types the driving force for mass transfer through the membrane is a concentration gradient.

2.3.2 Membrane structure

The ideal membrane to use in an MBR would be of a material that:

- is mechanically and chemically resistant;
- provides a high throughput of permeate; and
- has a high degree of selectivity.

For a sieving membrane to have a high degree of selectivity requires that the pores in the membrane are small. The only way then, for a membrane with small pores to have a high throughput of permeate (high permeability), is for the skin layer of the membrane to have a high degree of porosity (i.e. a large number of pores per unit surface area). However, to maintain a high degree of selectivity, it is also necessary for the pores in the membrane skin layer to have a narrow pore size distribution (isoporosity). To reduce resistance to convective transport through the membrane, it is best for the membrane skin layer to be thin and supported on a more open honeycomb or spongy substructure.

2.3.3 Membrane configurations

The membrane configuration refers to the geometry of the single membrane element, as well as the way in which the elements and modules (collections of membrane elements housed together in units) are arranged with respect to each other and the MBR. The aim of membrane configuration development for MBRs has usually been to suppress fouling and to address the resulting problems.

Membrane geometries employed for MBRs can be divided into planar, tubular and hollow fibre [Stephenson *et al.* (2000)]. Modules may either be submerged in the bioreactor or placed externally of the MBR in a side stream configuration as shown in Figure 2. Both configurations pose distinct advantages [Shimizu *et al.* (1996), Ueda *et al.* (1997), Bouhabila *et al.* (1998), Gander *et al.* (2000)].

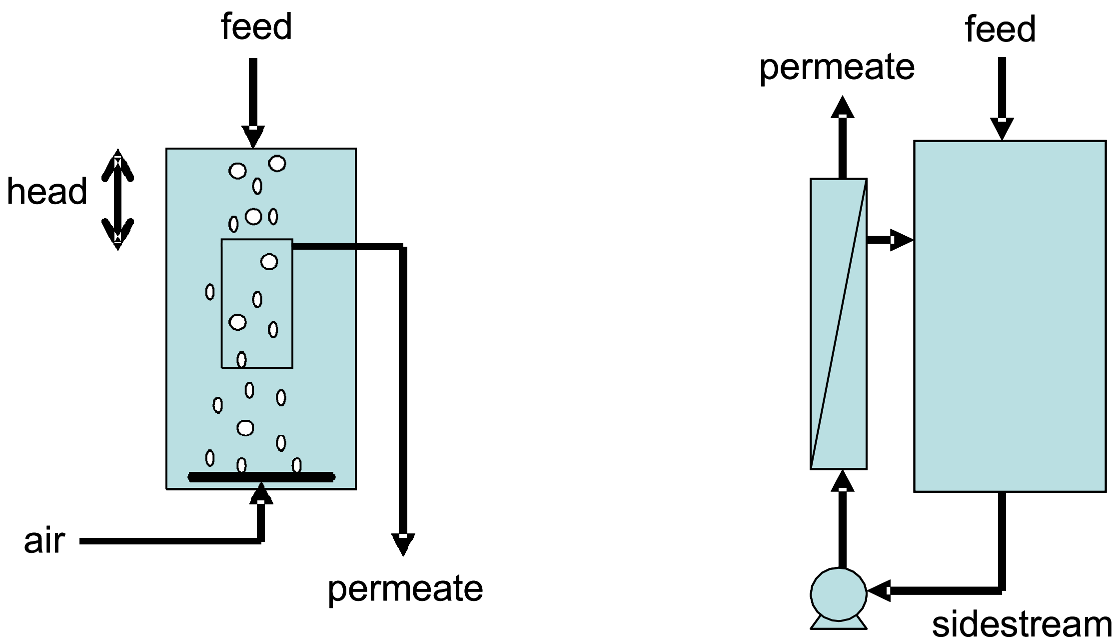

Figure 2: Difference in the submerged and side stream configurations.

With the membranes submerged in the bioreactor, a small or even no permeate suction pressure is required, since the hydraulic head of the water above the membranes is enough for the treated water to gravitate through the membranes and out of the MBR. Unfortunately this configuration requires coarse bubble aeration to produce the necessary turbulence and crossflow across the membranes to provide for the back-transport of retained material from the membrane surfaces. The turbulence created at the membrane surface is not as intensive as in the high cross-flow side-stream configuration and permeate fluxes are subsequently lower in the submerged configuration to reduce fouling. Lower fluxes necessitate an increase in membrane area with a consequent increase in capital expenditure.

If the side-stream configuration is used, the membranes are externally located and thus easy to clean or to replace. High cross-flow velocities are maintained through the membranes at relatively high TMP values to produce high permeate flux rates. Since the volume of the recycled feed is 10 to 20 times as much as the permeate produced [Shimizu *et al.* (1996)], the side-stream configuration requires high-rate recirculation pumping. It is believed that the microorganisms are sensitive to shear, exposure to the excessive shear produced by the recirculation pumps results in a loss of sludge activity [Brockmann and Seyfried (1996)] and a decreased nitrification rate [Ghyoot *et al.* (1999)]. Recirculation pumping makes side-stream treatment more expensive than immersed membrane treatment [Gander *et al.* (2000)].

2.4 Process Phenomena

2.4.1 Concentration polarisation

The two most significant mechanisms of mass transport in an MBR are convection and diffusion. Convection and diffusion is the result of bulk fluid motion and concentration gradient respectively.

TMP is the driving force for the mass transfer of permeate through the membrane with a concomitant increase in concentration of retained material at the membrane/solution interface. This phenomenon of solute accumulation within a concentration boundary layer at the membrane surface is known as concentration polarisation (CP). Since this layer is at the membrane/liquid interface, the liquid velocity is near zero. Diffusion is thus the only mechanism of mass transport away from the membrane surface, and it is significantly slower than the convection mechanism in the bulk liquid.

CP therefore increases:

- the chance of precipitation of slightly soluble solutes onto the membrane to form a gel layer under ultrafiltration or microfiltration conditions;
- the concentration of suspended matter near the membrane; and
- the permeation of retained material, because of the greater concentration gradient across the membrane.

The CP effect can be considerable in MBR applications, because fluxes can be high, while the diffusion coefficients of macromolecular solutes and colloids are low [Wakeman and Williams (2002)]. It is therefore necessary to increase turbulence at the membrane surface to reduce the thickness of the CP layer, or to operate at lower permeate fluxes to reduce the build-up of retained material at the membrane interface. CP, together with the two mass transport mechanisms: convection and diffusion are illustrated in Figure 3.

2.4.2 Fouling

Fouling refers to all the processes that collectively increase the hydraulic resistance of the membrane [Stephenson *et al.* (2000)]. They can be categorised into cake formation of relatively high molecular mass or large particles retained at the membrane surface (external fouling), which is usually reversible, and adsorption and deposition of small particles inside the membrane pore structure (internal fouling), which are normally irreversible [Wakeman and Williams (2002)].

It has been found that the three fractions of sludge: suspended solids (1 μm to > 100 μm), colloids (0.001 μm to 1 μm) and solutes (< 0.001 μm) each displays a certain tendency to foul the membrane [Bouhabila *et al.* (2001), Tardieu *et al.* (1998)]. The liquid fraction of sludge, containing the colloids and solutes, proved to be the main contributor to internal fouling (adsorption, as well as deposition). These compounds have strong physico-chemical interactions with the membrane, as well as with other elements, to induce the deposition of material on to the membrane [Wisniewski *et al.* (2000)].

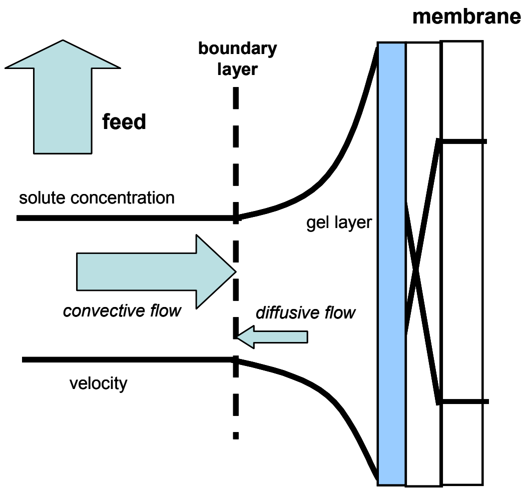

Figure 3: Concentration polarisation and the transport mechanisms.

It is also widely documented that, when filtrating activated sludge in an aerobic (air is supplied for microorganisms) MBR, that the extracellular polymeric substances (EPS), excreted from cells are the main fouling constituent [Hodgson *et al.* (1993), Baker and Dudley (1998), Nagaoka *et al.* (1998, 2000)].

Membrane fouling has been the main impediment to fully utilise the potential of MBRs [Flemming *et al.* (1997)]. Intensive research has been conducted to understand fouling mechanisms [Bouhabila *et al.* (2001)] and reduce fouling, not just in MBRs, but as a matter of fact, in any other membrane filtration operation.

There are three basic methods to reduce fouling [Wakeman and Williams, (2002)]:

- pre-treatment of the feed to remove any particulates, which may cause clogging or deposition, or to reduce the contaminant load;
- right choice of membrane material, e.g. a hydrophilic material will be less prone to protein deposition, and
- flow manipulation, which includes increased cross-flow velocity, air scouring to reduce the CP layer or back-flush (reverse permeate flow) for effective back transport of retained material from the membrane.

At some stage in operation the membranes may be fouled to such a degree, that the flux is reduced to only a fraction of the initial start-up flux (constant TMP operation) or producing a flux at an increased TMP (constant flux operation), so that the process is uneconomical. The membranes must then be taken off line to be cleaned by either a mechanical or a chemical process, or even both.

Fouling leads to uneconomical operation, downtime for cleaning purposes and a reduction in membrane lifetime. Incentives therefore exist to optimise every aspect of MBR operation to improve control of fouling.

2.4.3 Critical flux

For microfiltration, critical flux is defined as that flux, at start-up, below which no irreversible fouling takes place [Field, *et al.* (1995)]. Therefore, when operating below the critical flux the TMP and permeate flux will always be directly proportional in a steady state. The moment the flux is increased above the critical flux, the TMP will continue to increase with constant flux operation or the flux will continue to decrease with constant TMP operation. This has been visually confirmed by Li *et al.* (1998) when cross-flow of particulate suspensions at low fluxes was observed under a microscope. There were distinct conditions of operation where the particles did not deposit onto the membrane. The reversibility of the fouling at sub-critical fluxes and the irreversibility at supra-critical fluxes was also confirmed by Defrance and Jaffrin (1998).

It is believed that the critical flux is a function of the system hydrodynamics and the nature of the membrane, as well as the nature of the material retained at the membrane interface [Stephenson *et al.* (2000)]. It is therefore desirable to optimise these factors so as to operate the MBR at a high sub-critical flux.

2.5 Biological Processes

2.5.1 Aerobic and anaerobic oxidation

Microorganisms obtain the necessary energy for life functions and the material for cell growth from the oxidation of carbon substrates, which are usually measured as chemical oxygen demand (COD) or biochemical oxygen demand (BOD). The oxidation of organic carbon can occur in the presence of oxygen (aerobic) or in the absence of oxygen (anaerobic). Oxygen is the final electron acceptor in aerobic processes, whereas carbon dioxide is the final electron acceptor for the oxidation of organic carbon in anaerobic processes. However, other electron acceptors exist for anaerobic oxidation, depending on the substrate.

In contrast to aerobic oxidation, anaerobic oxidation is only a partial combustion process and produces less energy to make anaerobic a much slower process [Stephenson *et al.* (2000)]. Consequently, anaerobic processes require larger reactor volumes than aerobic processes for the same throughput. Where the aerobic process requires energy for aeration purposes, the anaerobic process produces an energy source in the form of biogas, which mainly consists of methane. Anaerobic processes also have a much lower sludge production rate than aerobic processes. Advantages of the aerobic system are that they operate almost odourless and achieve rapid start-up, unlike anaerobic systems. However, the energy requirement of the aerobic process is by far greater.

2.5.2 Nutrient removal

2.5.2.1 Nitrification

Nitrification is the two-step process in which ammoniacal-nitrogen (NH_4-N) is first oxidized to nitrite-nitrogen (NO_2-N), which in turn is oxidised to nitrate-nitrogen (NO_3-N). Nitrification, needing oxygen as final electron acceptor, occurs in aerobic systems.

Nitrification is very sensitive to dissolved oxygen (DO) concentration levels. Compared to complete nitrification at a DO concentration of 1 mg/L for an influent with total nitrogen concentration between 20 and 50 mg/L, it was shown that nitrification was considerably slower at a DO concentration of 0,5 mg/L [Chiemchaisri *et al.* (1992)].

2.5.2.2 Denitrification

Denitrification is the process where NO_3-N is reduced to gaseous products such as molecular nitrogen and dinitrogen oxide. Nitrification and denitrification allow for the complete removal of nitrogen to harmless products, rather than just concentrating it like conventional physico-chemical methods do [Nuhoglu *et al.* (2002)]. Unfortunately, denitrification utilises NO_3^- as the final electron acceptor and cannot occur alongside nitrification in an aerobic environment. Denitrification organisms are facultative aerobes, meaning that they can change their metabolic pathways when they are introduced to aerobic conditions. In an aerobic environment these organisms will change to utilising oxygen as the final electron acceptor for COD removal.

It has been shown that nitrification and denitrification can still be effectively accommodated together in MBRs with:

- intermittent aeration [Chiemchaisri *et al.* (1992), Yeom *et al.* (1999)];
- anoxic zones created by the hydrodynamic flow [Chaize and Huyard (1991)];
- addition of an anoxic tank prior to the aerobic tank [Churchouse and Wildgoose (1999)];
- high loading feed rates to produce large flocs where anoxic conditions prevail inside the floc [Chaize and Huyard (1991), Ueda *et al.* (1996)]; and
- a membrane interface between supplied oxygen and wastewater with an attached biofilm, containing aerobic and anoxic zones, like in the MABR configuration [Semmens and Hanus (1999)].

2.5.2.3 Phosphorus removal

It seems as if assimilation alone will not remove all the phosphorus, since biological processes are normally carbon limited [Stephenson *et al.* (2000)]. Some form of coagulant dosing may be necessary for the complete removal of phosphorus. Stephenson suggests that biological phosphate removal for an MBR may be improved by the addition of an anaerobic section prior to the aerobic section with free-of-nitrate-sludge recycle back to the anaerobic section.

2.6 Biomass Retainment

The one feature that distinguishes the MBR from any other conventional biological wastewater treatment process is the fact that the MBR retains the biomass completely. This property enables the MBR to:

- assimilate a wide variety of microorganisms;
- operate at very high MLSS concentrations; and
- operate at a high sludge age.

2.6.1 Microorganism consortia

The dewatering membranes used may even be able to keep viruses inside the bioreactor [Mallon *et al.* (1999)] and can therefore disinfect the permeate. Instead of losing microorganisms as result of washout as is the case with conventional systems, the membranes also give the bioreactor the opportunity to build up a rich variety of microorganisms with more complex interaction and symbiosis.

With a more intricate microorganism population the MBR may be able to biodegrade more substances more rapidly with greater robustness towards changes in the feed composition. The MBR also harbours slow-growing organisms such as nitrifiers. Nitrification is reported to be almost twice as effective in an MBR as a CAS plant [Zhang *et al.* (1997)]. It was generally found that the suspended ecology in an MBR hosts higher class organisms such as rotifers, nematodes and protozoa, which is not the case in CAS processes. The MBR ecology mainly contains heterotrophic organisms, but it is uncertain to what extent this matters.

2.6.2 High MLSS concentrations

MLSS concentration may be set to any desired value, but generally MBRs are operated at LSS between 8 to 14 g/L. High MLSS concentrations the MBR is more resistant to shock loadings, but more oxygen is needed in an aerobic MBR just to maintain biomass. Therefore, at low MLSS the airflow volumes required to maintain flux is scouring-controlled and at high MLSS values the airflow requirement is biomass-controlled. Viscosity increases with MLSS concentration with a resulting energy penalty. Also, at high MLSS concentrations the fouling seems to be more severe, because an EPS with a higher degree of hydrophobicity is produced. It was found that at low MLSS values the fouling propensity also increases. It is advised to operate at concentrations greater than 5 g/L.

2.6.3 Sludge age

Sludge age is the key control parameter in a bioreactor and effectively controls the microbial growth rate. The sludge age may be set to any desired value in an MBR. he sludge retention time is though to be the most important factor for effective nitrification [Kishino *et al.* (1996)]. It was found that the activity of the sludge decreases with sludge age, possibly due to the accumulation of inert biomass and the impeded oxygen transfer to the inside of suspended floc [Muller *et al.* (1995), Huang *et al.* (2001)]. The greater the sludge age the less EPS is produced (but with a higher proportion of protein) and the less active the biomass becomes. It is important to waste sludge at that point in order to get rid of inert materials.

3 DEVELOPMENT OF A FLAT-SHEET MEMBRANE MODULE

3.1 Introduction

One of the aims of the project is to develop a membrane module that would be used to dewater MBRs. The criteria for such a module include:

(i) it should simple and robust, and inexpensive in construction,

(ii) it should give a good permeate quality,

(iii) it should give a good flux, that would be viable for MBR applications,

(iv) it should require easy and inexpensive cleaning strategies,

(v) for thermophilic operations, the module should be able to operate at temperatures up to 60°C, and

(vi) it should preferablyutilise membranes that are readily available in South Africa, obviating the research and development costs to develop new membranes.

The development of the module occurred in parallel with investigations into system hydrodynamics in immersed filters, with the latter guiding the former. For reasons of simplicity, the module development is reported in this section, and system hydrodynamics is reported in Section 4.

3.2 Current commercial MBR modules

At present two membrane-module geometries dominate the commercial membrane market, viz. hollow fibre modules (capillaries) and flat-sheet modules. The VSEP® process uses a third geometry, viz. vibrating flat discs, but this is an emerging technology that is not widely employed at present.

The most common example of hollow fibre modules is the Zeeweed® module of Zenon. This consists of a large number of hollow fibre membranes manifolded together at the top and bottom, to form a *cassette* (Figure 4). The hollow fibres operate in an outside-in filtration configuration. The fibres are not stretched taut, but are fairly “loose” in the cassette. The cassettes are immersed into the reactor. Coarse bubble aeration is introduced below the cassettes, inducing turbulence in the fluid surrounding the fibres. This causes lateral motion in the individual fibres, leading to scouring of the membrane surface and hence the reduction of fouling.

Figure 4:- Zeeweed® hollow-fibre module

The most common flat-sheet module is that developed by Kubota (Figure 5) This consists of a central plate which has grooves for permeate flow. Spacers are placed over this, and the flat-sheet membranes are placed over the spacers. The membranes are welded to the central plate ultrasonically. The individual modules are then inserted into a *membrane pack*. Each module has its own permeate off- take moulded into the frame. The off-takes are connected to a permeate offtake manifold using individual flexible tubes.

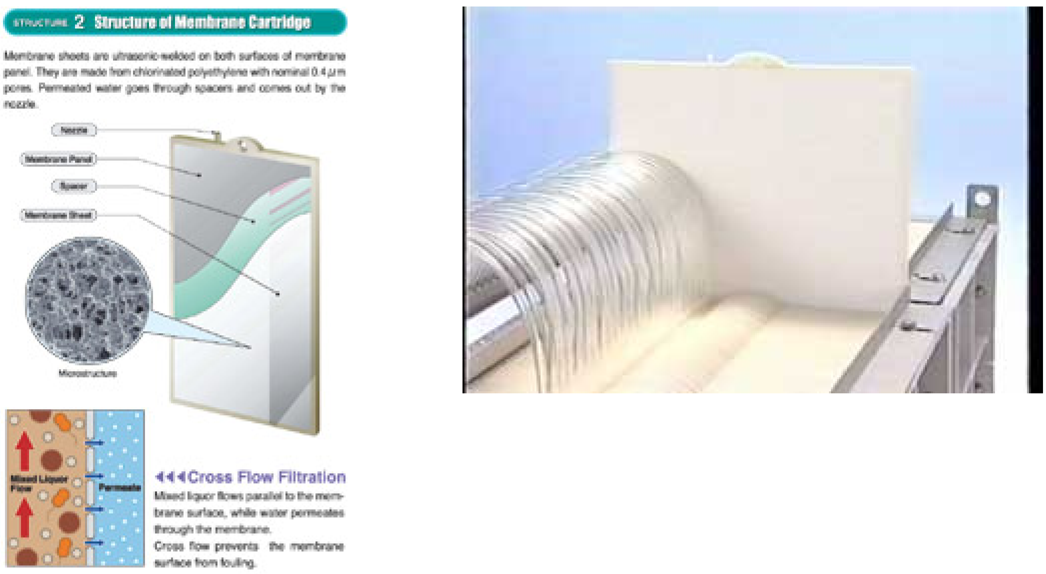

Figure 5:- Kubota flat-sheet module

The hollow-fibre geometry appears to offer various advantages over the flat-sheet geometry. These include :

(i) the hollow-fibre module has a significantly greater filtration area to volume ratio than flat-sheet modules. Hence, the footprint of a hollow-fibre MBR is smaller than that employing flat-sheet modules, and

(ii) the hollow-fibre module is *self-sealing*, i.e. if a fibre breaks, contaminants would be drawn into the broken fibre, and hence seal off the broken fibre.

The advantages offered by the flat-sheet module include :

(i) the system can be operated under a gravity head. Conversely the hollow-fibre installations employ a suction pump for permeate withdrawal, and

(ii) individual modules may be easily accessed if physical cleaning is required.

At the onset of this project, both module geometries enjoyed significant market shares internationally, with no clear distinction as to which was the "better" system. However, towards the conclusion of this project, it was slowly emerging that the hollow-fibre geometry could have significant disadvantages from the point of view of fouling. This is discussed further in Section 3.3.2.

3.3 Module development

3.3.1 Choice of module geometry and membrane type

At the initiation of this project it was decided that development of both the capillary (hollow-fibre) and flat-sheet modules would be pursued. Both modules would be assessed in terms of the criteria listed in Section 1, and hence a final module type would be decided on.

The starting point in terms of the capillary module was to use the capillary ultrafiltration membranes that had been developed at the University of Stellenbosch for use in potable water production. These membranes are fabricated from polysulphone, have a diameter of 1,8 mm, and a molecular mass cutoff of approximately 35000 Dalton.

The membrane material selected for the flat-sheet module was the woven fibre microfiltration (WFMF) fabric developed by a South African company, Gelvenor. In a previous WRC project, K5/1232 – *The Development of a Reverse Flow Microfilter* [Pillay and Jacobs (2005)] it was shown that this woven polyester fabric had a good potential for use as an immersed filter, and offered various potential advantages over the current commercial inversion-cast flat-sheet membranes.

3.3.2 Initial investigations – capillary vs flat-sheet

Various tubular woven fabric and capillary membrane immersed-filter designs were evaluated during the first phase of the project. However, it was soon realized that the flat-sheet woven-fabric membrane filter elements had significant advantages over the capillary membrane modules:

(i) the WFMF modules were substantially more robust than the capillary modules,

(ii) the locally produced ultrafiltration capillary membranes necessitated higher operating pressures for an equivalent product yield than the more porous woven fabric microfiltration membranes,

(iii) because of the relatively large internal diameter of the local capillary membranes (1,2 mm), the membranes did not prove to be self-sealing when a fibre would break, and

(iv) it was substantially easier to mould and fabricate sheet filter devices than was the case with capillary- type membranes. Figure 6 shows one type of mould that was used to cast a manifold onto the one side of a membrane bundle. This was one of a number of approaches used to prepare double-manifolded capillary membrane elements. It was also not trivial to cast the second manifold in a way that all the fibres experienced the same amount of tension. By producing capillary membrane elements with one manifold only, the problem of uneven membrane tension was overcome (Figure 7b). It also simplified element fabrication

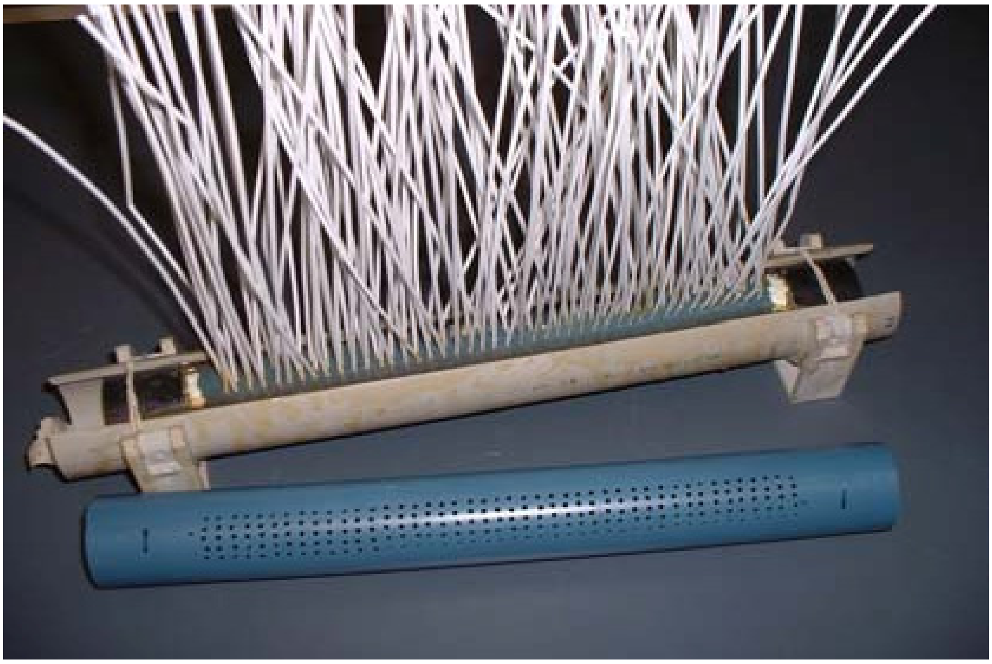

Figure 6:- Moulding system to produce an immersed capillary membrane filter element.

.

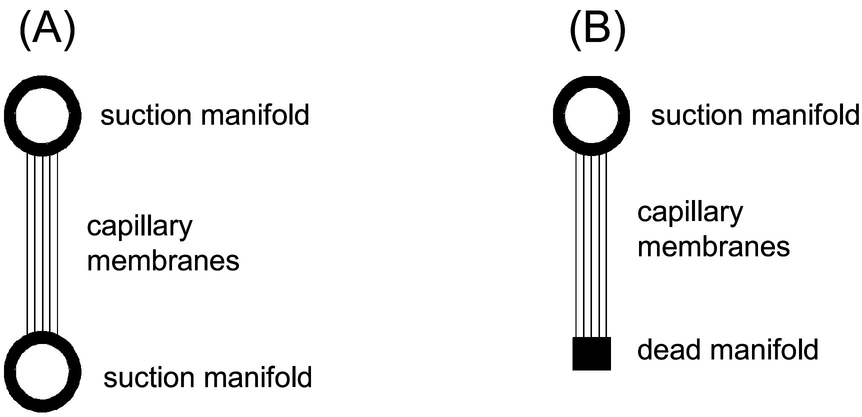

Figure 7:- Two approaches to capillary filter element design:
a) double manifolded capillary membranes,
b) single manifolded element.

At this stage it also began emerging that some of the commercial hollow-fibre plants were experiencing significant problems with fouling. These included:

(i) Material accumulating near the manifolds. Whilst the central parts of the fibres move about under turbulence induced by coarse bubbles, the ends near the manifolds are almost stationary. Hence, these regions could foul rapidly (Figure 8a), and

(ii) In order to control fouling, it is essential that the hollow-fibre in a bundle move about individually under turbulence. If however any fibrous material, e.g. hair, gets entangled in the hollow-fibre bundle, it can quickly lead to the hollow-fibres being bound together. This rapidly leads to the formation of a cake within the bundle (Figure 8b).

Figure 8:- Fouling in capillary/hollow fibre modules

In view of all the above, it was decided that work on the capillary membrane modules be terminated, and that the project should focus solely on the WFMF flat-sheet modules.

3.3.3 WFMF flat-sheet module – First Prototype

The initial development of WFMF modules utilised the *tubular* WFMF fabric. In the original application for which the WFMF fabric was developed, the individual tubes were manifolded into end-blocks on either end of the filter curtain. These membranes were operated under pressure from the inside (Figure 9).

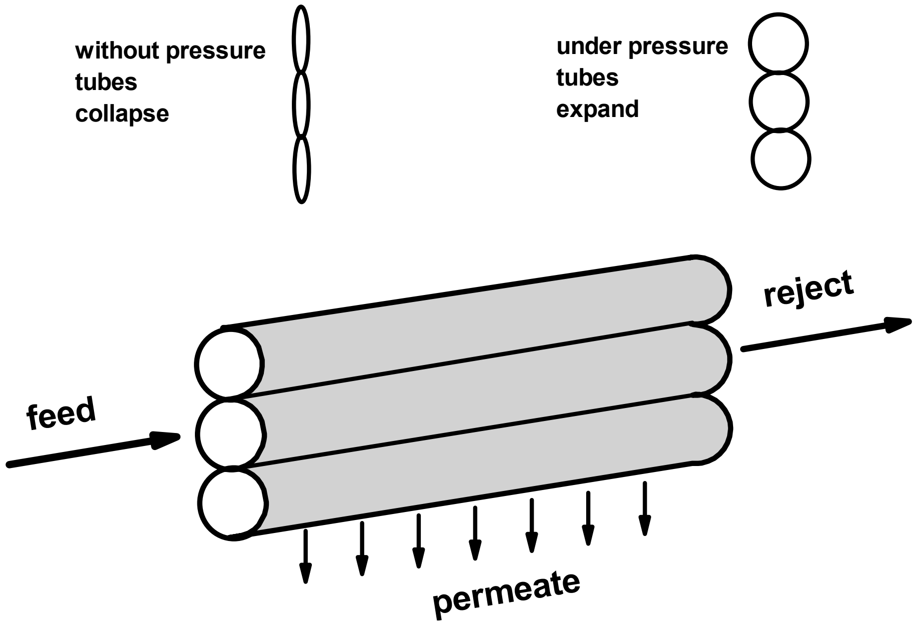

Figure 9:- Original (inside-out) operation of tubular WFMF membrane (From WRC Project K5/1232)

In the MBR application, the filter element is placed under water, and the permeate is drawn from the reactor and collected in a manifold positioned only at one end of the curtain under suction pressure. The other end is blocked off. In order to provide for the permeate to flow with as little restriction as possible to the point of collection, spacers had to be inserted to keep the inside faces of the fabric apart (Figure 10b).

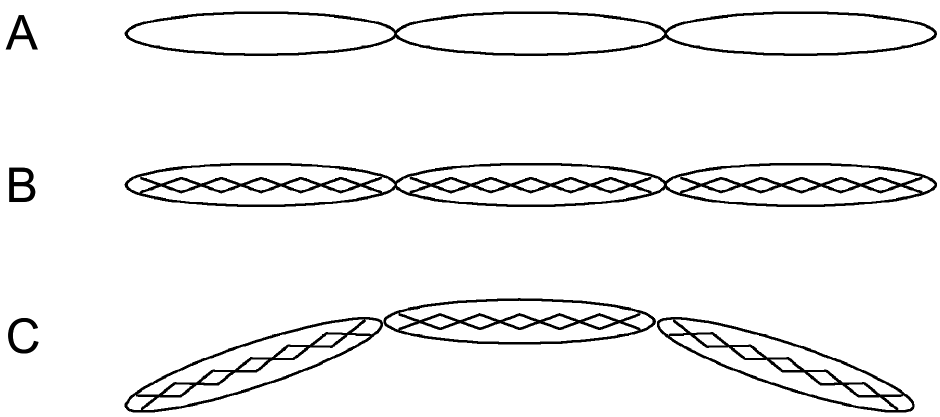

Figure 10:- Schematic of the woven tubular membrane filter:
a) without permeate side spacer,
b) with permeate side spacer and c) lateral flex in the segmented panel.

Figure 11 shows two filter panels under construction. One of the problems with this filter was the bulkiness of the product collector manifold, which had an outside diameter of 40 mm. Another problem, that also interfered with positioning of a multitude of filters in a vessel was, the flexibility of these filter elements (Figure 10). Although the stainless steel provided some rigidity to the individual tubular sections, the element as a whole was still flexible in both the lateral and vertical direction. In another embodiment of an immersed filter (Figure 10c) this feature may be to advantage since the filter element could be in the form of a coil as result of the unsupported section in-between the filter ducts.

Figure 11:- Tubular woven fabric immersed membrane under construction.

Nonetheless, in most of the experimental work use was made of the tubular woven fabric membrane elements. The very first bioreactor that operated in the laboratory also made use of immersed filters of this kind (Figure 12). It was during these bioreactor experiments that the project team first learned about uneven membrane fouling as result of poor hydrodynamic design of the bioreactor.

Figure 12:- Bioreactor vessels with one woven tubular fabric membrane envelope.

Choice of the spacer material also needed some consideration. The membrane is under suction pressure and although the fabric used was fairly stiff, the fabric did take to the contours of the spacer insert on the inside. This imparted some surface topography on the exposed side of the membrane which lead to localized build-up of foulants. A series of experiments were conducted in which various inserts were evaluated as spacers. Single-tube elements with different inserts were manifolded in panels and tested on bentonite as model foulant. From these studies the woven stainless steel mesh, covered with a non-woven fabric gave the best result. These panels were used in subsequent hydrodynamic studies and development.

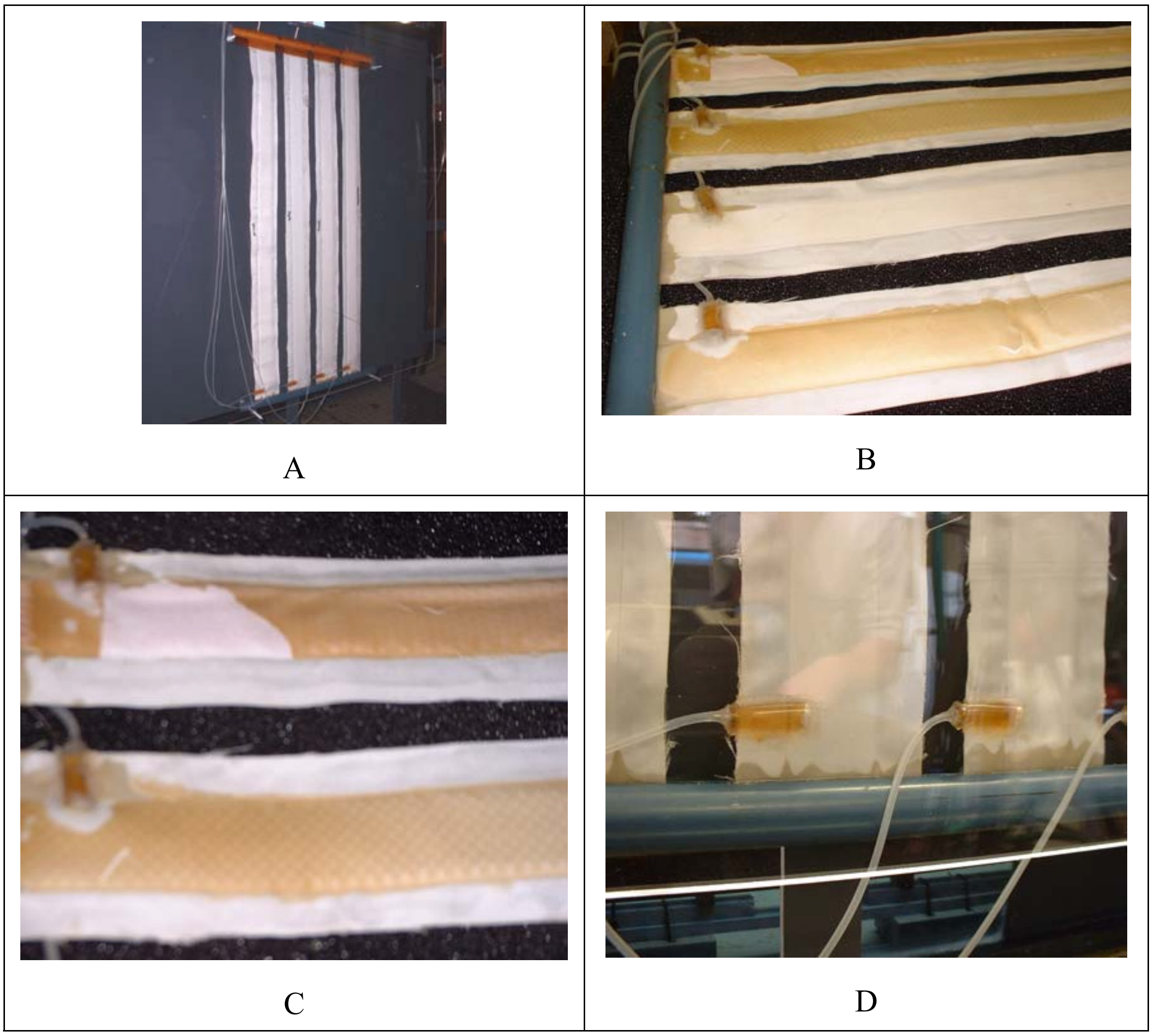

Figure 13: (a) Four tubular 1-m tubular sections with different permeate-side spacer materials,
(b) different fouling behaviour of membranes as result of the type of spacer insert used,
(c) close-up of the pressure sampling points, and
(d) pressure sampling points on a different set of tubular filter elements.

It was noticed during the studies on different spacers that the fouling layer (bentonite film) came loose and peeled off when the membrane is allowed to dry out. This can be seen in Figure 13c, where the consolidated film of bentonite came loose near the pressure take-off point. The reactor contained a small percentage biocide to reduce bacterial activity, and it was thought that this would not happen when the membranes were operated on biologically active water. However, the same happened when membranes that had been operating inside a bioreactor treating a mixture of domestic and winery effluent was allowed to dry out. Figure 20 shows how the biofilm peels and comes loose on own accord after the membranes dried out. Cleaning these membranes with compressed air completely restored the pure water flux performance of the fouled membrane elements.

It was not a problem to experiment with single tubular sheet membrane elements. However, the bulkiness of the permeate collecting manifolding system used (Figure 14), posed a problem when a number of these elements were used together. When the layout shown in Figure 15b is used to position the elements in a membrane stack, with the collector manifold positioned horizontally and at the top, the collector manifold interfered with the air flow and fluid circulation. The membranes are also spaced very far apart and air scouring becomes less effective.

Figure 14: Biofilm peeling from a tubular filter panel, operated in a bioreactor, after the panel has been allowed to dry out completely.

A better arrangement is that shown in Figure 15c, in which case the manifold is positioned vertically and the air flow is out of the plane of the paper. However, the membrane spacing is still dictated by the relative size of the collector manifold. The manifolding system could be improved on and the size reduced, but it will always remain a problem with the tubular-type sheet filter devices.

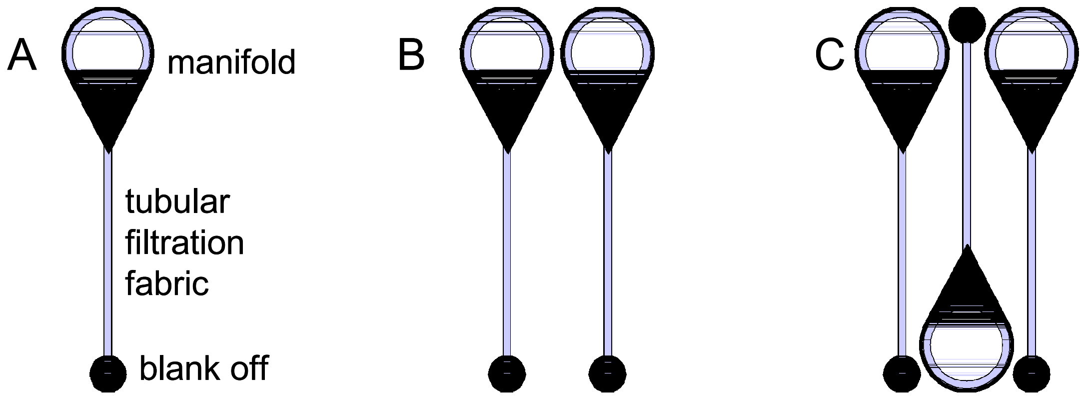

Figure 15: Schematic presentation of tubular cloth element design, showing:
a) single element,
b) two elements in filter rack in one arrangement and
c) more elements in another arrangement.

One way in which the relative size of the collector manifold could be reduced is to do away with the tubular-type manifold, which was a standard PVC tube for convenience, and cast a square block in a fixed mould. A simplified version of the design envisaged is shown in Figure 16.

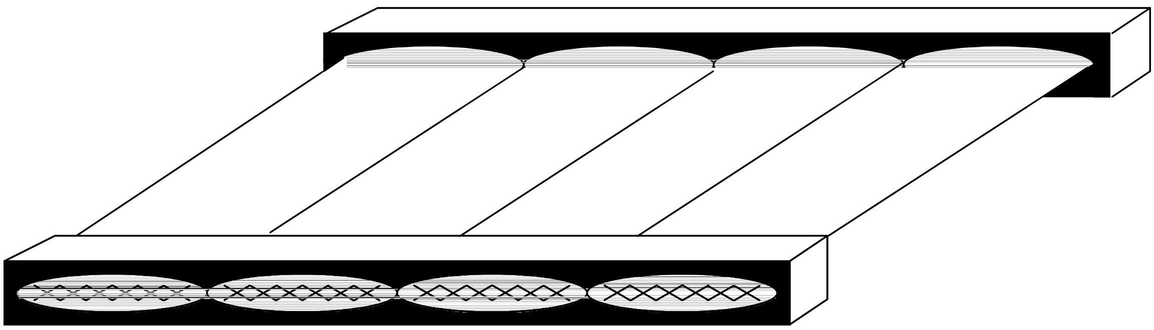

Figure 16:- Improved tubular-type filter element envisaged.

Some features, specifically the hydrodynamics of 2-phase flow across the face of the element and the moulded sections would still need thorough investigation. The moulded sections will always stand proud of the filtration surface and will always dictate minimum spacing of the elements. But, it is only through rigid research and development that one will be able to establish whether reduced surface area packing density is outweighed by other attributes of the tubular-type membrane filter

The tubular sheet filters do offer certain advantages, apart from their proven record of accomplishment as excellent filtration devices, in that each filter element is partitioned into small filter segments. When these tubular-type filters are back-washed the filter does not inflate to the same extent that a flat-sheet filter does because of the interference of the permeate spacer. If the spacer inserts (in this case stainless steel wire mesh) are rigid enough and fit snugly inside the opening, the spacers prevent the tube from inflating excessively. Pulsed backflush would be an appropriate manner to backwash these elements.

3.3.4 WFMF flat-sheet module - second prototype

Earlier work on flow patterns and system hydrodynamics (See Section 4) indicated the importance of providing for unhindered flow past the membrane surface to reduce the potential of fouling as result of stagnating fluid flow. All the panel filter elements constructed up to this point had some or other feature that interfered with fluid or gas flow distribution.

One way in which unhindered flow across the face of the filter element could be ensured was to design a flat-faced filter element. It emerged that the manufacturer of the tubular WFMF fabric also manufactured a flat-sheet fabric, of a similar weave to the tubular fabric. This provided the opportunity to develop a full flat-sheet module that would obviate some of the problems experienced with the tubular fabric.

A mould and moulding technique was devised by which such a filter could be fabricated. This filter element consisted of a core and permeate spacers that are sandwiched by the flat woven fabric (Figure 17).

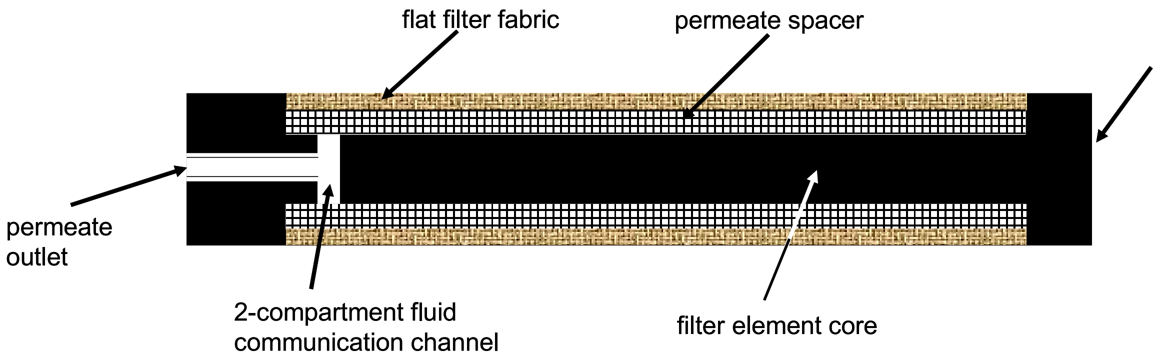

Figure 17:- Schematic of the flat filter element showing the membrane, permeate spacer and filter core.

The membrane panel consists of three major parts :- a combined insert/manifold sheet, mesh spacers and the woven fabric membrane. The mesh spacers are placed on either side of the insert/manifold (Figure 18) and the membranes are then placed over the spacers. These are then placed into a mould where casting epoxy is used to seal all edges and form a full shroud (Figure 19). A draw-off point for permeate is integrated into the mould. The final product is shown in Figure 20.

Figure 18: mesh spacer on membrane

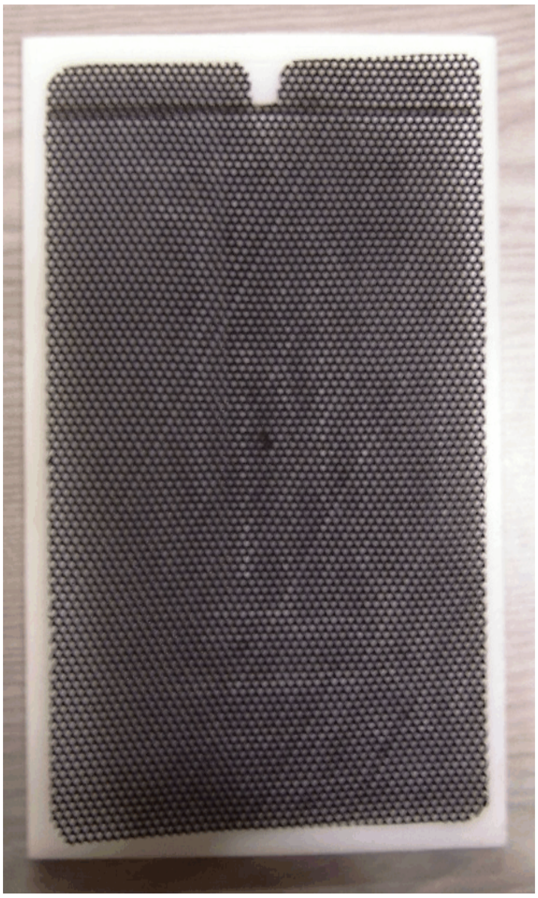

Figure 19 : moulded product

Figure 20: Final module with permeate offtake

The membrane panel is completely flat (Figure 20) and there is a smooth cross-over from the epoxy that encapsulates and anchors the membrane into the element surrounds. It is extremely simple to load the mould and cast the element. The core of the element is currently machined from plastic material, which is costly, but a machine drawing for a mould to cast the core from an inexpensive resin such as polyester has been prepared.

Figure 21: Flat A4 membrane panel after operation on a bentonite feed solution for a number of hours.

As can be seen from Figure 21, membrane discolouration, indicative of bentonite fouling, is completely even across the face of the panel. It would appear that the problem of localized fouling, experienced with previous module design attempts has been solved. The black edge around the element is the epoxy used to encapsulate the fabric edges and seal the membrane in place. The filter is robust and scale-up to larger sizes does not pose a problem at all. The moulding technique and mould developed will equally suite larger-sized filter elements. Fabrication of the filter panel is extremely simple and does not require complex machinery.

The new flat-sheet module design seems to meet all the criteria stated in Section 3.1. Accordingly this new design was used in all further work done in the project.

It should be noted that the approach developed to fabricate flat membrane panels is generic and any type of flat membrane may be used. In other words, it would be possible to use exactly the same panel configured with either woven membranes of different weave and web and compare their performance and attributes to those of conventional phase inversion ultra- and microfiltration membranes.

4 DESIGN GUIDELINES FOR IMMERSED MEMBRANE BIOREACTORS

4.1 Introduction

The critical operational feature of IMBRs is that coarse bubble aeration induces scouring of the membrane surface, controlling the fouling of the membranes, and also induces a gross circulation of the bioreactor contents around the membranes. Both are essential to ensure stable operation of the IMBR. In terms of hydrodynamic designing of IMBRs, therefore, the following criteria must be met:

(iii) there should be stable circulation of the biomass around the membranes

(iv) the hydrodynamics of the flow across the membranes should ensure stable scouring of the entire membrane surface

The geometric parameters of an IMBR that are expected to affect the hydrodynamics include the reactor vessel, the membrane module, the membrane pack, and the air sparger. The main operating parameter that influences the hydrodynamics is the air flowrate.

In Section 3, a design for the membrane module was presented. In this section, the effects of the above parameters on system hydrodynamics are investigated. From this, and based on a factorial experimental design, guidelines for IMBR geometries are developed.

At the initiation of the project, it was expected that one of the project outcomes would be a *hybrid* MBR (HIMBR), which would include silicone tube aerators that would also act as scourers of the membrane surface. It emerged that this was not feasible, and this is discussed in Section 4.2.

The Design of IMBRs forms the topic of an MSc study undertaken by M Hamman at the University of Stellenbosch, and which is in the process of being written up. Various excerpts from the draft thesis are included in this report.

4.2 Feasibility of the proposed HIMBR concept

4.2.1 The concept

In the proposed HIMBR, vertical plate-and-frame flat-sheet (ultrafiltration/microfiltration) cartridges (or horizontally mounted narrow-bore skinless capillary membranes) will provide for bioreactor dewatering (similar to conventional MBRs). These filter cartridges will be aerated with air from below to provide oxygen to the bioreactor and scour the flat-sheet membranes to facilitate cleaning, consistent with current commercial IMBRs.

However, completely different from current commercial IMBR systems, it was proposed that an array of narrow-bore silicone rubber membranes will be installed in-between the flat-sheet plates, in a transverse orientation to the stream of rising air. These silicone rubber membranes tubes would serve the following functions:

(i) act as a surface for biofilm attachment and development. It was expected that different microbial populations will exist in the floc contained in the bulk of the bioreactor and in the biofilm that develops on the silicone rubber membranes. This greater diversity in microbial population would lead to better breakdown efficiencies of the hybrid reactor compared to that of the conventional MBRs.

(ii) provide a means for pure oxygen transport to the biofilm by diffusion. This is of specific interest when the bioreactor is operated in the thermophilic temperature range, where the equilibrium solubility concentration of oxygen is reduced.

(iii) facilitate the cleaning of flat-sheet modules. Back-flushing with permeate was shown to be effective to control fouling of capillary membranes, however flat-sheet membranes cannot be back-flushed. This is where the secondary function of the silicon rubber membranes in the HIMBR comes into play. The silicon rubber membranes will be positioned such that the rising aeration air will agitate them in a random fashion and cause them to touch both each other as well as the flat-sheet membrane cartridges. In the HIMBR therefore, the respective thickness of the fouling layer on the dewatering membranes and the biofilm on the silicone rubber tubes will be controlled by both the scouring action of the rising aeration air and the mechanical rubbing action caused by the silicone rubber membranes.

4.2.2 The Reality

After the initiation of this project, it soon became that the HIMBR concept would not be feasible at this stage for, *inter alia*, the following reasons:

(i) cost – it emerged that silicone rubber membranes were extremely expensive, primarily because they are marketed for specialist applications in the microbiology and medical fields. Whilst their incorporation into an IMBR would effect operational advantages, the cost of the HIMBR system would be substantially greater than "conventional" IMBRs, and hence the HIMBR would be unlikely to enjoy a market

(ii) fouling – recent studies on immersed hollow-fibre bundles employed in IMBRs indicate that these systems could be particularly prone to fouling (see Section 3.3.2). These problems are expected to be worse in the proposed silicone rubber membranes, since they would be transverse to the direction of the flow of the biomass. Whilst the central portions of the silicone membranes would sway about under the action of the coarse bubble aeration, the potted ends would be relatively stationary. This would undoubtedly result in the accumulation of foulants at the potted ends. Further, if any fibrous material entered the HIMBR, the fibres would bind the silicone membrane together, effectively stopping the sweeping motion of these membranes, and providing further dead zones for the accumulation of foulants.

In view of the above, the Steering Committee decided that the HIMBR concept should be shelved, and that the project should focus on the development of a "conventional" IMBR.

Prior to the above decision, a study was undertaken into the effects of geometry and operating variables on the mass transfer of oxygen from silicone rubber membranes. This was written up as an MTech thesis [Mbulawa (2005)].

4.3 Investigations into effects of air flowrate and system geometry on hydrodynamics and fouling

Coarse-bubble aeration is typically employed to induce shear across immersed membranes to remove retained material. In the case of MBRs, this aeration can amount to more than 90% of the operating costs [Gander, *et al.* (2000)]. The cross-flow velocity achieved with aeration in an immersed membrane system is usually much lower than the velocities achievable when fluid is pumped across externally placed membranes. An immersed membrane system is consequently, in an attempt to avoid excessive fouling, limited to low permeate fluxes and requires a larger total membrane area with a resulting higher capital expenditure. The critical flux for a given system therefore dictates the threshold flux value above which the system should rather not be operated to maintain steady flux performance.

Increasing the air-flow rate increases the ability of the air to scour the immersed membrane surfaces when operated at constant flux [Bouhabila *et al.* (2001)], but Ueda *et al.* (1997) found that for a given system a critical value exists above which further increase in the air-flow rate had no effect on the scouring efficiency. Without increasing the air-flow rate, however, they found that when aeration was intensified from fewer diffusers and the membranes rearranged, the scouring efficiency was increased. Shim *et al.* (2002) studied immersed MBRs with airlift geometries where the membranes were located in the riser section of the reactor. They reported that the membranes in those reactors with the highest downcomer area (A_d) to riser area (A_r) ratios displayed better filtration stability at the same air-flow rate and permeate flux

(Figure 22). These findings suggest that air-scouring efficiency is dependent on the system hydrodynamics and configuration.

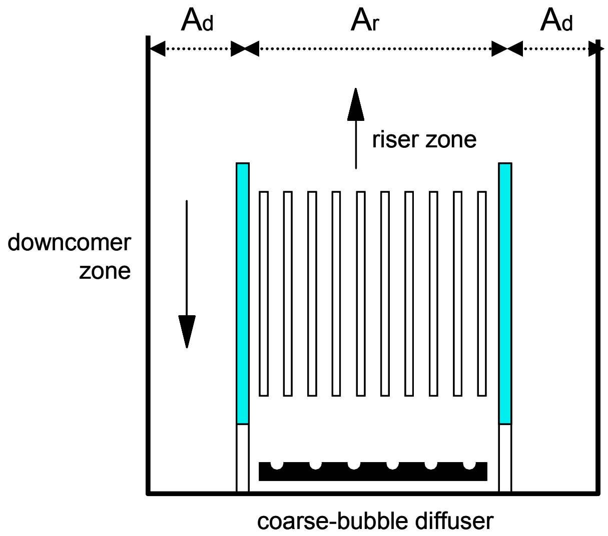

Figure 22: Coarse-bubble aerated membrane bioreactor showing the membrane pack, riser and downcomer zones respectively.

An incentive therefore existed to develop an immersed membrane system with more favourable system hydrodynamics to improve the air-scouring efficiency. Such a system will be able to operate stably at a lower aeration intensity, which is defined as the supplied air-flow rate per cross-sectional area to be aerated, and at a higher critical flux values as was defined and described by Field *et al.* (1995).

The influence of air flowrate on fouling and circulation is investigated in Section 4.3.1, and the effect of geometric parameters on fouling is investigated in Section 4.3.2.

4.3.1 Effect of Air Flowrate

4.3.1.1 Experimental set-up

The experimental set-up is shown in Figure 23. A peristaltic pump with variable speed connected to a submerged woven fabric flat-sheet membrane, produced the necessary constant permeate flux. The total active surface area of the membrane was 0,12 m^2. The TMP was measured with a water-filled manometer. The cross-flow across the membrane was induced by coarse aerating the tank with air from a compressor, which was measured with an air flow meter and fed to a diffuser at the bottom of the tank.

Ocean bentonite was suspended in a tank filled with 60 L reverse osmosis tap water to give a concentration of 1 g/L. The permeate was pumped back to the tank to operate at a bentonite concentration which was assumed to be constant.

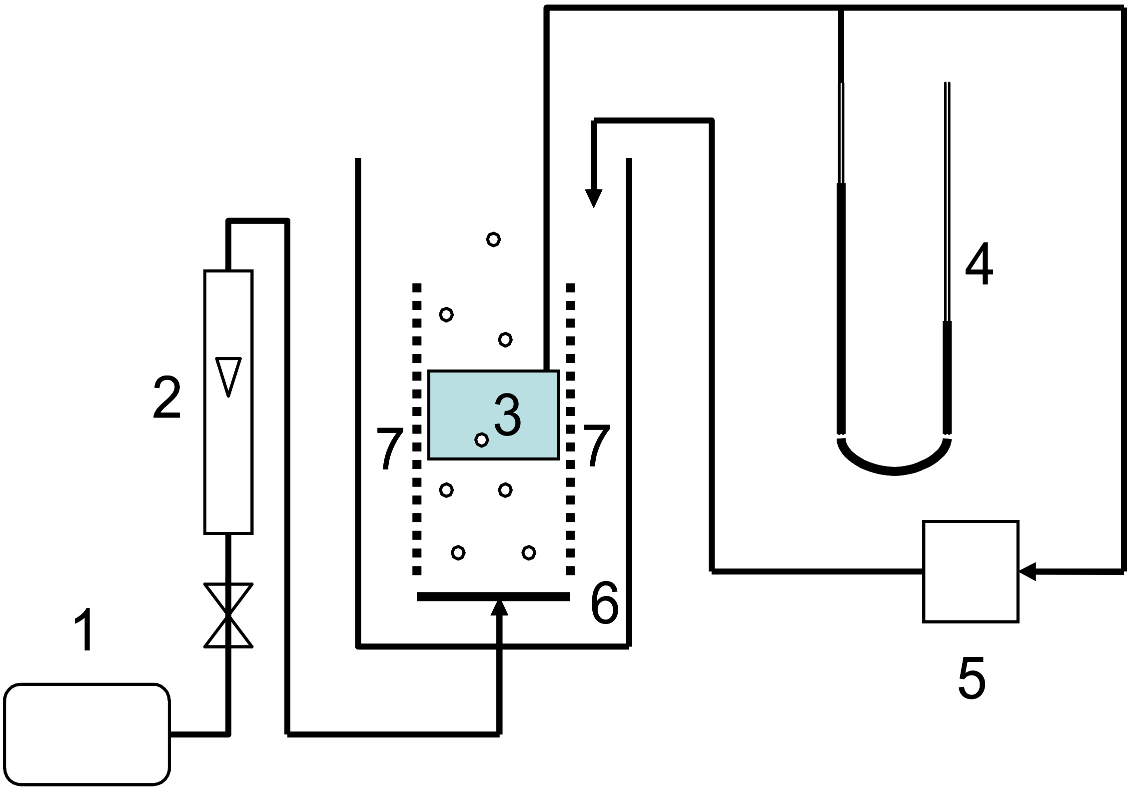

Figure 23: The experimental setup: (1) compressor, (2) air flow meter, (3) membrane, (4) manometer, (5) peristaltic pump, (6) diffuser and (7) baffle.

Adjusting the air flowrate to the tank created different turbulent conditions. For each air flowrate setting used the peristaltic pump was set to deliver consecutive fluxes of 5, 10, 15, 20 and 25 LMH, for 2 h each. The change in TMP with time was read from the manometer and recorded.

4.3.1.2 Results and discussion

It was observed that, for a specific tank geometry, a region of stagnant bubbles would develop above the riser section. When the air flowrate to the tank was increased the region grew towards the bottom of the tank. This phenomenon is depicted in Figure 24.

This is because an increase in air flowrate leads to an increased air hold-up in the riser section and an increased difference in density between the riser and the downcomer sections with a consequent higher recirculation velocity. The resistance for the water to enter the down comer sections also increases to a point where some of the water starts to recirculate towards the bottom in the riser section and force-balances the rising bubbles – therefore the visual effect of stagnant (stationary) bubbles.

When the stagnant region grew downwards and crossed the membrane it was also observed that the most fouling seemed to occur where the membrane crossed the stagnant region as shown in Figure 24. The stagnant region, therefore, is unable to remove particles from the membrane, and will rather deposit matter.

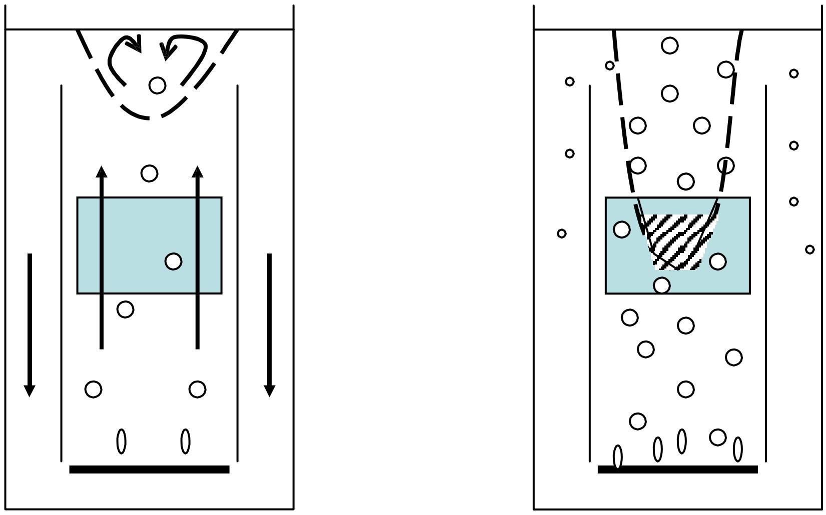

(low air rate) (high air rate)

Figure 24:- System hydrodynamics at low and high air sparging rates

The fouling, as manifested in the increase in TMP with time, for each flux at a specific air flowrate was found to be a linear function. In Figure 25 these fouling rates for each flux for a specific system geometry were plotted against the supplied air flow for scouring.

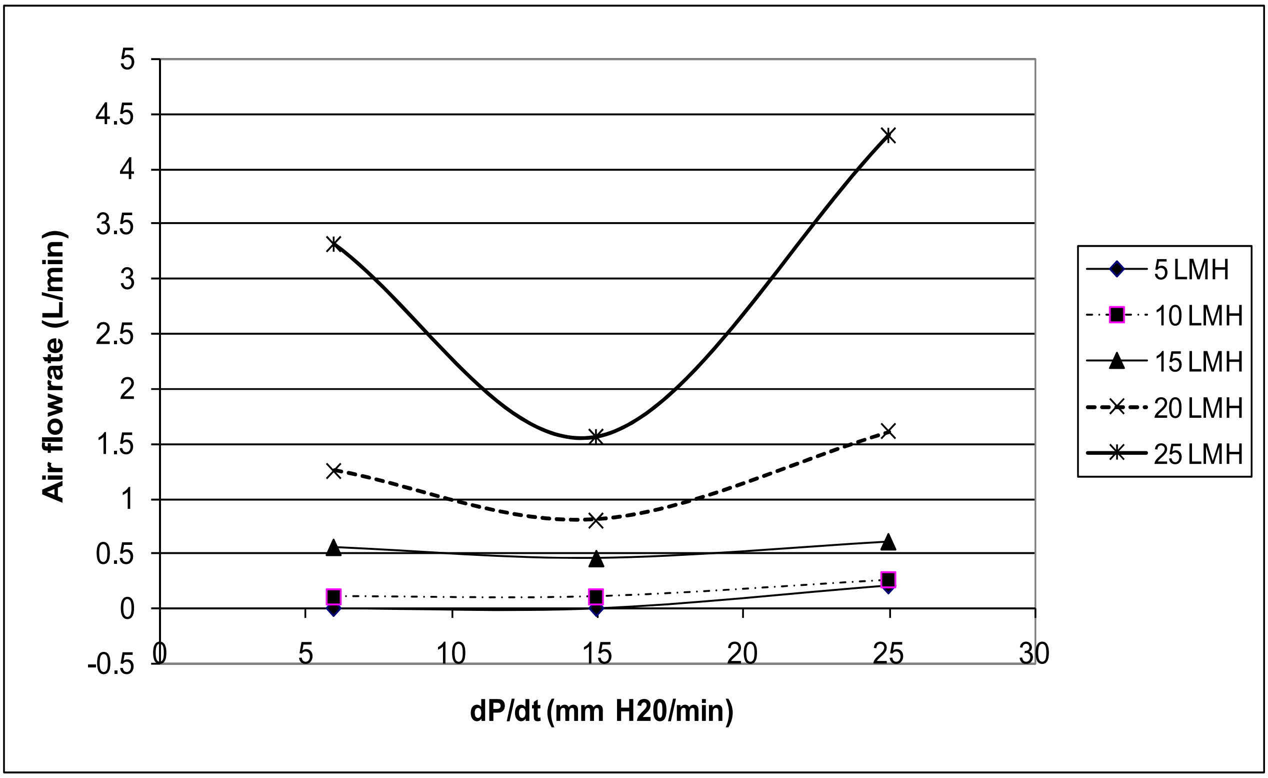

Figure 25: Fouling rates at different air flow rates

From Figure 25 it is evident that, for a given air flow rate, an increase in flux results in an increase in TMP. Also, the increment step in the fouling rate continues to increase with an increase in flux for any given air flow, in other words $d^2(TMP)/dt^2 > 0$.

It can be seen that an increase in the air flow rate from 6 L/min to 15 L/min increased the scouring effect and reduced the fouling rate. Sub-critical flux operation would mean that the effective fouling rate in terms of TMP increase with time must be zero. It seems as if a flux of 5 LMH is below the critical flux at airflows up to approximately 15 L/min.

However, when the air flow rate was increased from 15 to 25 L/min, the fouling rate for each flux increased, even the former sub-critical flux of 5 LMH. These drastic changes can be attributed to the crossing of the stagnant region with the membrane and the increased deposition of clay.

4.3.2 Effect of Area Ratio (A_d/A_r)

In this study, fouling behaviour was investigated for different internal-loop airlift reactor configurations. Unlike the case where Shim *et al*. (2002) studied various A_d/A_r ratios at the same airflow rate, different A_d/A_r ratios were investigated at the same aeration intensity, as well as at the same permeate flux. The investigation used a model particulate suspension (bentonite) for the sake of simplicity and reproducibility. An in situ ultrasonic technique was employed to observe and quantify the fouling as a function of time and location on the flat-sheet membranes in the different configurations studied.

4.3.2.1 Experimental Setup

The experimental set-up used is shown schematically in Figure 26 and a photograph of the reactor is shown in Figure 27.

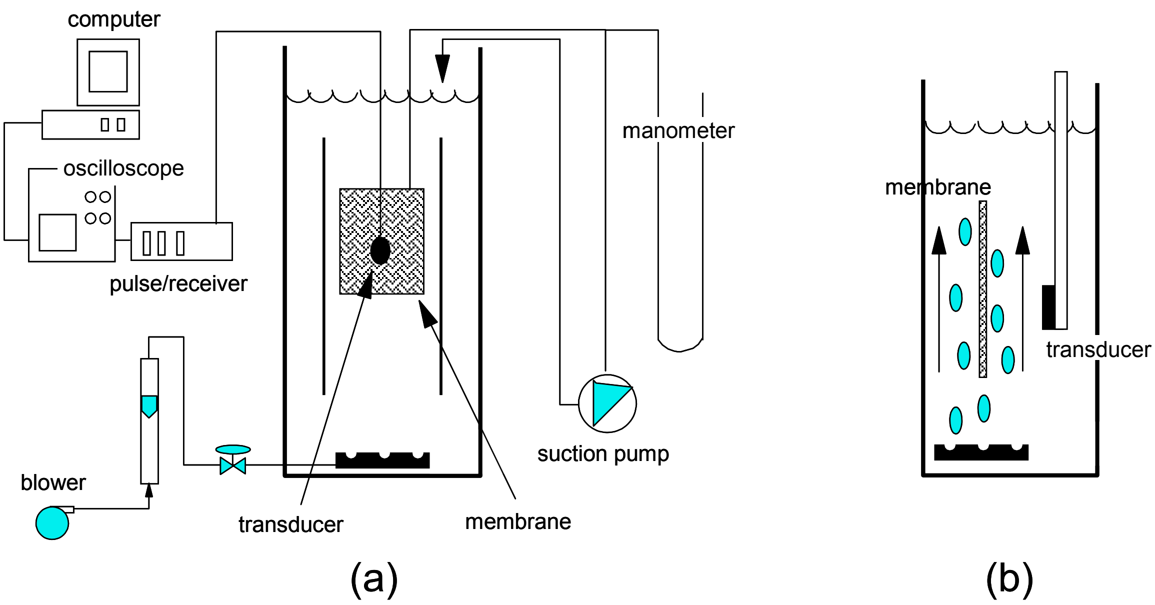

Figure 26: (a) Experimental set-up,
(b) Side-view of the riser zone of the airlift reactor.

Flat-sheet membrane elements were constructed from a fabric that is interwoven in a manner to produce longitudinal arrays of filter tubes [Swart *et al.* (1994)]. Stainless steel meshes were inserted in the individual filter tubes to act as a spacer. The combination of the fabric and stainless steel spacer material provided a rigid and durable membrane envelope. The membranes can be back-flushed under low-pressure head.

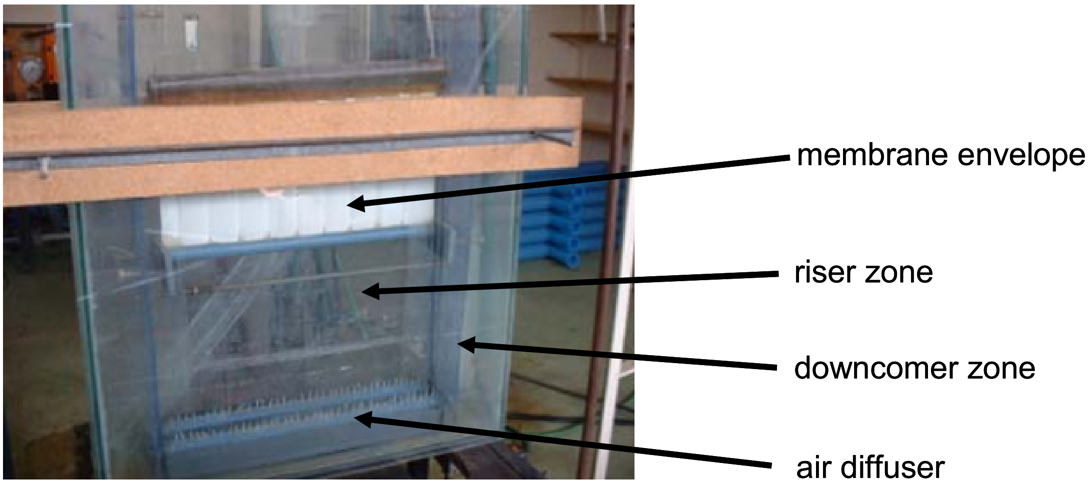

Figure 27: Photograph of reactor vessel with membrane envelope mounted in the riser section of the reactor.

4.3.2.2 Woven material membrane and reactor configuration

The membrane envelopes (Figure 28) used in these experiments had the same overall dimensions, but differed in widths, which were 156 mm, 235 mm and 350 mm, to produce total active filtration areas of 0,056 m^2 , 0,085 m^2 and 0,12 m^2 respectively. The membrane envelopes were tightly secured inside an adjustable framework, which divided the rectangular tank into a riser and downcomer section with A_d/A_r ratios of 1,45 , 0,71 and 0,31 for the 0,056 m^2 , 0,085 m^2 and 0,12 m^2 membranes respectively. The membranes were located in the riser zone of the reactor basin (Figure 26a). For each configuration a double-pipe diffuser, with 0,6 mm holes, was located at the bottom of the tank and stretched the width of the respective riser.

Figure 28: Smaller version of membrane envelopes used for studying flow profiles in aerated reactors and fouling profiles.

4.3.2.3 Ultrasonic instrumentation set-up

Increased membrane resistance and calculation of cake deposition according to the cake filtration model normally quantify fouling of ultrafiltration and microfiltration membranes. This, together with differential pressure increases and/or flux decline can be plotted against a time scale and some information gained with respect to membrane behaviour operating under a certain set op operating conditions. However, what one measures is the averaged effect of fouling on measured responses and does very little to elucidate whether the fouling is even over a length of a membrane conduit. The latter information is important, especially if one is to experiment and compare spacer materials with each other. One way out of this dilemma would be to make use of a technique that could distinguish between areas of low fouling deposition and higher fouling deposition or concentration polarisation. A technique studied under WRC research project K5/1166 ultrasonic time-domain reflectometry (UTDR), offered a possible solution to quantify uneven deposition/fouling and assist in improving the hydrodynamics of the filtration pack.

A 7,5 MHz ultrasonic transducer (Panametrics V120) was attached to a pole and hung inside the tank (Figure 26a), so that the fouling medium was the only barrier between the transducer and the membrane surface. The transducer and the membrane were tightly secured to remain immovable during aeration. This enabled the transducer to detect the fouling process accurately with UTDR as explained by Mairal *et al.* (1999).

The distance between the transducer and the membrane was varied between 20 mm and 30 mm so as not to disturb the fluid-flow behaviour near the membrane surface. The transducer was connected to a pulser-receiver (Panametrics 5058PR), and an oscilloscope (HP 54602B) was used to observe the reflected waveform. The waveform data was captured as 2000 time-amplitude value pairs on a computer for further data processing.

4.3.2.4 Experimental procedure

A simple backwash procedure, prior to a filtration experiment, proved to be adequate to restore the original hydraulic resistance of the membrane, therefore removing all particles within and on the membrane surface. The tank was filled with reverse osmosis (RO) tap water and permeate was drawn off at the desired flux with a peristaltic pump. Once the membrane was compressed, the transmembrane pressure (TMP), as measured by the water-filled manometer, was stable, indicating the membrane hydraulic resistance. The received waveform was saved on the computer hard drive as the reference signal to which the signal of the fouled membrane would be compared. When the permeation was stopped, the membrane would slowly relax to a fraction of its original volume before permeation, but on re-commencement of permeation the membrane would quickly assume the stable compressed form. With the permeation stopped, the fouling agent, a suspension of bentonite (Ocean Bentonite, G&W Base & Industrial Minerals, South Africa) in RO water, was then added to the tank to create a particulate suspension of 1 g/L bentonite. The bentonite particles in suspension were measured (Malvern Mastersizer) to have an average particle size of 19 µm.

Permeation was maintained at 15 ± 0,4 LMH for all experiments, while air was supplied to the specific geometry to produce an aeration intensity of 1 130 ± 20 L/m^2 .min. When sampling the reflected ultrasonic signal from the membrane surface, the aeration was momentarily stopped (less than 10 s), while permeation was allowed to continue. Without the interference of the bubbles the transducer was able to receive a clear reflected ultrasonic signal.

If permeation were stopped during the sampling process the membrane would relax, creating an uneven surface with increased scattering of the reflected signal, thereby complicating data interpretation. It was assumed that the increased fouling in the brief absence of aeration was negligible. Sampling was done in successive experiments on the left, middle and right of the membrane envelope in the respective configurations studied. Sampling was conducted at suspension temperatures of 25 ± 2^{o}C.

4.3.2.5 Results and discussion

Preliminary Visual observations

The general effect of the A_d/A_r ration on fouling can be visually inferred from Figure 29.

(a) (b) (c)

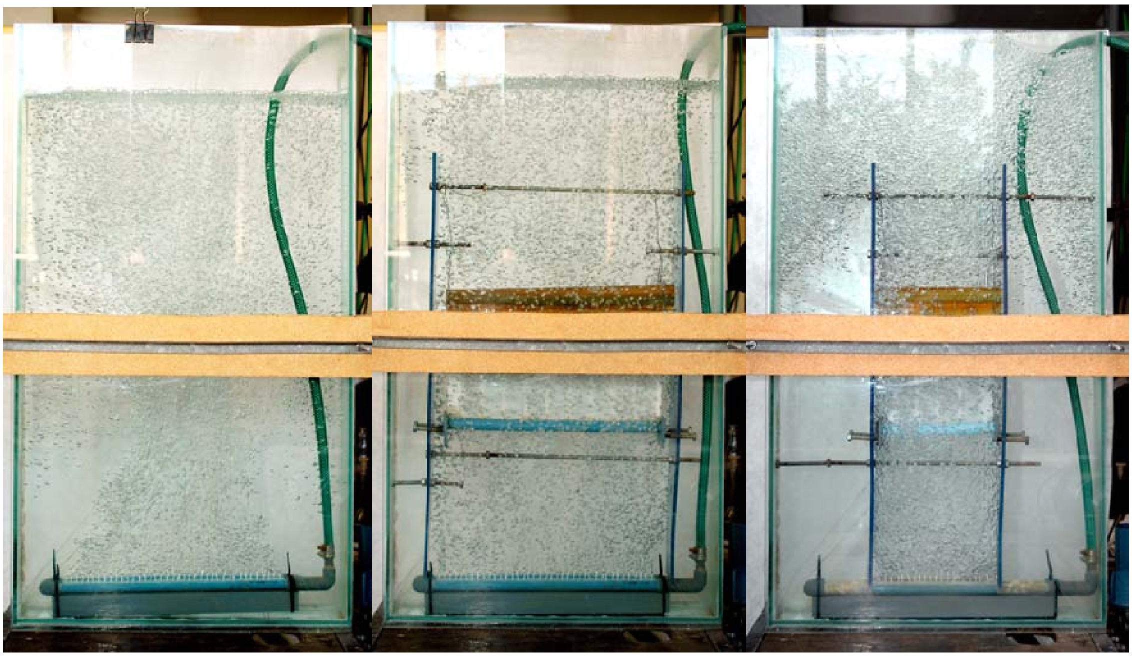

Figure 29:- Photographs of the mini basin in which the first experiments concerning air-flow patterns was conducted. Vessel A had no down-comer section, vessel B had a larger riser to down-comer area ratio and vessel C the riser to down-comer ratio was the smallest.

On examining the flow patterns of the rising bubbles in Figure 29 a, it is easy to realize how it is possible for greater localized fouling to occur, as indicated in Figure 30. It is also easy to infer that the positioning of the membrane within such a reactor is important, and that the positioning of the air sparger relative to the membrane and inlet to the riser section is also of relevance.

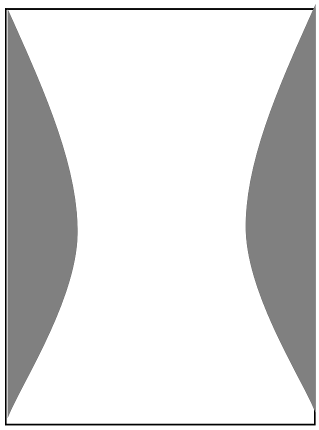

Figure 30: Typical fouling pattern on membrane. Grey area shows increased deposit of bentonite on the white surface of the membrane.

Reflected waveform

Wave energy sent from the transducer is reflected back to the transducer on the principle of difference in acoustic impedance. Acoustic impedance is a function of the medium's density and the velocity of sound in the particular medium. Therefore, when a propagated wave encounters a medium of different density, some of the energy is reflected. The larger the difference in the acoustic impedance of two media, the higher the proportions of reflected energy at the media interface. This phenomenon enables UTDR to measure distances and to differentiate between media along the propagation direction in a composite system non- invasively. The application of UTDR for fouling layer thickness measurement is explained in Figure 31.

The ultrasonic waves propagate from the transducer and through the suspension to meet the clean membrane (Figure 31a). The water/membrane interface (A) is the first difference in media density that the waves meet. A fraction of the transmitted energy is reflected from the interface and received by the transducer. This is converted to a signal by the pulser/receiver and displayed as peak A of a waveform on the oscilloscope. The remainder of the energy continues to propagate through the membrane to meet the membrane-water interface, B, where again a certain fraction of the energy of incidence is reflected to produce peak B of the displayed waveform. In this case, the difference in amplitude value between peaks A and B is ascribed to the difference in the available incidence energy at each interface. Given that the speed of sound through the membrane is known, the measured arrival time difference between peaks A and B can be translated into a distance between interfaces A and B. The membrane thickness can be determined from the relationship:

$$\Delta S = \frac{1}{2} c \, \Delta t \qquad (1)$$

where ΔS is the determined thickness, c is the speed of sound in the medium and Δt is the measured difference in arrival time.

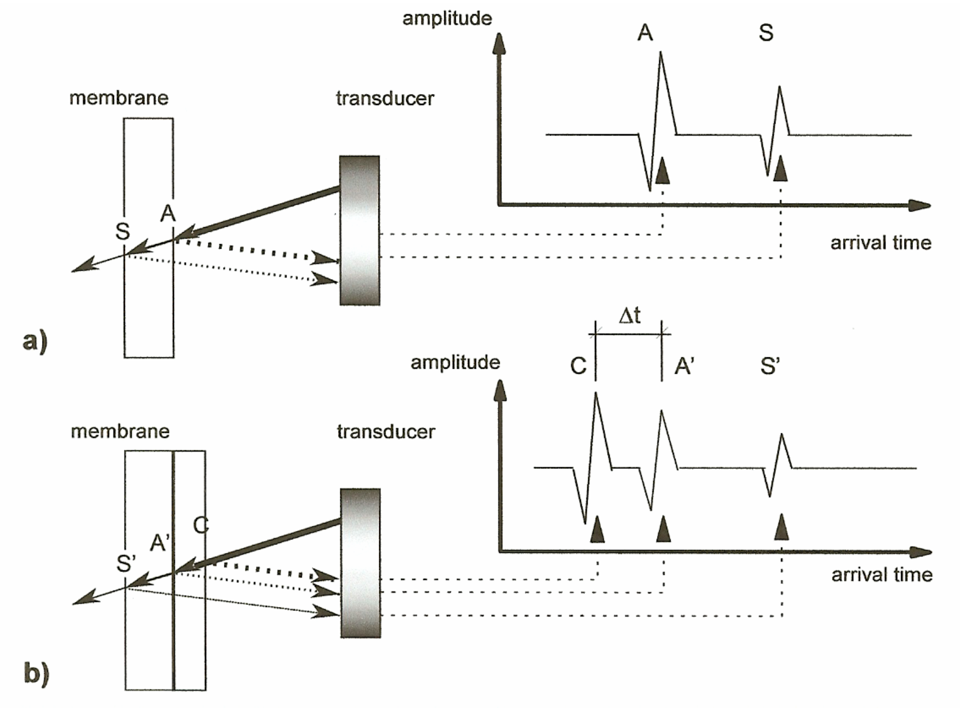

Figure 31:- (a) UTDR for clean membrane and (b) UTDR for a membrane with a fouling layer.

Consider Figure 31b, showing the same membrane as in Figure 31a, but after some filtration time to have acquired a fouling layer on the membrane surface. Comparing the displayed waveforms of Figure 31a and Figure 31b, it can be seen that the presence of the fouling layer has resulted in the appearance of a new peak, C, in the waveform. By using Eqn.1 the arrival time difference between peaks C and A' can be used to determine the thickness of the fouling layer. The consequent growth in the fouling layer will manifest in the movement of peak C to an earlier arrival time. However, the time-domain positions of peaks A and B in Figure 31 will not change, but their relative amplitude values will have decreased with the decrease in incidence energy at interfaces A' and B', as more energy is reflected from the fouling layer. A larger proportion of incidence energy will be reflected from the fouling layer if its density increases through compression and entrapment of smaller particles.

Although Figure 31 presents hypothetical waveforms, it serves as explanation for the basic concepts of UTDR. In this study the fouling layer was not found to be a clearly defined layer on the membrane surface with a uniform density, but a transition from concentration polarisation to an external cake layer to internal fouling. A differential waveform, which is the difference between the test waveform and the initial reference waveform, was therefore employed to highlight any density changes [Sanderson *et al.* (2002)]. These density changes were ascribed to the presence of different fouling mechanisms. In Figure 32 real and typical waveforms obtained during the study are shown.

Figure 32 shows a reflected waveform from a clean membrane at the start of filtration. Peak B represents the membrane surface. This waveform is saved on the computer's hard drive as the reference or base waveform as a fingerprint of the unfouled membrane. When permeation starts, small particles are drawn into the relatively open weave of the membrane matrix where they adsorb onto the material and plug the pores (passages between the individual fibres and weave). The membrane quickly densifies with resulting higher acoustic impedance and increased reflection of wave energy. This is depicted in the sudden increase in height of peaks A and B to form peaks A' and B' 1 minute after start-up (Figure 32b). At this stage the differential waveform distinguishes a difference in density and the onset of concentration polarisation.

After the initial internal fouling, another fouling mode starts to dominate, namely external or surface fouling, where particles are deposited onto the membrane surface to form a cake layer. This cake layer shelters the membrane from the transducer, causing a decrease in the peaks B' and A' as the effective reflected energy from the membrane is reduced, as is shown in Figure 32c, sampled 25 minutes after start-up. The existence of polarised particles, a cake layer and internal fouling complicated the fouling interpretation of the experiment waveform, but with the use of the differential waveform the state of fouling inside and on the membrane surface (Figure 32c) was known. The time-domain shift of peak C'' from the membrane surface at peak C' indicates that deposition has occurred. A'' indicates the time-domain position of the concentration boundary layer (concentration polarisation) where the accumulation of material is responsible for energy reflection.

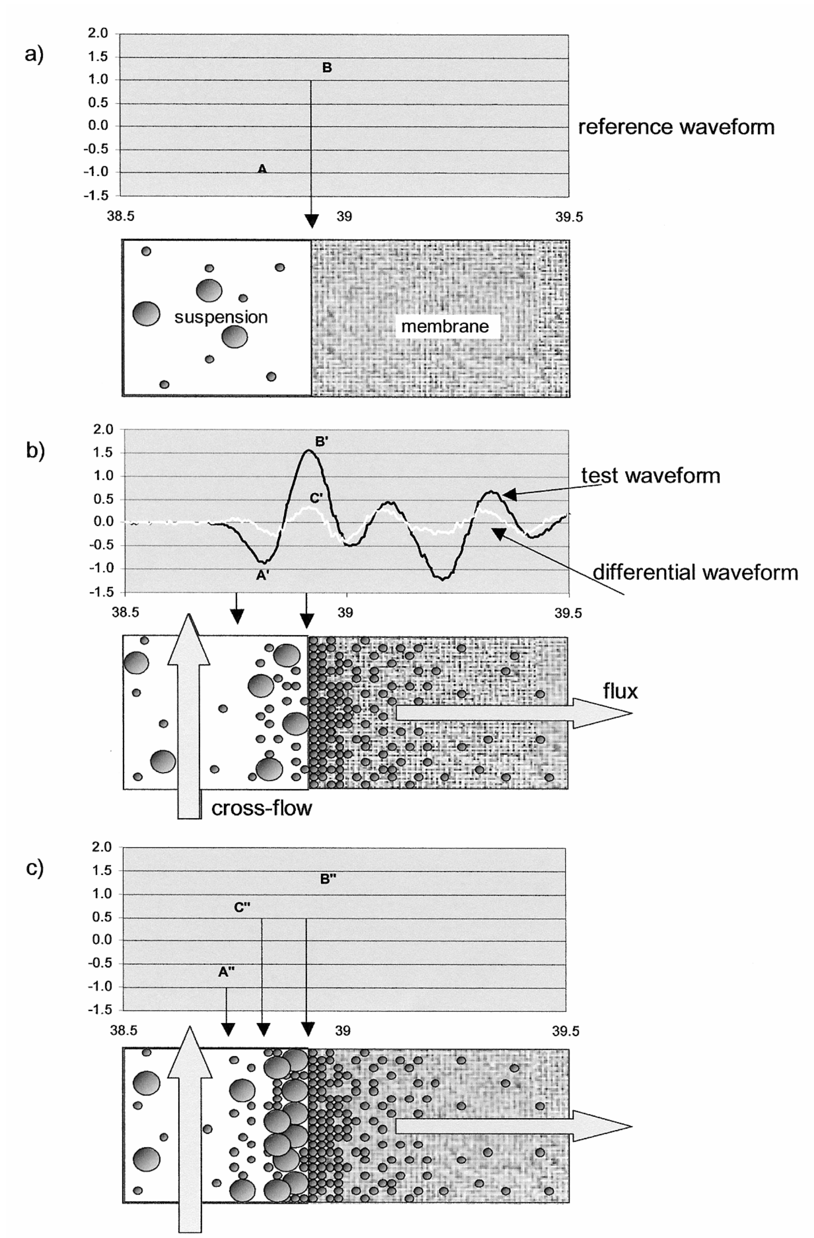

Figure 32: Hypothesis for surface and subsurface fouling as interpreted from UTDR data.

Fouling

In the reactor configuration with an A_d/A_r ratio of 0,31, it was observed that very high riser cross-flow velocities occurred on the sides, just next to the dividing frame, compared to the very slow, almost stagnant, cross-flow that occurred in the remaining middle of the riser. As the A_d/A_r ratio was increased, the variance in the cross-flow velocity seemed to decrease. Assuming that the density of the cake layer is approximately 2 g/cm^3, the velocity of sound in the cake layer was measured to be 2 800 m/s. After 20 h of operation the fouling layers in the mid-section of the membrane envelope had arrival time differences of 90 ns, 105 ns and 130 ns for the airlift reactor configurations with A_d/A_r ratios of 1,45, 0,71 and 0,31 respectively. By using (Eqn. 1) these arrival times equate to fouling layer thicknesses of 0,126 mm, 0,147 mm and 0,182 mm respectively. Figure 33 shows the calculated fouling layer thickness after 20 h of operation at the various relative distances for the configurations investigated. The thicker fouling layer on the right side of the large membrane can be ascribed to the positioning of the manifold outlet on the right side of the membrane envelope with a significant pressure loss from right to left to produce higher local trans-membrane pressure values on the right-hand side than, for example, the left-hand side.

By comparing the evolution of the relative height of peak B in each experiment, it was found that for a low A_d/A_r ratio such as 0,31, deposition mainly occurred in the middle of the membrane with pore plugging mainly on the sides. For the higher A_d/A_r ratios the fouling behaviour was more uniform across the whole membrane.

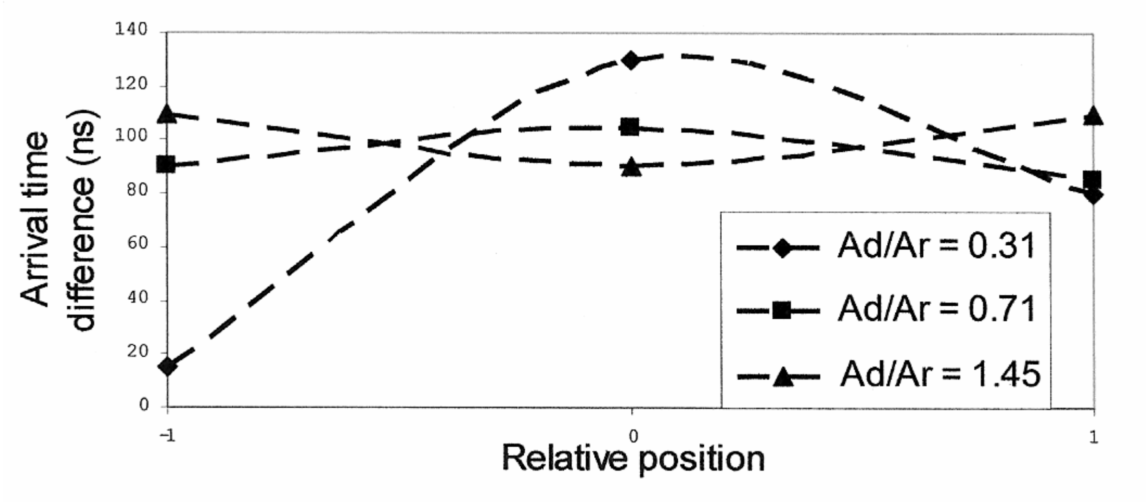

Figure 33: Arrival time differences at the relative positions after 20 hours of operation.

4.3.3 Summary

System hydrodynamics influence the fouling behaviour in IMBR systems. By increasing the air flowrate to the diffuser, turbulence near the membrane surface is promoted and more retained material can be transported back from the membrane surface. Increased air flowrate is therefore expected to increase the critical flux for a given membrane system.

However, increasing the air flowrate for membrane scouring may not always reduce fouling. The system geometry may distort the usual fluid flow pattern observed at lower airflows to produce a fluid flow pattern with zones of relative low turbulence. Particle deposition may occur if the membrane or parts of the membrane are situated within these zones. Therefore a local minimum air flowrate may exist for a given system to achieve the optimum scouring of the membranes.

The back-transport of retained particles at the membrane surface is a function of particle size. The findings with the UTDR technique are in agreement with the deposition theories, where the larger particles are swept away from the membrane surface at higher cross- flow velocities, leaving the smaller particles to penetrate into the membrane. This was observed on the sides of the membrane envelope, especially for the configuration with an A_d/A_r ratio of 0,31, with very rapid local fluid flow. In the stagnant zones, however, larger particles were also deposited on the membrane surface to form a cake layer. The UTDR technique employed is therefore able to distinguish, in real-time and non-invasively, between internal (inter fibre and weave) and external (surface) fouling.

Ignoring secondary effects, there is an overall decrease in fouling layer thickness with an increase in the A_d/A_r ratio. This is a result of the higher fluid-rising velocities that are generated in the riser zone for higher A_d/A_r ratios. Internal-loop airlift reactors with high A_d/A_r ratios therefore seem to produce favourable system hydrodynamics for immersed membrane systems by increasing the air-scouring efficiency for reduced fouling.

In overview, typically three hydrodynamic flow patterns may be obtained, depending on the combination of air flowrate and reactor geometry. These are summarized in Figure 34.

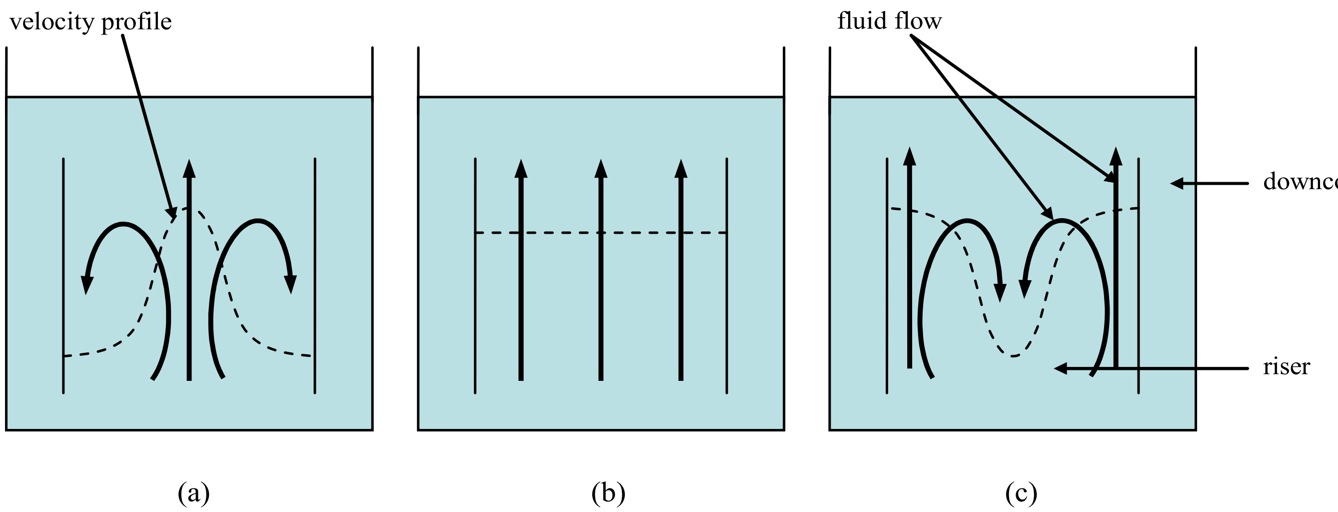

Figure 34:- Typical hydrodynamic field patterns that were observed in the riser section of an airlift reactor: (a) fast rising bubbles in the middle with stagnant bubbles, and consequent severe fouling, on the sides; (b) uniformly fast rising bubbles with overall low fouling; and (c) fast rising bubbles on the sides with stagnant bubbles, and consequent severe fouling, in the middle.

4.4 Development of Design guidelines for IMBRs

4.4.1 Approach

The investigations reported in the previous sections showed that the fouling in aerated immersed filtration systems is a complex function of geometry and operating variables. This section concerns the development of design guidelines for an IMBR.

Information on features of immersed flat-sheet membrane reactor design is sparse in the open literature. However, by considering the design and hydrodynamics of an airlift reactor [Majeed and Bekassy-Molnar, (1995)], it was possible to identify certain design factors that should have an effect on the hydrodynamic behavior inside an aerated MBR system. Those factors were translated into a proposed MBR membrane stack configuration and are shown in Figure 35.

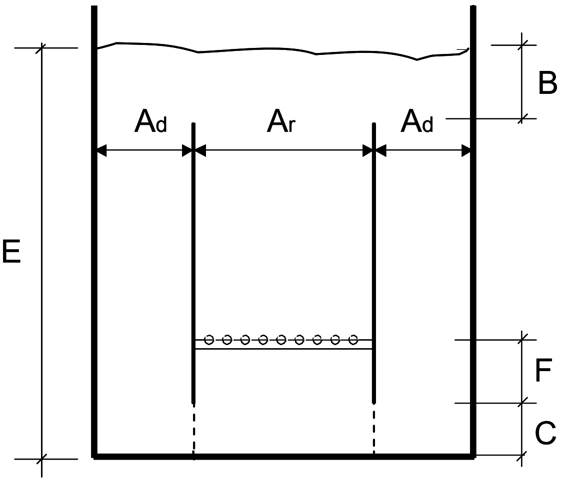

Figure 35:- Schematic of a membrane bioreactor, showing the membrane stack in the centre of the vessel.

With reference to Figure 34, the more important parameters of the membrane stack are:

A_d	area of the down-comer section
A_r	area of the riser section
B	clearance height between the top of the membrane stack and the liquor level
C	bottom entry clearance for fluid recirculation
F	position of the air sparger relative to the top of the bottom entry clearance (liquor level)
E	total liquor head in reactor vessel

The rate of aeration is also of importance, and particularly the size and size distribution of the bubbles that are released by the air sparger. The size of the bubbles is important because one would like to reduce the slip between the air slugs and the water. The volumetric density (concentration of bubbles in the liquid) of the air bubbles is also of significance because bubbles will coalesce, forming larger air slugs, which result in increased slip between the bubble and the water. Furthermore, high air flowrates causes excessive acceleration losses accompanied by large air fractions collecting at the top of the membrane stack. Large air flow rates were therefore found to give greatly reduced water circulation.

Overall, it is a matter of optimization to arrive at some initial design for the membrane stack. It is important that the effect of geometric factors and air flowrate on the scouring ability should not be investigated in isolation, since very numerous and significant interactions seem to exist, but rather simultaneously with the help of a factorial design experiment. It would consequently be possible to design and operate an airlift reactor with ideal system hydrodynamics for efficient air supply and improved scouring ability if the effects of these studied factors were known.

The approach taken in this work was to make use of a single membrane panel, arranged within a structure inside the glass reactor in such a way as to simplify altering the variables depicted in Figure 35. A two-level factorial experimental design was conducted to assist in establishing the coefficients of the main factors and interactions that need to be considered in the design of the first prototype membrane stack.

4.4.2 Factorial Experiments

4.4.2.1 Approach

The 6 factors shown in Figure 35 (above) were investigated in the factorial design experiment to establish their effects on the system hydrodynamics in an airlift reactor set-up. No membrane filtration or fouling tests were performed in this experiment; only the hydrodynamic behaviour was studied to be optimised in later work for improved air scouring of immersed membranes. The sparged air flow to the riser section was studied in the form of aeration intensity; a factor which could be set to the same value for any cross-sectional riser area.

4.4.2.2 Equipment

A PVC tank was used for this experiment with inside dimensions of 1558 x 1600 x 60 mm. The tank was made from grey PVC sheets, but half of the one side contained a clear PVC sheet to enable visual observation of the hydrodynamic behaviour inside the tank. The use of the clear PVC sheet was restricted to only half of the one side, since the clear PVC sheet had a thickness of 6 mm compared to the grey PVC sheet thickness of 10 mm that consequently limited the ability of the clear PVC sheet to withstand water pressure. PVC sheet baffle plates were slotted inside the tank to divide it into riser and downcomer sections. The baffle plates were connected with steel rods for stability as well as to allow for the baffle plates to be shifted to create any required ratio of the downcomer to riser cross-sectional area. Additional PVC sheets could also be fitted on top of these baffle plates, when required, to change the top clearance distance. The baffle plates rested on steel rod feet, which could also be adjusted, when required, to change the bottom clearance distance. A blower supplied air, which was measured with a flow meter, to an air sparger at the bottom of the tank. The air sparger was a 15 mm (ID) PVC pipe that stretched from baffle plate to baffle plate; containing a single line of 2 mm holes, spaced 50 mm apart, on the top. The baffle plates could support the air sparger at two positions: 200 mm above the bottom of the baffle plates inside the riser section or at the bottom of the tank at the baffle plates' steel rod feet. Figure 36 shows the PVC tank and the baffle plate framework that was slotted inside the PVC tank.

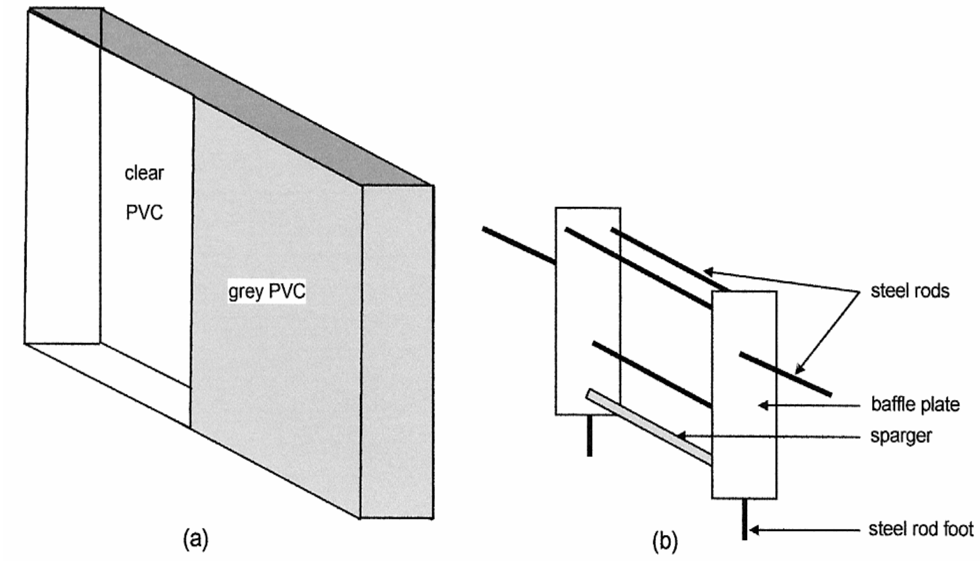

Figure 36: Equipment used in Factorial Experiments : (a) PVC tank with one half of the one side containing a clear PVC sheet and (b) the baffle plate framework which could be changed to create different airlift reactor geometries when slotted inside the PVC tank.

4.4.2.3 Experimental procedure

The key output measure of this factorial design experiment, as was mentioned earlier, was the system hydrodynamics of the airlift reactor, and more specifically, the hydrodynamic behaviour in the riser section. The riser section will house the membranes in an immersed membrane application, because it is here where the sparged air can be utilised to scour the membrane surfaces to reduce fouling. Two aspects of the hydrodynamic behaviour in the riser section must be optimised simultaneously to produce a fluid flow field that will promote scouring efficiency:

- fluid flow velocity
- distribution of the fluid flow velocity profile (uniformity of flow)

The faster the fluid flow velocity, the faster the bubbles will sweep the membrane surfaces to produce increased shear forces for better removal of deposited material from the surfaces. But the fluid flow must be uniform through the riser section, because if a distribution exists in the velocity profile, as is shown in Figure 33, fouling will be concentrated in the regions of low velocity that cross the membrane surfaces. Both these aspects can be assessed by measuring the linear fluid flow velocities across the riser section.

Polypropylene (PP) pieces of approximately 1 cm^3 with a measured density of 0,97 g/cm^3 were added with the tap water in the tank and used as tracers to indicate the fluid flow velocity. With the airlift reactor in operation, the circulation flow would drag the PP pieces down the downcomer sections and again up in the riser section (see Figure 37 (a)). The PP pieces were well distributed below the riser section to rise up across the whole riser section. The times it took the PP pieces to travel the distance from the bottom of the baffle plate to the top of the baffle plate in the riser section were measured and converted to linear velocities. This was an inexpensive velocity measurement technique and could be quickly repeated for any number of trials. Although this may not be an accurate measurement of the linear fluid flow velocities, because of the slight buoyancy of the PP pieces, this technique still produced comparable indications from which the hydrodynamic effects of the factors could be calculated.

The baffle plate frameworks that were slotted in the tank were symmetrical - each time creating the riser section in the middle with the downcomer sections on the sides. As a result, one downcomer and exactly one half of the riser section could be seen through the clear PVC sheet that made up one half of the tank's one side. It was assumed that, since the geometry is symmetrical, the fluid flow pattern in the riser section would also be symmetrical and that it would only be necessary to attain a fluid flow velocity profile of the visible half of the riser section. The bottom of the riser section was divided into quadrants. The calculated linear velocities of the PP pieces were allocated to the specific quadrant where they entered the riser section, as is explained in Figure 37 (a). For each quadrant an average fluid flow velocity was calculated from 10 measurements. Therefore, 40 measurements were required for each experimental run to calculate 4 average fluid flows from which a fluid flow velocity profile could be compiled. From the fluid flow velocity profile, the area under the profile, as well as the average gradient of the profile, were calculated as outputs for the effects on fluid flow velocity and distribution of the fluid flow velocity profile respectively. Figure 36 explains this procedure. For the fluid flow velocity in the riser section to be optimised the area of the integrated velocity profile in the riser section must be maximised, and for the distribution of the fluid flow to be optimised the gradient of the velocity profile in the riser section must be equal to zero.

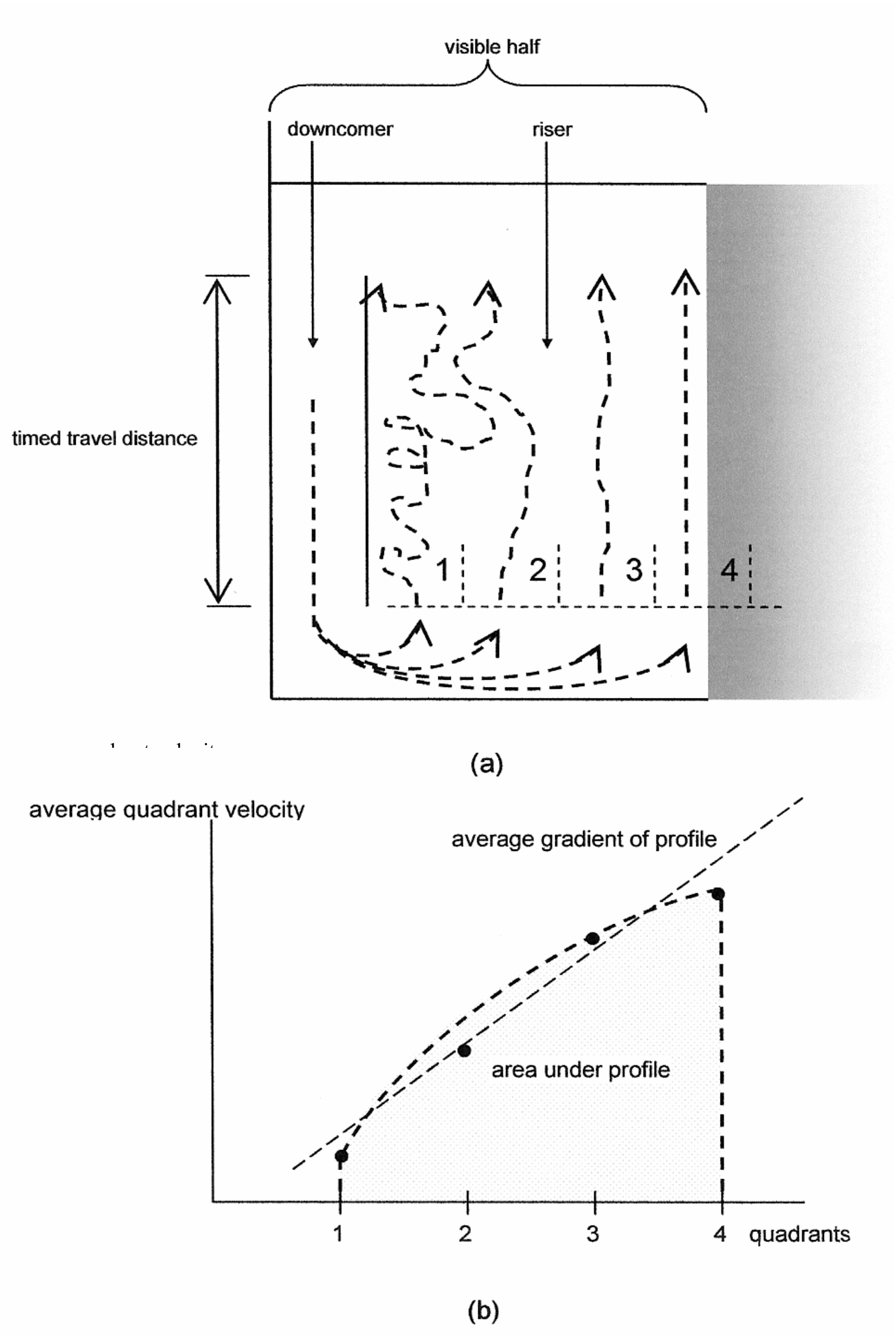

Figure 37: Typical fluid flow velocity profiles :
As observed through the clear PVC sheet, the rising pathways of the PP pieces, and therefore the linear velocities, can be quite different for the different quadrants as shown in (a). The average linear velocity of each quadrant is plotted to attain the fluid flow velocity profile for the experimental run as shown in (b). The calculated area under the profile is an indication of the fluid flow velocity behaviour in the riser, whereas the average gradient of the profile is an indication of the distribution of fluid flow velocities in the riser.

4.4.2.4 Factorial design

The 6 identified factors will most probably exhibit polynomial behaviours, but to reduce the experimental work of the factorial design experiment, the factors were assumed to be linear and that evaluation at 2 levels would provide for adequate estimations of their effects. Table 1 shows the different levels at which each factor were evaluated. The "+1" indicates the high level and the "-1" indicates the low level. The values of these levels were determined by the physical limitations of the experimental set-up, ease of measuring and practicality for continuously changing the baffle plate framework for the various geometrical arrangements. For simplification the 6 factors will be referred to by the symbols A to F as is indicated in Table 2.

Table 2: Values of the levels at which each factor was evaluated.

Factors	**Levels**	
	+ 1	**- 1**
A: A_d/A_r	2	0.5
B: Top clearance distance	200 mm	100 mm
C: Bottom clearance distance	100 mm	30 mm
D: Aeration intensity	1 350 L/m^2.min	800 L/m^2.min
E: Water depth	1 400 mm	1 100 mm
F: Sparger position	Riser section (200 mm above bottom of baffle plates)	Bottom

A full factorial design of these 6 factors would require 64 (26) independent experimental runs, and when replication is included to determine the experimental error, a total amount of 128 (26 + 26) independent experimental runs would be required. A full factorial design would therefore have consumed a lot of experimental time, and it was decided that a screening design, an 8 run Plackett-Burman design with 7 factors, would be utilised. In this case the 7th factor was a so-called dummy factor, since it did not represent any process parameter. Unfortunately, in a screening design the factors' effects could be confounded with each other and is an additional reflection run required to determine the main factor effects. A reflection run is an inverse of a base run where the factors are evaluated at opposite levels as compared to the levels they were evaluated at in the base run. In this case the base and reflection runs would require 16 independent experimental runs, and including replication to determine the experimental error, a total of 32 runs would be required. Since it was expected that numerous two-factor interaction effects existed, a further 16 runs with replication would be performed to determine all the significant interactions. Consequently, this factorial design experiment consisted of 64 independent experimental runs; each run providing a value for the integrated area under the velocity profile and a value for the average gradient of the velocity profile.

The 32 base runs and reflection runs of the Plackett-Burman design, as well as all their replication runs, were first performed randomly and independently to determine the experimental error. The experimental error is an estimation of the inherit variation in the experiment because of the measurement variation, the inability of the experimenter to repeat the conditions and the inability of the process to repeat the same response for the same conditions. For these 32 runs the degrees of freedom were 32, and for evaluating the effects at a 95% significant level, the tabular t-value of 2.04 from statistical tables was used to determine the experimental errors for both the integrated area under the velocity profile and the average gradient of the velocity profile outputs. These same experimental errors were also used to determine the significance of the interactions in the following 32 runs.

4.4.3 Results

4.4.3.1 Area under the velocity profile

Factor A and interaction DF were found to be 99.9% and 95% significant respectively in determining the area under the velocity profile. The model to predict the area under the velocity profile includes the average of all the runs' responses, the determined effects of all the significant factors and interactions, as well as the determined effects of the factors of the significant interactions. The 95% significant model for the prediction of the area under the velocity profile can therefore be written as:

$$Y = \bar{Y} + \frac{E(A)}{2}A + \frac{E(D)}{2}D + \frac{E(F)}{2}F + \frac{E(DF)}{2}DF$$

where Y is the predicted value, $\bar{Y}$ is the average of all the runs' responses and E refers to the determined effect of a factor or interaction. A, D, F and DF, the factors and interaction, are represented at the levels +1 or -1, as shown in Table 1.

When including the average value of all the runs' responses and the effects on the area under the velocity profile, as was determined in this experiment, the model can be written as:

$$Y = 0.6003 + \frac{0.2732}{2}A + \frac{0.0189}{2}D + \frac{-0.0317}{2}F + \frac{0.1710}{2}DF \quad (1)$$

Consequently, if Y has to be maximised for improved fluid flow velocity in the riser section, and considering the +1 and -1 levels of this experiment, A and DF must both be equal to 1. For DF to be equal to 1, the product of D and F must be equal to 1. To counter factor F's negative effect, F must be equal to -1, and consequently D too. Therefore, only considering the chosen levels, as shown in Table 1, the airlift reactor arrangement which would have the highest fluid flow velocity in the riser section would have an Ad/Ar ratio of 2, be operated with an aeration intensity of 800 L/m2.min and have the sparger positioned at the bottom of the tank. The other factors did not seem to affect the fluid flow velocity in the riser section.

4.4.3.2 Average gradient of the velocity profile

Factors C and F, and interactions CF and DF, were found to be 99.9% significant. Interactions AD, BD, BF, CD, DE and EF were found to be 99% significant. As was described in Section 3.1, using the average of all the runs' responses and the determined effects on the average gradient of the velocity profile, the same procedure can be followed to arrive at the 95% significant model for the prediction of the average gradient of the velocity profile:

$$Y = -0.0122 + \frac{0.0136}{2}A + \frac{0.0181}{2}B + \frac{0.0615}{2}C + \frac{-0.0112}{2}D + \frac{0.0226}{2}E +$$

$$\frac{-0.0987}{2}F + \frac{0.0343}{2}AD + \frac{0.0410}{2}BD + \frac{-0.0431}{2}BF + \frac{0.0387}{2}CD + \frac{-0.0817}{2}CF +$$

$$\frac{0.0428}{2}DE + \frac{-0.0813}{2}DF + \frac{-0.0388}{2}EF \quad (2)$$

To optimise the uniformity of the fluid flow in the riser section, the average gradient of the velocity profile needs to be equal to zero. Using the solver function of Microsoft's Excel, and considering the +1 and -1 levels of this experiment, an optimised average gradient of the velocity profile could be achieved by evaluating the factors at the following levels:

A → +1

B → +1

C → -1

D → -1

E → -1

F → +1

Therefore, only considering the chosen levels, as shown in Table 2, the airlift reactor arrangement which would have the most uniform fluid flow in the riser section would have the following geometry:

(i) an A_d/A_r ratio of 2

(ii) a top clearance distance of 200 mm

(iii) a bottom clearance distance of 30 mm

(iv) be operated with an aeration intensity of 800 L/m^2.min

(v) have a water depth of 1 100 mm

(vi) have the sparger positioned inside the riser section (200 mm above the bottom of the baffle plates).

4.4.4 Summary

The amount of air that is supplied for air-scouring of immersed membranes is not an indication of how well fouling is limited. Increased aeration can result in very unfavourable system hydrodynamics that will even promote membrane fouling. Numerous interactions exist between aeration and the geometrical parameters of the system in creating the system hydrodynamics. Therefore, in an attempt to improve the scouring ability and to increase the efficiency of the supplied air, it is important that aeration is considered together with geometrical factors to create system hydrodynamics that will optimally utilise the scouring action of the rising bubbles across the membrane surfaces. Equations 1 and 2 must consequently be optimised together with the same factor levels.

With the effects of the factors and interactions known, and given the values of the levels (see Table 2) at which the factors were evaluated in this experiment, it is possible to interpolate between these values and arrive at different levels that could be used in Equations 1 and 2 for optimisation of other systems.

4.4.5 Final IMBR geometries

Once the regression equation was obtained and verified, variables were generated for three membrane stack designs operating at different liquid height settings (Table 3).

Table 3: Optimal design dimensions for membrane stack for different liquid levels with reference to Figure 34.

Liquid Height	1000 mm	1300 mm	1500 mm
Factor			
A	4	4	4
B (mm)	315	245	195
C (mm)	125	65	30
D ($L/m^2.min$)	1350	1350	1350
E (mm)	1000	1300	1500
F (mm)	200	200	200
D = specific air volume flow (air flowrate per riser cross-sectional area) A = A_d/A_r ratio			

The performance of one of the above designs is evaluated in Section 5.

5 PERFORMANCE OF SELECTED IMBR DESIGN

5.1 Introduction

In the previous section, the geometric and operating variables that affect IMBR fouling were investigated. From a factorial experimental design, optimized IMBR designs were developed. In this section, the performance of one of the designs is evaluated.

The design selected for evaluation is summarized in Table 4.

Table 4: Dimensions chosen for experimental IMBR

Liquid Height	**1300 mm**
A_d/A_r	**4**
Height of liquid above membrane pack (mm)	**245**
Bottom clearance below membrane pack (mm)	**65**
Aeration intensity (L/m^2.min)	**1350**
Overall liquid level (mm)	**1300**
Sparger position above bottom of pack (mm)	**200**

The construction of the IMBR based on the variables listed in Table 4 is described in Section 5.2. Laboratory evaluations of the system form the topic of Section 5.3. The performance of the IMBR on activated sludge is discussed in Section 5.4.

5.2 Experimental IMBR Unit

The reactor was a cylindrical plastic tank from a local supplier, having a nominal diameter of 0,5 m. The standard tank was converted by extending its height by the addition of a further cylindrical section. A membrane panel stack was constructed to hold 10 A4-sized membrane panels. The pitch, i.e. the spacing between the panels, was set at 8 mm, following values reported for current commercial IMBR units [Churchouse (1997), Cui *et al.* (2003)]. All the other dimensions are illustrated in Table 4 above. Various photographs of the unit are shown in Figure 38.

Overview of membrane case

View from side, showing air inlet for gas spargers

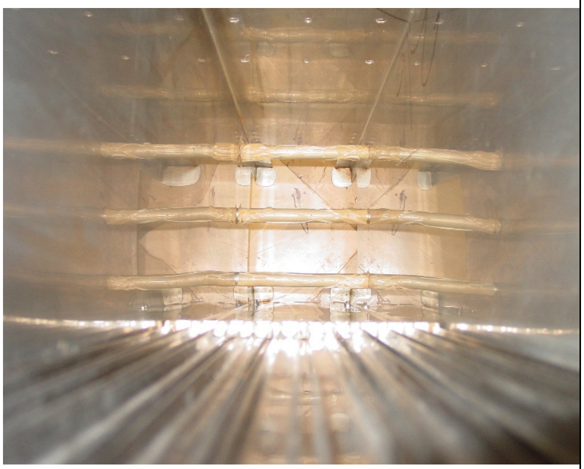

Top view, showing gas spargers

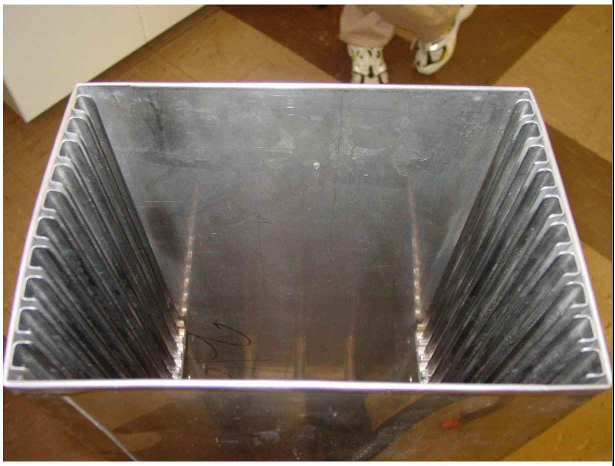

Top view, showing spacers for membrane panels

Membrane panel being inserted into pack

Permeate off-takes on modules

Figure 38: IMBR membrane pack constructed following Table 4.

5.3 Laboratory evaluation on a bentonite suspension

The membrane stack was placed inside the cylindrical reactor vessel and the vessel charged with bentonite suspension concentrations of 0.2 mg/L, 0.5 mg/L and 1 mg/L respectively. The flux was determined under three different air scouring flow rates, namely 6 L/min, 12 L/min and 18 L/min (direct flow meter measurement, no correction for density as result of pressure losses in the diffuser and hydrostatic head). If the area posed by the bottom cross-section of the membrane panels is deducted from the cross-section area of the membrane stack, these air flow rates are equivalent to specific volumetric flow rates of 325, 649 and 974 L/min.m^2 respectively. A peristaltic pump was used to draw permeate from the membrane panels. The action of the pump is pulsatile, and the maximum flux that can be drawn from the 10 membrane panels was 50 LMH. This imposed certain limitations on the experimental set-up.

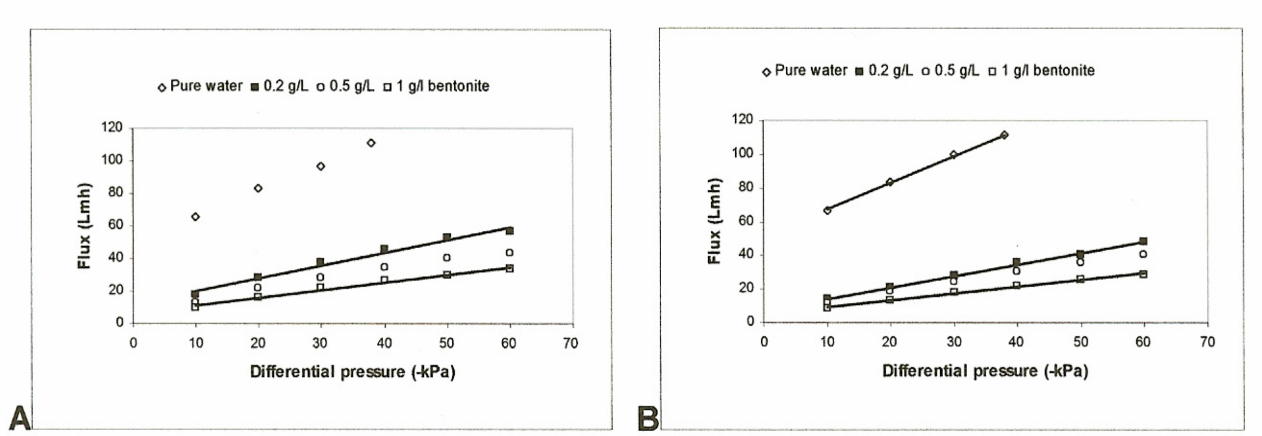

Figure 39: Flux-differential pressure relationship for flat membrane elements operating on pure water and three bentonite suspensions at two air-sparge flow rates: a) 6 L/min and b) 12 L/min.

The pure-water flux (PWF) differential pressure relationship for both air flow rates was the same, and a linear relationship between flux and pressure was found as one would have expected (Figure 39). Two points must be raised though. The weave of the cloth used is fairly dense (Figure 40) and the membrane resistance obviously has an effect on the flux/pressure relationship. There was also a small lowering in membrane flux at the higher sparger flow rate evaluated in this experiment (12 L/min) compared to the lower flow rate of 6 L/min. This was surprising since one would have expected the flux to be lower at the lower sparging rates as result of the lower scouring effect (air flow rate of 6 L/min is about 25% of the reference air flow indicated in Table 4).

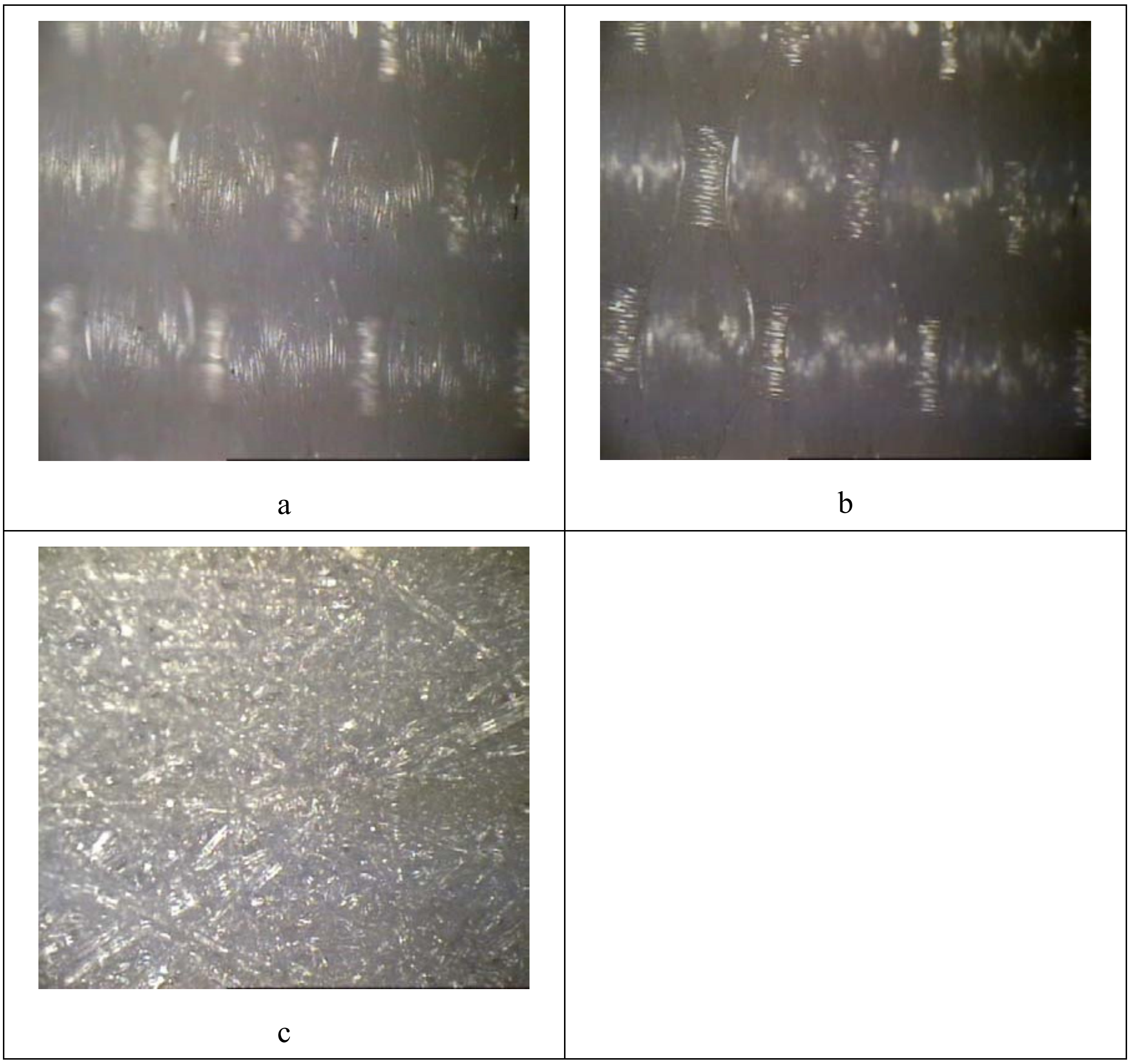

Figure 40: (a) and (b) :- 50x magnification of the filter cloth used in the membrane panel showing the topology of the membrane at two focus lengths; (c) surface of a non-woven spunbonded filter material with a smoother surface.

There appears to be some deviation from linearity in the bentonite flux curves generated at aeration rates of 6 and 12 L/min (Figure 38 (a) and Figure 38 (b)). From the data in Table 5, it appears as if all the flux relationships are still pressure dependent, but that those generated under 6 L/min air-sparge flow deviate slightly from linearity. This may indicate that mass transfer may become a factor at higher differential pressure. For the bentonite system one would then argue that it is better to operate the sparger at air-flow rates of 6 L/min or at a specific volume flow of 650 L/min.m^2.

Table 5: Regression performed on bentonite flux curves

Air-flow rate (L/min)	Bentonite concentration (g/L)	Regression Coefficient (R^2)
6	0,2	0,981
	0,5	0,982
	1,0	0,982
12	0,2	0,997
	0,5	0,995
	1,0	0,995

Another point that needs consideration, but which also needs substantiation, is that of particle size distribution and the action of smaller particles under the influence of shear caused by the 2-phase flow across the plane of the membrane. Particle deposition rate is a function of convective transport towards the membrane surface and is a function of the rate of permeate withdrawal. Larger particles will tend to migrate across the membrane surface because of there greater momentum and surface area, but smaller particles would rearrange into a tighter packing order. This would result in increased cake resistance and therefore reduced flux.

The specific fluxes of the membranes were also lower at higher operating pressure (Figure 40). There could be various reasons for this. Head-loss within the membrane body would be higher at higher permeate velocities as result of frictional losses within the membrane. The other possibility could be that the permeate spacer material used was not of optimal design and may have added to frictional losses as at higher permeate velocities as the operating pressure was increased. Densification of the membrane material at higher operating pressure may also have added to frictional losses. These factors must be considered individually and in combination to elucidate the observed trend since the cause could be due to the design of the panels and not process-operation related. One approach would be to increase the pumping capacity of the system and establish whether there is a relationship between the PWF asymptote and membrane panel variables (membrane, permeate spacer material and panel core design). The specific flux for all the bentonite operations seemed to have reached some asymptote beyond operating pressures of 40 kPa and this may be a starting point for further experimentation.

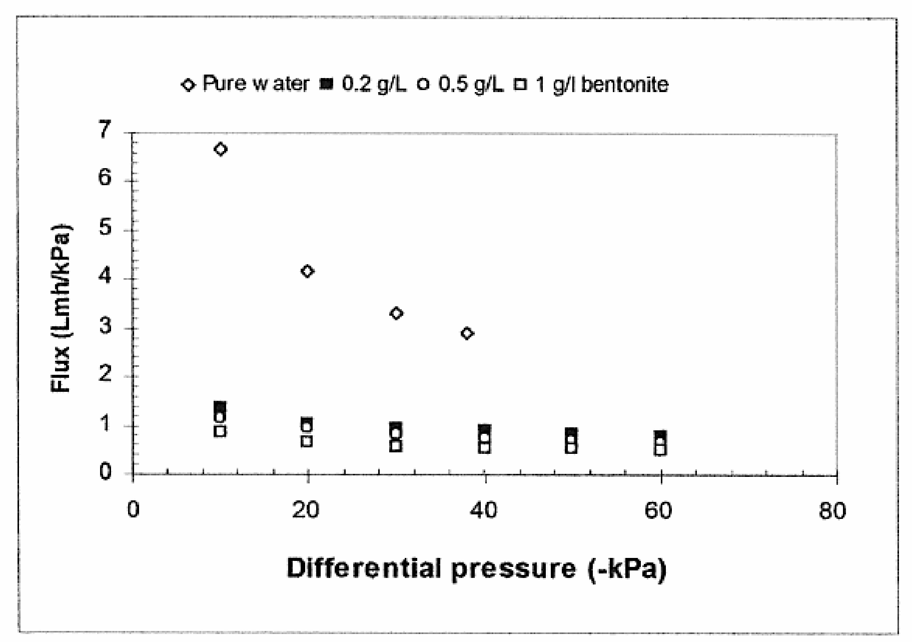

Figure 41: Specific flux behaviour as a function of differential pressure.

The variation in permeate turbidity is shown in Figure 42 as function of bentonite concentration and air sparging rates of 6, 12 and 18 L/min. In all instances there appears to be a minimum in permeate turbidity at differential pressures around 30 and 40 kPa. One hypothesis is that membrane compaction increased as the pressure increased from 10 to 30 kPa and hence caused better sieving ability of the woven membrane. Particle diffusion through the membrane weave as the cake layer builds up could explain the increase in turbidity beyond operating pressures of 40 kPa. This convoluted behaviour needs further investigation. It is known that the woven fabric cross-flow microfiltration membranes operate best if the membranes are first coated with particulate matter such as limestone, fumed silica or, even better, powdered activated carbon. However, in the case of the internally pressurized tubular- type membranes, the membrane weave tightens up as the pressure increases and the sieving ability should increase.

In the case of the woven flat-sheet membranes, the forces acting on the membrane are one- dimensional and not two-dimensional as in the case of the tubular membrane. The flat woven membranes will therefore rely more on the presence of a fouling layer for improved performance than the tubular-type would, since the structure (weave) of the flat membrane will not tighten up to the same extent as the tubular counter-part would as the operating pressure increases. Further, the woven-type microfiltration membranes are not surface filters as is the case with phase inversion membranes. These membranes are more a depth-type filter, whereby the internal structure initially tends to trap particles that eventually contribute to improved membrane sieving properties. In the flat membranes, these particles may become dislodged as the pressure is increased and migrate to the product side of the filter. Repeat experiments with different filter materials will allow the observed phenomenon to be elucidated.

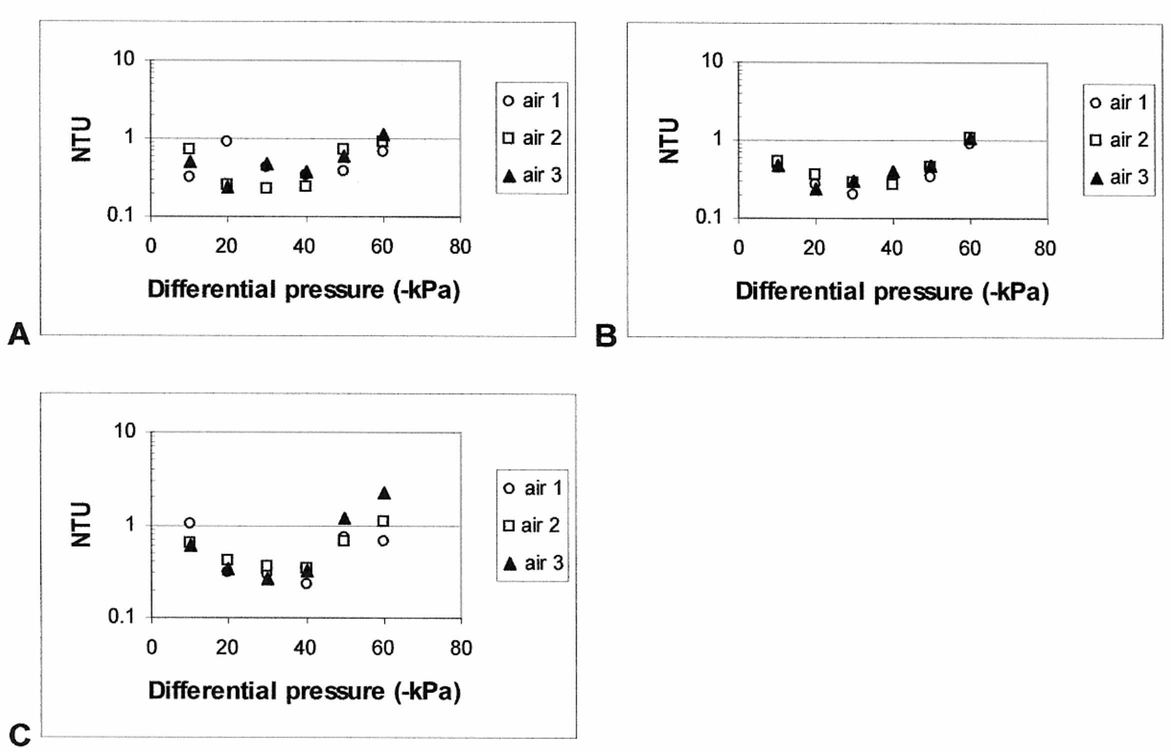

Figure 42: Turbidity determination for plate membranes operating on three different bentonite suspensions and air sparge volume flow rates. (a) 0,2 mg/L; (b) 0,5 mg/L; and (c) 1 mg/L.

The critical flux was determined under different airflow conditions. In the earlier discussion concerning flux and differential pressure, the data in the 3 L/min sparging rate experiment suggested the onset of mass-transfer dependent product flow. The data in Figure 43 substantiates this. The critical flux of the membranes was found to lie between 16 and 19 LMH when the air scouring was set at a rate of 3 L/min (Figure 43 a). There was no evidence of an increase in pressure (increase in concentration polarization) when the flux was drawn at a rate of 19 LMH using an air-scouring rate of 6 L/min. At a differential suction pressure of 40 kPa the turbidity of the permeate is at its minimum, as was seen earlier.

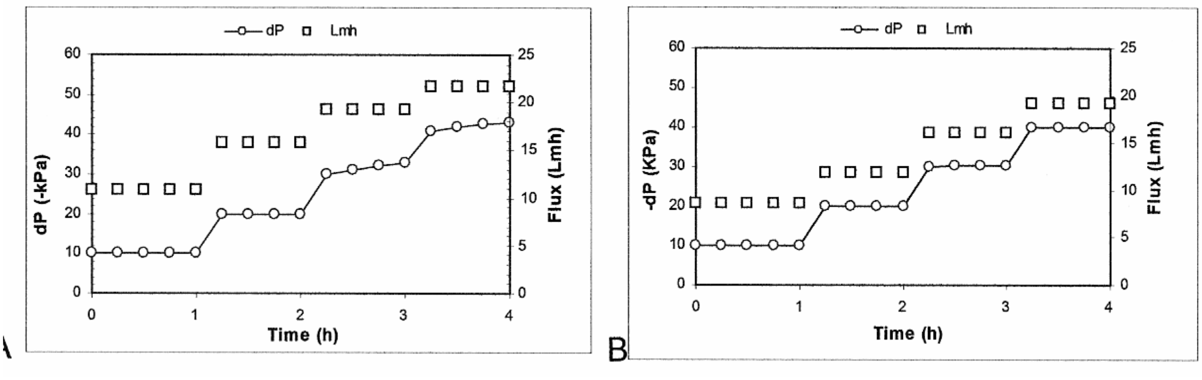

Figure 43: Results of critical flux determination with a 1 g/L bentonite suspension: a) air flow 3 L/min (160 L/min.m^2) and b) 6 L/min (325 L/min.m^2).

5.4 Evaluation on activated sludge

The objective of this evaluation is solely to determine whether the membrane module and IMBR configuration developed in the project technically adequate for IMBR systems. Further detailed and longer term evaluations would be required before the system may be compared to current commercial IMBR systems.

5.4.1 Experimental

A pilot scale IMBR having a volume of about 350 L was set up at the Northern Waste Water Treatment Works (NWWTW) in Durban. The IMBR used the membrane pack developed earlier (Table 4) and the experimental setup is shown in Figure 44.

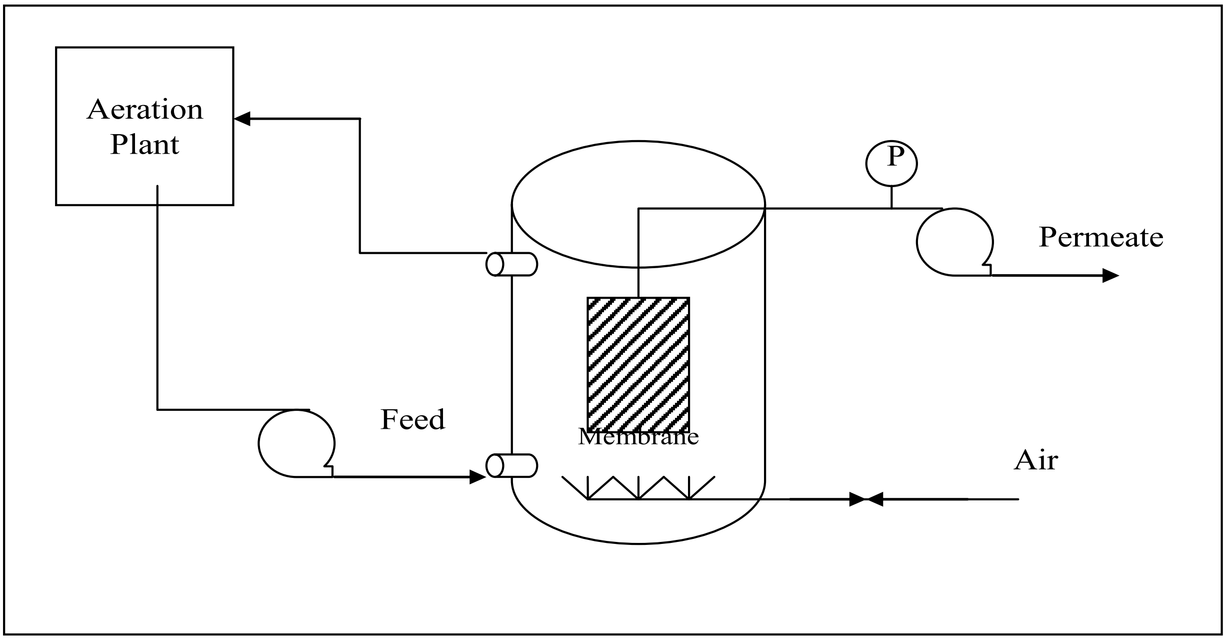

Figure 44: Experimental setup at NWWTW

Activated sludge was pumped from the main activated sludge (AS) plant into the reactor. The overflow from the reactor was returned to the activated sludge plant. Permeate drawoff was effected by a peristaltic pump, with variable speed control. A compressor provided aeration to the IMBR, via a diffuser.

The ambient MLSS of the AS plant was about 3 g/L. To perform experiments at elevated concentrations, the sludge was settled, the supernatant decanted, and the concentrate loaded into the IMBR.

Two variables were investigated:- biomass concentration (MLSS) and aeration rate. The combinations investigated are as follows:

MLSS (g/L)	**Total air flowrate into Reactor (L/min)**	**Specific air flowrate (L/min per module)**
3	3	0,3
3	25	2,5
9	3	0,3
9	25	2,5

Selected results are presented below. All analyses were performed at the NWWTW laboratory, and the results are presented here in their format.

5.4.2 Turbidity rejection

The effect of flux on permeate turbidity was investigated, for each of the operating condition sets above. This is presented in Table 6.

Table 6: Permeate Turbidity at Different Biomass Concentrations and Air-sparge Flowrates

Flux (LMH)	**Turbidity (NTU)**			
	3g/L 3L/min	3g/L 25L/min	9g/L 3L/min	9g/L 25L/min
5	0,53	0,91	0,92	0,9
10	0,35	0,29	0,67	0,6
15	0,39	0,38		
20	0,28	0,25		
25		0,23		
30		0,26		

Permeate turbidities were consistently below 1 NTU. The initial turbidity is fairly high and drops off rapidly with time. There is an indication that permeate turbidity increases marginally as the feed concentration increases.

MLSS removal at the different operating conditions is shown in Table 7.

Table 7: MLSS Results for Feed and Permeate at Different Biomass Concentrations and Air-sparge Flowrates

Operating Condition	MLSS (mg/L)		% MLSS Removed
	Feed	Permeate	
3g/L biomass 25L/min air	1 866	< 1	100
	1 648	< 1	100
9g/L biomass 3L/min air	7 700	< 1	100
	8 928	< 1	100
9g/L biomass 25L/min air	7 952	< 1	100
	9 012	< 1	100

5.4.3 Critical Flux investigations

Critical fluxes were determined for each operating set following the conventional procedure, i.e.

(i) the permeate flux was set at a low value, and the differential pressure across the membrane was measured.

(ii) the flux was then increased in small increments, and the new DP measured at each flux.

Below the critical flux, the DP should remain constant with time. Above the critical flux, the DP should increase with time, as fouling occurs. Hence, by noting the flux at which the DP ceases to remain steady, the critical flux may be inferred.

A typical critical flux determination is shown in Figure 45. Here, the critical flux is between 10 LMH and 15 LMH.

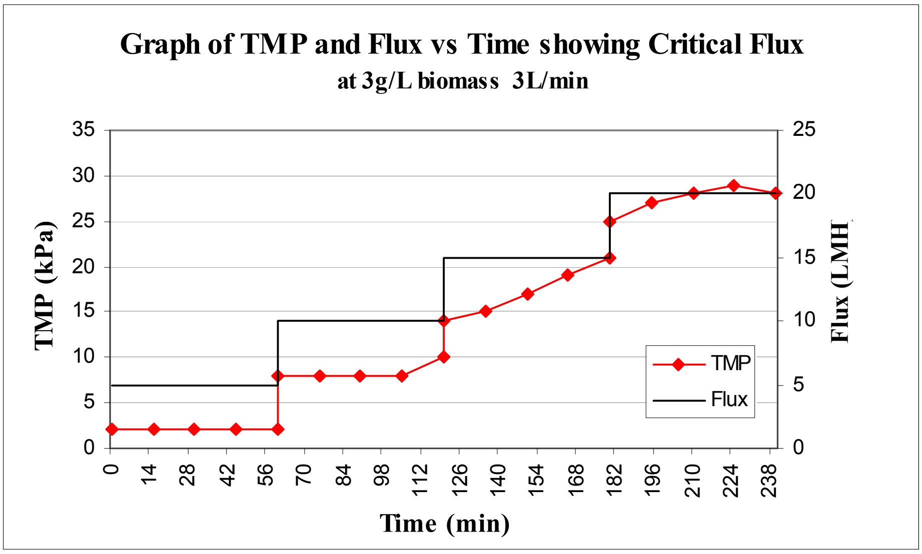

Figure 45: Typical critical flux experiment

The critical fluxes so determined are shown in Table 8, and follow the expected trends. However, the value obtained at 9 g/L and 25 L/min air is doubtful, and could be due to non-homogeneity in the reactor vessel when the experiment was performed.

Table 8: Summary table of Critical Flux Results

Operating Condition	Critical Flux (LMH)
3g/L biomass 3L/min air	15
3g/L biomass 25L/min air	30
9g/L biomass 3L/min air	10
9g/L biomass 25L/min air	[10]

5.4.4 COD removal

The overall COD removals are shown in Table 9.

Table 9: COD Results for Feed and Permeate at Different Biomass Concentrations and Air-sparge Flowrates

Operating Condition	COD (mg/L)		% COD Removal
	Feed	Permeate	
3g/L biomass 25L/min air	3 191,6	16,6	99,5
	3 364,9	35,9	98,9
9g/L biomass 3L/min air	3 716,4	7,2	99,8
	3 228,6	52,1	98,4
9g/L biomass 25L/min air	3 430,3	57,8	98,3
	3 520,2	11,0	99,7

5.4.5 Fouling and Cleaning of modules

During the above investigation, the modules were cleaned by simply brushing them in water. This seemed to be adequate to remove the biological fouling layer.

After the above investigation, the used modules were stored in the DUT lab for about two weeks. When the modules were subsequently used in laboratory trials, on bentonite, it was found that all the modules had high starting differential pressures (DPs), and that the DP increased substantially faster than normal. Typically, this is indicative of irreversible fouling in a module.

This prompted an investigation into cleaning of the modules. Before attempting any of the “exotic” cleaning solutions, the modules were soaked in a dilute commercial bleach solution overnight (Jik). They were then washed out, and run on a bentonite suspension.

The initial DP profiles, before soaking, are compared to the DP profiles obtained after soaking in Figure 46.

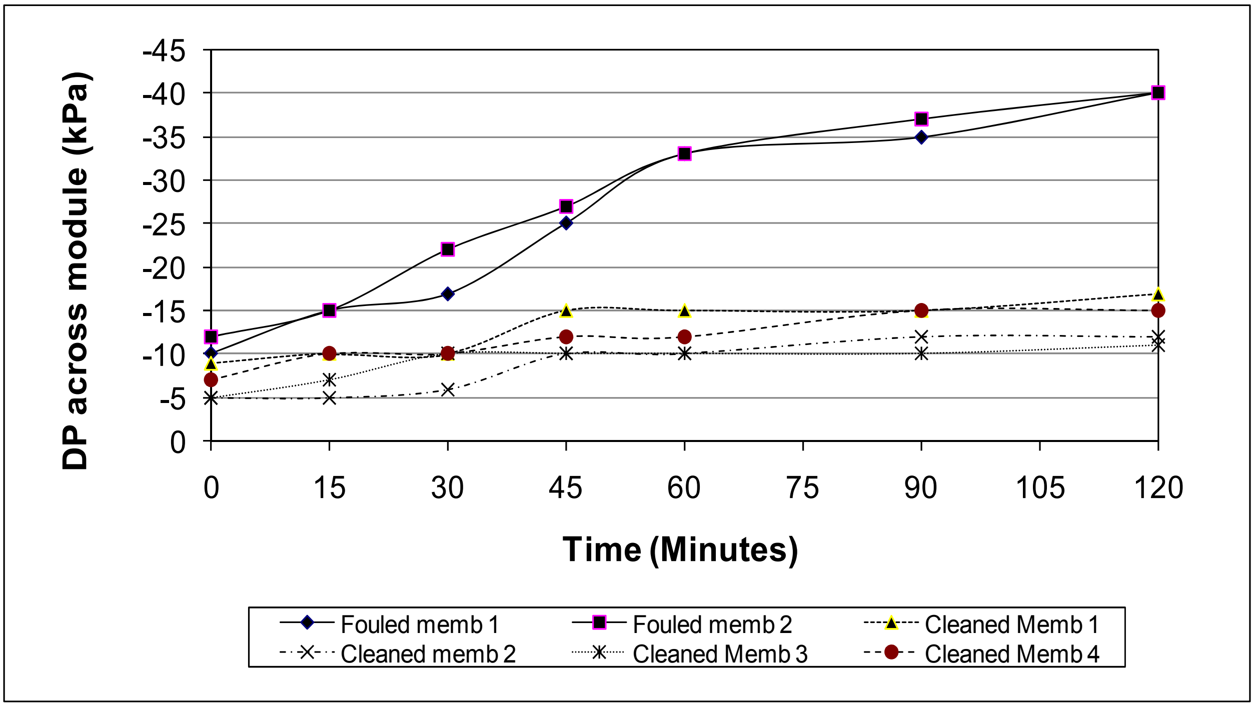

Figure 46: DP profiles for fouled and cleaned modules

In determining whether a fouled membrane has been successfully cleaned, it is important to consider both the starting DP and the subsequent rate of increase in DP. From Figure 45 it is clear that simply soaking the modules in a commercial bleach was sufficient to remove residual foulants from the membrane and restore their performance.

5.5 Overall assessment

<u>Hydrodynamics</u>

In both the laboratory and on-site evaluations, smooth and stable circulation was obtained within the reactor, with no indication of the stagnant zones obtained in the preliminary experiments in this project. On examination of the membranes after each run, there were no signs of preferential fouling zones.

It would thus seem that the proposed IMBR design meets the hydrodynamic criteria, i.e. to ensure stable circulation and uniform scouring of the membrane modules.

<u>Permeate Quality</u>

The permeate turbidities are consistent with values expected from current commercial systems (0,2 NTU to 0,8 NTU). The turbidities are also consistent with results obtained on the WFMF membranes in previous WRC projects. Note that in these previous projects the WFMF membranes were operated in a tubular mode or a flat-sheet mode without aeration. It was then believed that the removal ability of WFMF was dependant on a fouling layer (or precoat) forming on the membrane surface. Hence, there was some doubt as to whether a good turbidity removal would be obtained when the membrane surface is vigorously scoured. The results obtained in this project indicate that the separation efficiency is primarily determined by the fabric itself, and is probably assisted when a precoat exists.

Critical fluxes

The system shows the typical characteristics of commercial IMBRs, i.e. a critical flux exists which is function of feed concentration and aeration intensity.

Commercial IMBRs operate at critical fluxes of about 15 LMH to 25 LMH, for MLSS values between 12 g/L and 15 g/L. In the evaluation performed at NWWTW, a critical flux of about 10 LMH to 15 LMH was achieved at a MLSS value of 9 g/L. However, the aeration intensity used here was substantially below that used in commercial IMBRs. One of the leading suppliers recommends an air flowrate of 7 L/min to 10 L/min per membrane module. In this study, the flowrates ranged from 0,3 L/min/module to 2,5 L/min/module, about 5% to 35% of the commercial units. Hence, further detailed and long term evaluations would have to be performed at equivalent conditions before the critical fluxes obtained with the proposed design can be compared to commercial plants.

Cleaning of fouled modules

As with previous WRC projects on WFMF membranes, it was found that the modules were fairly easy to clean, and there were no indications of irreversible fouling. It is notable that when the modules were allowed to dry out with biological foulants within the fabric, the system could be cleaned with simple soaking in a commercial hypochlorite solution. This would be unique advantage to the system, since most commercial membranes are destroyed if they are allowed to dry out.

6 INVESTIGATIONS INTO FACTORS AFFECTING MORPHOLOGY OF SKINLESS CAPILLARY ULTRAFILTRATION MEMBRANES

6.1 Introduction

During a previous Water Research Commission supported project, the Institute of Polymer Science, University of Stellenbosch, developed a membrane that had morphological features distinctly different from other commercially available membranes [Jacobs and Sanderson (1997)]. This membrane became known as the *skinless* membrane, essentially because the closely packed microvoids present in the membrane substructure opened up in the outer layer of the capillary membrane.

Two applications emerged from the development of these skinless membranes. The first was in the production of potable water by from sources containing coloured water. The second application was in the immobilization of a white rot fungus in a "Gradostat" membrane bioreactor. Here a nutrient gradient through the membrane wall and fungal mat can be established and manipulated in order to stimulate continuous production of secondary metabolites (extra-cellular enzymes). The WRC holds RSA, American and European patents on the continuous production of enzymes from filamentous fungi using the Gradostat reactor. Other possible applications for the membranes include reactor oxygenation and to immobilise microorganisms in a biofilm.

The membranes are somewhat difficult to fabricate and very stringent process control is required to obtain the requisite structure. Also, for the other potential applications mentioned above, it could be of advantage to develop a skinless membrane that has either a thinner or thicker wall thickness, or an outside diameter larger or smaller than that of the current membrane, i.e. 1,8 mm. Hence, it was deemed necessary to revisit and study the different factors that affect the morphology of the skinless membrane.

The production process for capillary membranes is described elsewhere [Jacobs *et al.* (2003)]. The skin and microvoids formation depend mostly on the rate of solvent/non-solvent exchange between the bore fluid and the polymer dope [Wijmans *et al*. (1983), Cabasso *et al.* (1977), Young and Chen (1995)]. In view of the importance of relative volumetric flow rates, it was decided to study the effect of changing the volumetric flow rates of both the bore fluid and dope fluid, and determine the effect they may have on membrane structure and performance. Accordingly the main production variables selected for investigation in this study were:

(i) composition of the spinning bath

(ii) dope extrusion rate (DER) and viscosity of dope fluid

(iii) bore fluid flowrate (BFFR)

(iv) spinnerette size

This investigation was performed as an Mtech study and is reported in Jack (2005). Selected excerpts from that thesis are reported here. For the detailed experimental protocol, the reader is referred to the Mtech thesis.

6.2 Experimental

Capillary ultrafiltration membranes were produced using the spinning laboratory at the Institute of Polymer Science, University of Stellenbosch, at different combinations of spinning bath composition, DER and BFFR. The dope formulation, bore fluid composition and spinning bath composition is shown in Table 10. The combinations of these variables that were investigated are shown in Table 11.

Table 10: Compositions of Dope, Bore Fluid and Spinning Bath

Constituent	Mass %
DOPE	
NMP (N, Methyl 2- pyrrolidone)	35
MC (Methyl cellosolve)	10
PSF (Polysulfone)	23
PEG 600 (polyethylene glycol)	32
BORE FLUID	
NMP	2
Water	98
SPINNING BATH	
NMP	93 to 99
Water	7 to 1

Table 11: Combinations of Variables investigated

Experiment	DER (mL/min)	BFFR (mL/min)	Spinning Bath NMP %
Effect of spinning bath composition	2,5; 3,0	4,5	93; 94; 96; 99
Effect of DER	2,5; 3,0; 4,0; 4,5	4,5	93; 94; 96; 99
Effect of BFFR	4,0	1,5; 2,5; 3,5; 4,0; 4,5	94; 96

The membranes that were produced were then subjected to the following characterization tests :

(i) permeate flux and rejection: Test cells were fabricated from 10 membranes, 35 cm long. Rejection was determined by pumping a 0,5% solution of PEG (MW 35 000) through the membrane and gravimetrically determining the concentration of

PEG in the permeate. Permeate flux was determined by the standard procedure of monitoring the permeate flowrate with time, when operating on pure water.

(ii) diameter determination: Sample membranes were fractured at liquid nitrogen temperatures in order to obtain smooth surfaces. A traveling microscope was used to determine their diameters and an average of three samples was taken.

(iii) examination of membrane morphology: Membranes were fractured in liquid nitrogen (70K) and then gold sputtered. Specimen membranes were observed with a Leo Model at 1430 variable pressure. The voltage used was 7 kV and the working distance = 6 mm.

6.3 Results

6.3.1 Interpretation of SEMs

The objective is to produce *externally unskinned* membranes with microvoids extending from the inner membrane to the outside surface.

Figure 47 (a) shows a membrane that is *externally skinned*, and hence unacceptable. Figure 47 (b) shows a typical *externally unskinned*, i.e. *skinless,* membrane with desirable microvoids. Hence, from the SEM scans, the morphology of the produced membrane may be assessed, and hence whether the membrane is acceptable as a *skinless* membrane or not.

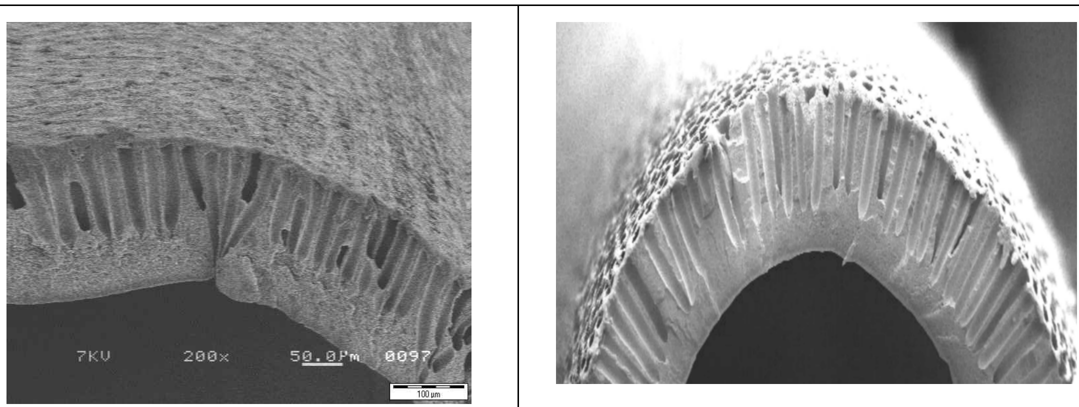

(a) (b)

Figure 47: SEM of (a) externally skinned (b) and externally unskinned i.e. skinless membrane

All the descriptions of membrane morphology reported here are supported by SEMs that are available in the MTech thesis [Jack (2005)].

6.3.2 Effect of spinning bath composition

Membranes spun at the extreme NPM spinning bath compositions, i.e. 99 and 93% NMP, had an external skin layer, for DER rates of both 2,5 mL/min and 3,0 mL/min. Even at these low DER no externally unskinned membranes were formed. Acceptable externally unskinned membranes were produced at 94 and 96% NMP external bath compositions.

6.3.3 Effect of DER

Once again, membranes produced at a spinning bath NMP content of 93% and 99% produced unacceptable externally skinned membranes. Only the experiments at NMP contents of 94% and 96% produced skinless membranes, and these results are presented here.

The morphology of membranes produces with spinning bath compositions of 94% NMP and 96% NMP are shown in Tables 12 and 13 respectively. The permeate fluxes and rejections are shown in Figures 48 and 49.

Table 12: Morphology on varying DER, BFF held constant at 4,5 ml/min and external spinning bath composition = 96% NMP

DER (mL/min)	Membrane Dimensions			Burst Pressure (kPa)	Morphology
	ID (mm)	OD (mm)	Thickness (mm)		
2,5	0,13	0,19	0,053		Thick inner skin, few finger like voids, polymer rich in between. Distorted on the inner surface. Externally unskinned
3,0	0,11	0,18	0,071		Thick inner skin, voids becoming many, starting just below the inner skin and extending to the outside. Externally unskinned.
4,0	0,11	0,21	0,101	1300	Thick inner skin, voids becoming short, some start far from the inner skin while some do not reach the outer skin
4,5	0,11	0,2	0,093	1700	Thick inner skin, voids narrow and extend to the outer skin. Small pores at the end of the voids. Thick outer skin
5,0	0,12	0,23	0,103	1700	Inside skin reduced, too many needle like voids starting just below the inner skin and extend to the outer skin. Thick outer skin

Table 13: Morphology on varying DER, BFF held constant at 4,5 ml/min and external spinning bath composition = 94% NMP

DER (mL/min)	Membrane Dimensions			Burst Pressure (kPa)	Morphology
	ID (mm)	OD (mm)	Thickness (mm)		
2,5	0,13	0,19	0,053		Thick inner skin, few finger like voids, polymer rich in between. Distorted on the inner surface. Externally unskinned
3,0	0,15	0,22	0,067		Thick inner skin, finger like voids starting below the skin and extending outwards. Externally unskinned
4,0	0,11	0,21	0,094	900	Thin inner skin, narrow needle-like voids. Pores on the underlying outer skin.
4,5	0,12	0,22	0,098	1700	Thin inner skin, needle-like voids extending to the outer skin. Pores at the end of voids. Thick outer skin.
5,0	0,13	0,23	0,092	1700	Thin inner skin, needle like voids starting just below the skin, extending to the thin outer skin.

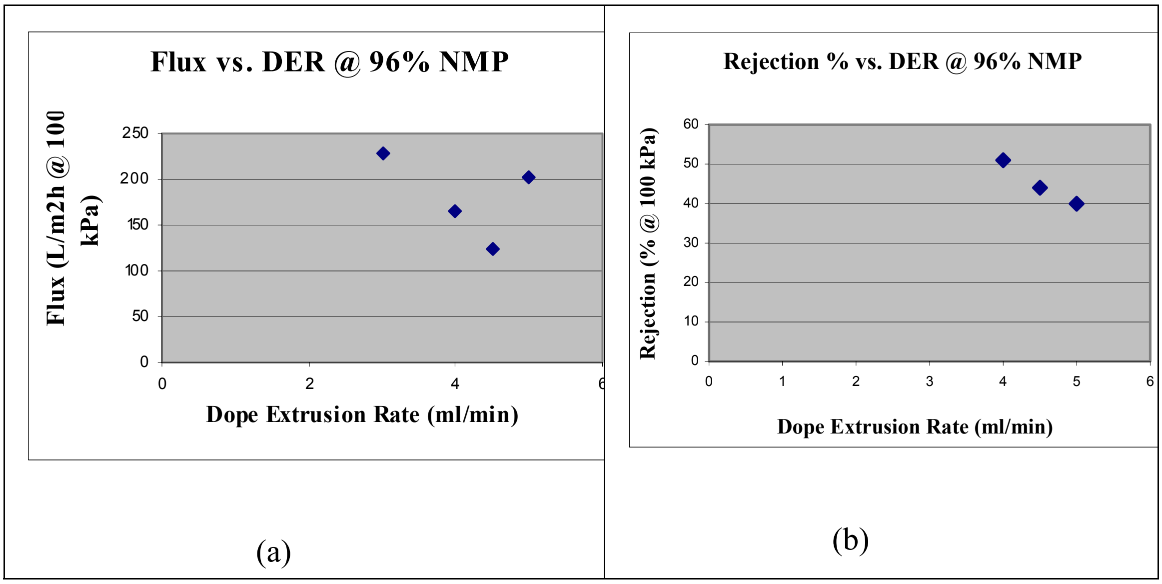

Figure 48: Effect of DER on (a) pure water flux, and (b) rejection [spinning bath NMP = 96%]

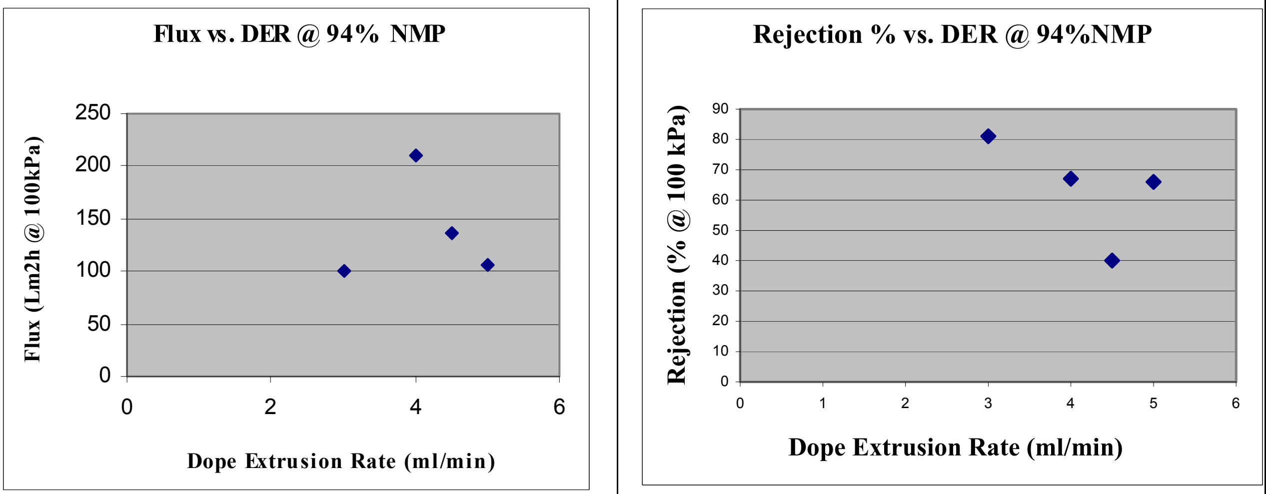

(a) (b)

Figure 49: Effect of DER on (a) pure water flux, and (b) rejection [spinning bath NMP = 94%]

Externally unskinned membranes were formed at low dope extrusion rates (2,5 and 3,0 ml/min). At higher DER, that is, greater than 3,0 ml/min, an external skin layer was formed. The membrane performance results showed a decrease in flux with increasing DER. That can be caused by the external skin layer getting thicker with increasing DER. Rejection also seemed to decrease with increase in DER and that is a rare situation.

Membranes formed at 2,5 mL/min DER showed signs of distortion on the inner surface. That could be the result of shear stress caused by the bore fluid at high flow rate of 4,5 ml/min whilst the dope is extruding at a very low rate.

6.3.4 Effect of BFFR

The morphology of membranes produced at spinning bath NMP contents of 96% and 94% are shown in Tables 14 and 15 respectively. The pure water flux and rejections are shown in Figures 50 and 51.

Table 14: Morphology on varying BFFR, DER held constant at 4 mL/min and external spinning bath composition = 96% NMP

BFFR (mL/min)	Membrane Dimensions			Burst Pressure (kPa)	Morphology
	ID (mm)	OD (mm)	Thickness (mm)		
1,5	0,1	0,2	0,098	2000	Thick skin inside, voids wide not close to each other, thin outward skin
2,5	0,11	0,19	0,083	> 1000	Thick inner skin, voids wide, elongated to the outer skin. thick polymer rich in between voids
3,5	0,11	0,21	0,098	1500	Thick inner skin, voids extending to outer skin
4,0	0,12	0,22	0,078	1300	Thick inner skin, voids wide and not much elongated, some starting from inner skin, some not reaching outer skin
4,5	0,11	0,21	0,101	1300	Thick inner skin, voids becoming short, some start far from the inner skin, some don't reach outer skin

Table 15: Morphology on varying BFFR, DER held constant at 4 mL/min and external spinning bath composition = 94% NMP

BFFR (mL/min)	Membrane Dimensions			Burst Pressure (kPa)	Morphology
	ID (mm)	OD (mm)	Thickness (mm)		
1,5	0,11	0,2	0,089	1800	Inside skin thin, too many needed like voids extending to outer skin
2,5	0,11	0,2	0,088	1700	Thin inner skin, too many needle-like voids. Small pores at the end of voids. thinner outer skin
3,5	0,12	0,2	0,085	1600	Inside skin reduced, too many needle like voids starting just below the inner skin and extend to the outer skin. Outer skin reduced.
4,0	0,12	0,25	0,134		Inner skin getting thin, voids narrow and extend to outer skin. Thin outer skin
4,5	0,11	0,21	0,094	900	Thin inner skin, narrow needle like voids. Pores on the underlying outer thin skin.

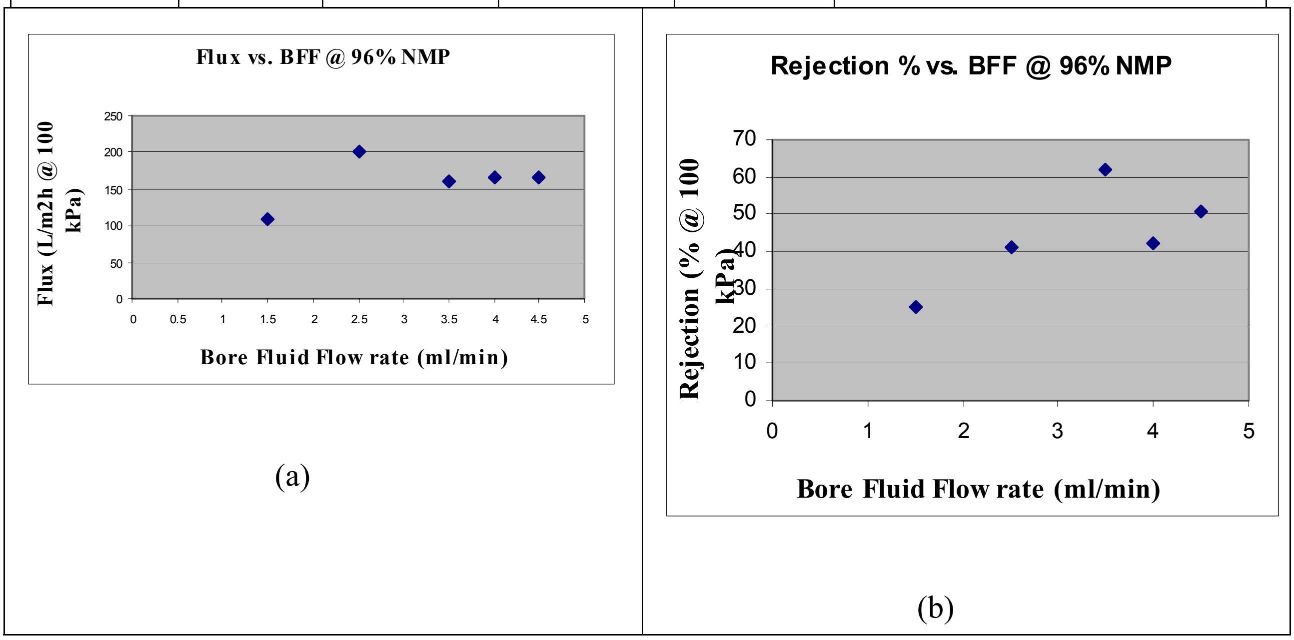

Figure 50: Effect of BFFR on (a) pure water flux, and (b) rejection [spinning bath NMP = 96 %]

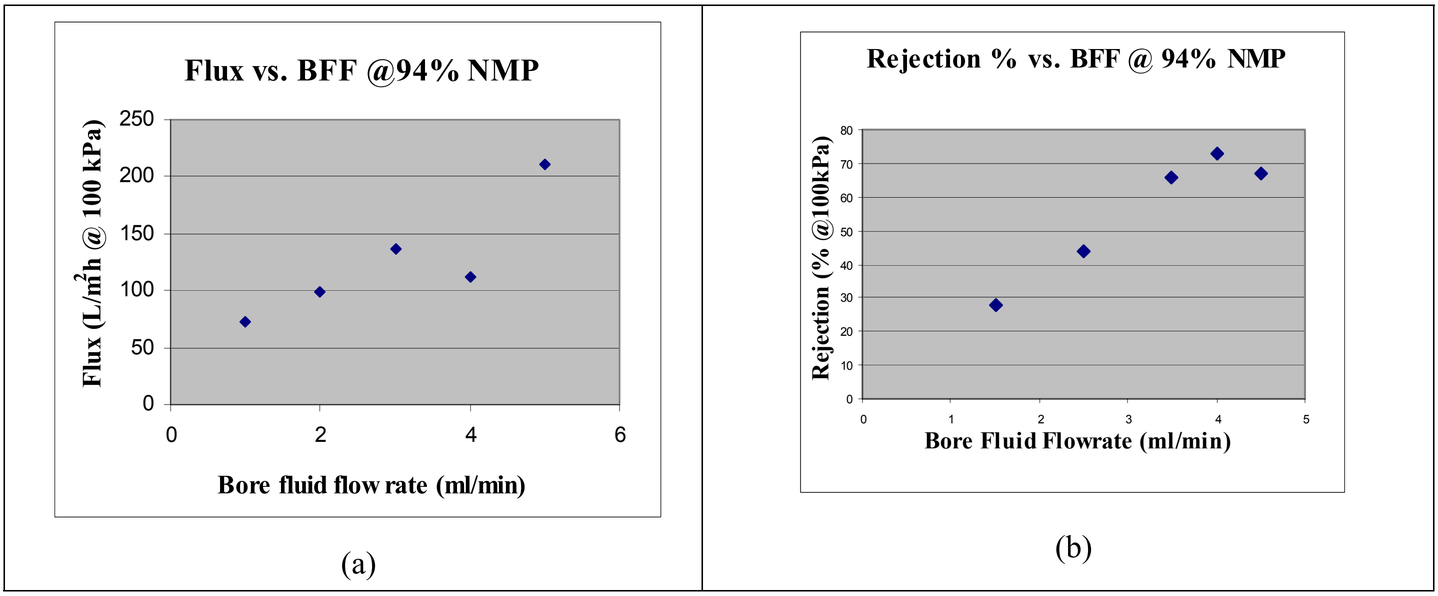

Figure 51: Effect of BFFR on (a) pure water flux, and (b) rejection [spinning bath NMP = 94 %]

The SEM photos showed that the microvoid length and number increased with an increase in bore fluid flow rate. The inner skin layer was reduced with an increase in bore fluid flow rate.

When the external spinning bath composition was 94% NMP aqueous content, membranes formed had thin external skin. The flux increased with BFF increase, because the major hydraulic resistance was the inner thin skin layer, which also got thinner with BFF increase. That explains the decrease in retention with increase in BFF.

When the external spinning bath composition was 96% NMP aqueous content, membranes formed had a thick inner skin layer. There was an increase in retention also with BFF increase. This is a rare situation, increase in flux and retention at the same time. The reason for an increase in retention could be the inner thick skin layer.

No externally unskinned membranes were formed. The constant dope extrusion rate must have been sufficiently high to allow for complete precipitation of the nascent membrane by the bore fluid before reaching the humidity chamber.

6.3.5 Effect of spinneret size

In the experiments reported above, the spinneret had an ID of 0.063 mm and an OD of 0.273 mm. To test the effect of spinneret size on membrane production, a small spinneret with an inside diameter (ID) of 0.012 mm and an outside diameter (OD) of 0.056 mm was used.

Six experiments were conducted at different dope extrusion rates of 1.1; 1.3; 1.5; 2.0; 2.5 and 3.0 mL/min. The BFFR was held constant at 3.5 mL/min.

Significant problems were experienced with the smaller spinneret. The maximum DER the spinneret could allow was 3,0 mL/min. At 3,0 and 3,2 mL/min DERs, the production line became slack and entangled. Increasing the roller speed and take up speeds did not help.

All the membranes produced using a small spinneret were externally unskinned. Very high fluxes, > 200 L/m^2h, were obtained but the retentions were very low. After some time of running pure water with the dye through the membranes, permeate came out with the dye. With UF tests, no clear permeate was obtained. For that reason, no samples were taken for retention tests. At 200 kPa pressures, permeate was also not clear.

6.4 Summary

(i) External spinning bath composition ranging between 94 to 96% NMP was found suitable for production of externally unskinned membranes

(ii) The DER where an externally unskinned membrane could be formed with a thick wall was found to be 3,0 mL/min.

(iii) The BFF of 4,5 ml/min was found to be satisfactory for production of externally unskinned membrane with the DER of 3,0 mL/min.

(iv) A small spinneret was found unsuitable for the production of thick-walled membranes.

7 CONCLUSION AND RECOMMENDATIONS

7.1 AIM: Development of a flat-sheet membrane module

Criteria

The criteria for a membrane module for dewatering in IMBR applications are:

(i) it should be simple and robust, and inexpensive in construction;

(ii) it should give a good permeate quality;

(ii) it should give a good flux that would be viable for MBR applications;

(iv) it should require easy and inexpensive cleaning strategies;

(v) for thermophilic operations, the module should be able to operate at temperatures up to 60°C; and

(vi) it should preferablyutilise membranes that are readily available in South Africa, obviating the research and development costs to develop new membranes.

Project Achievements

A fabrication protocol has been developed for a flat-sheet module. In this project, the module utilised the woven fibre microfiltration (WFMF) fabric developed by a local company, Gelvanor, and the module developed was approximately A4 in size.

In evaluations on both mineral and biological suspensions, the module gave very good rejections of suspended solids, with permeate turbidities ranging from 0,2 NTU to 0,9 NTU. Cleaning of the membrane is very simple, with either simple scrubbing or soaking in a commercial bleach solution to remove foulants. It was also observed that on drying, the fouling layer peels away from the membrane and can be easily removed. This is a unique advantage to the membrane, since the leading commercial IMBR membranes are destroyed on drying.

The protocol for the module is fairly simple, and does not require highly skilled technicians or specialist materials. The materials can be chosen to be resistant to temperatures up to 60°C, fulfilling the requirement for operation in thermophilic IMBRs.

The fabrication protocol may equally be applied to other flat-sheet membranes, including non-woven fabric membranes or polymeric membranes.

Recommendations

There is huge potential for flat-sheet alternatives to the Kubota membrane module in the rapidly growing IMBR and immersed filtration markets. The fabrication protocol developed in this project should be developed further towards producing a commercially competitive product. Amongst the issues to be addressed are:

(i) choosing less expensive materials;

(ii) increasing the size of the modules; and

(iii) industrialising the production protocol, using current mass-production fabrication techniques.

7.2 AIM: Development of a design for IMBRs

Criteria

The criteria for a hydrodynamic design for IMBRs, include the following:

(i) there should be stable circulation of the biomass around the membranes; and

(ii) the hydrodynamics of the flow across the membranes should ensure stable scouring of the entire membrane surface.

Project Achievements

A model for the optimization of IMBR hydrodynamics has been developed, based on an identification of the important geometric and operating variables that affect circulation and fouling, and on a factorial experimental optimization of these variables.

The model was implemented in the design and construction of a pilot plant IMBR, which was evaluated on both mineral suspensions and a biological suspension (activated sludge).

In both laboratory and on-site evaluations, smooth and stable circulation was obtained within the reactor, with no indication of the stagnant zones obtained in the preliminary experiments in this project. On examination of the membranes after each run, there were no signs of preferential fouling zones. It would thus seem that the proposed IMBR design meets the hydrodynamic criteria, i.e. to ensure stable circulation and uniform scouring of the membrane modules.

The IMBR showed the typical characteristics of commercial IMBRs in terms of critical flux, i.e. a critical flux exists which is a function of feed concentration and aeration intensity. Commercial IMBRs operate at critical fluxes of about 15 LMH to 25 LMH, for MLSS values between 12 g/L and 15 g/L. In the evaluation performed on the biological sludge, a critical flux of about 10 LMH to 15 LMH was achieved at a MLSS value of 9 g/L. However, the aeration intensity used here was substantially below that used in commercial IMBRs. Commercial flat-sheet IMBR systems use air-flow rates of 7 L/min to 10 L/min per membrane module. In this study, the flowrates ranged from 0,3 L/min/module to 2,5 L/min/module, about 5% to 35% of the commercial units.

Overall, the evaluations indicated that the IMBR membrane module design produced by this project were technically adequate and competent for IMBR applications.

Recommendations

The evaluation trials performed here were merely to determine the technical adequacy of the project outputs. Substantially longer and more detailed trials need to be performed on biological suspensions in order to determine the long-term performance of the system, and to obtain sufficient data for comparative evaluations with current commercial systems.

The current tendency is to divide the bioreactor into two zones, viz. a zone of fine bubble aeration for biological degradation, and a zone with coarse bubble aeration, where the dewatering membranes would be situated. Future trials should use this two-zone configuration. This would simplify and improve system hydrodynamics, since larger A_d/A_r ratios can be achieved in a two-zone system.

7.3 AIM: Morphology of *Skinless* capillary ultrafiltration membranes

Objectives

The main objectives here were:

(i) to identify the production parameters that influence the structure and performance of skinless capillary ultrafiltration membranes;

(ii) to identify their effect on membrane structure and performance; and

(iii) to identify regimes for the production of skinless membranes.

Project Achievements

The important production parameters were identified as dope extrusion rate (DER), bore fluid flowrate (BFFR) and spinning bath composition. Regimes have been identified where (undesirable) externally skinned membranes would form, and where (desirable) externally unskinned membranes would form. The qualitative effects of the production variables on membrane thickness, flux and rejections have been identified. This can be utilised to define regimes for producing unskinned membranes of the desired properties.

Recommendations

The membranes produced in this project were subjected to only short term evaluations. Longer term trials must be performed to unequivocally determine "recipes" for unskinned membranes of particular properties.

References

Baker, J.S. and Dudley, L.Y. (1998), Biofouling in membrane systems: a review, *Desalination*, 118(1-3), pp. 81-89

Bouhabila, E.H., Aim, R.B. And Buisson, H. (1998), Microfiltration of activated sludge using submerged membrane with air bubbling (application to wastewater treatment), *Desalination*, 118, pp. 315-322

Bouhabila, E.H., Aim, R.B. And Buisson, H. (2001), Fouling characterization in membrane bioreactors, *Separation and Purification Technology*, 22, pp. 123-132

Brindle, K. And Stephenson, T. (1996), The application of membrane biological reactors for the treatment of wastewaters, *Biotechnol. Bioeng*., 49, pp. 601-610

Brindle, K. And Stephenson, T. (1999), Interfacial oxygen transfer in a membrane aeration bioreactors, MBR2 – Proc. 2nd Intl. Mtg. Membrane Bioreactors for Wastewater Treatment, Cranfield University, Cranfield, UK, 9 pp.

Brindle, K., Stephenson, T. And Semmens, M.J. (1998), Nitrification and oxygen utilisation in a membrane aeration bioreactor, *Journal of Membrane Science*, 144(1-2), pp. 197-209

Brockmann, M. And Seyfried, C.F. (1996), Sludge activity and cross-flow microfiltration – a non-beneficial relationship, *Water Science and Technology*, 34(9), pp. 205-213

Cabasso, I., Klein, E., James K.S. (1977), Polysulfone hollow fibers II. Morphology. *J. Appl. Pol. Sci.* 21: 165 – 180

Chaize, S. And Huyard, A. (1991), Membrane bioreactor on domestic waste-water treatment: sludge production and modeling approach, *Wat. Sci. Technol*., 23(7-9), pp. 1591-1600

Chiemchaisri, C., Wong, Y.K., Urase, T. And Yamamoto, K. (1992), Organic stabilisation and nitrogen removal in membrane separation bioreactor for domestic wastewater treatment, *Wat. Sci. Technol*., 25(10), pp. 231-240

Churchouse, S. (1997), Membrane bioreactors for wastewater treatment – operating experiences with the Kubota submerged membrane activated sludge process, *Membrane Technology*, 83, pp. 5-9

Churchouse, S. And Wildgoose, D. (1999), Membrane bioreactors hit the big time – from lab to full-scale application, MBR2 – Proc. 2nd Intl. Mtg. Membrane Bioreactors for Wastewater Treatment, Cranfield University, Cranfield, UK, 14 pp.

Cui, Z.F., Chang, S. and Fane, A.G. (2003), The use of gas bubbling to enhance membrane processes, *Journal of Membrane Science*, 221, pp 1–35

Defrance, L. And Jaffrin, M.Y. (1998), Reversibility of fouling in activated sludge filtration, *Journal of Membrane Science*, 157, pp. 73-84

Field, R.W., Wu, D., Howell, J.A. And Gupta, B.B. (1995), Critical flux concept for microfiltration fouling, *Journal of Membrane Science*, 100, pp. 259-272

Flemming, H., Schaule, G., Griebe, T., Schmitt, J. And Tamachkiarowa, A. (1997), Biofouling – the Achilles heel of membrane processes, *Desalination*, 113, pp. 215-225

Gander, M., Jefferson, B. And Judd, S. (2000), Aerobic MBRs for domestic wastewater treatment: a review with cost considerations, *Separation and Purification Technology*, 18, pp. 119-130

Ghyoot, W., Vandaele, S. And Verstraete, W. (1999), Nitrogen removal from sludge reject water with a membrane-assisted bioreactor, *Wat. Res.*, 33(1), pp. 23-32

Gunder, B. And Krauth, K. (1998), Replacements of secondary clarification by membrane separation – results with plate and hollow fibre modules, *Wat. Sci. Tech.*, 38(4-5), pp. 383-393

Hodgson, P.H., Leslie, G.L., Schneider, R.P., Fane, A.G., Fell, C.J.D. And Marshall, K.C. (1993), Cake resistance and solute rejection in bacterial microfiltration: The role of the extracellular matrix, *Journal of Membrane Science*, 79, pp. 35-53

Huang, X., Gui, P. And Qian, Y. (2001), Effect of sludge retention time on microbial behaviour in a submerged membrane bioreactor, *Process Biochemistry*, 36, pp. 1000-1006

Husain, H. And Cote, P. (1999), The Zenon experience with membrane bioreactors for municipal wastewater treatment, MBR2 – Proc. 2nd Intl. Mtg. Membrane Bioreactors for Wastewater Treatment, Cranfield University, Cranfield, UK, 9 pp.

Jack, U. (2005), Fabrication of wet phase inversion capillary membrane, dimension and diffusion effects, *MTech Thesis*, Peninsula Technikon,

Jacobs, E.P. and Sanderson R.D. (1997), Capillary membrane production development, *WRC report* No 632/1/97

Jacobs, E.P, Yanic, C., Bradshaw, S.M., Marais, C., Bredenkamp, C.W. and Swart, P. (2003), Fabrication and production protocol for capillary ultrafiltration membranes and modules, *WRC Final Report* 769/1/03. ISBN 1-86845-843-1.

Jefferson, B., Laine, A.L., Judd, S.J. And Stephenson, T. (1999), Membrane bioreactors and their role in wastewater reuse, MBR2 – Proc. 2nd Intl. Mtg. Membrane Bioreactors for Wastewater Treatment, Cranfield University, Cranfield, UK, 10 pp.

Kimura, S. (1991), Japan's aqua Renaissance '90 project, *Wat. Sci. Technol.*, 23(7-9), pp. 1573-1582

Kishino, H., Ishida, H., Iwabu, H. And Nakano, I. (1996), Domestic wastewater reuse using submerged membrane bioreactor, *Desalination*, 106, pp. 115-119

Li, H., Fane, A.G., Coster, H.G.L. And Vigneswaran, S. (1998), Direct observation of particle deposition on the membrane surface during crossflow microfiltration, *Journal of Membrane Science*, 149, pp. 83-97

Livingston, A.G. (1994), Extractive membrane bioreactors: A new process technology for detoxifying chemical industry wastewaters, *J. Chem. Technol. Biotechnol.,* 60, pp. 117-124

Livingston, A.G., Arcangeli, J., Boam, A.T., Zhang, S., Marangon, M. And Freitas Dos Santos, L.M. (1998), Extractive membrane bioreactors for detoxification of chemical industry wastes: process development, *Journal of Membrane Science*, 151(1), pp. 29-44

Majeed, J.G. and Bekassy-Molnar, E. (1995), Design correlations of an air-lift tube reactor, *Gas separation and Purification*, 9(2), pp 101-109.

Mallon, D., Steen, F., Brindle, K. And Judd, S. (1999), Performance on a real industrial effluent using a ZenoGem® MBR, MBR2 – Proc. 2nd Intl. Mtg. Membrane Bioreactors for Wastewater Treatment, Cranfield University, Cranfield, UK, 7 pp.

Mayhew, M. And Stephenson, T. (1997), Low biomass yield activated sludge: a review, *Environ. Technol.*, 18, pp. 883-892

Mbulawa, X. P. (2005), Development And Evaluation Of Silicone Membrane As Aerators For Membrane Bioreactors, *MTech Thesis*, Durban University of Technology

Muller, E.B., Stouthamer, A.H., Van Verseveld, H.W. And Eikelboom, D.H. (1995), Aerobic domestic waste water treatment in a pilot plant with complete sludge retention by cross-flow filtration, *Wat. Res*., 29(4), pp. 1179-1189

Nagaoka, H., Yamanishi, S. And Miya, A. (1998), Modeling of biofouling by extracellular polymers in a membrane separation activated sludge system, *Wat. Sci. Tech.*, 38(4-5), pp. 497-504

Nagaoka, H., Kono, S., Yamanishi, S. And Miya, A. (2000), Influence of organic loading rate on membrane fouling in membrane separation activated sludge process, *Wat. Sci. Tech.*, 41(10-11), pp. 355-362

Nuhoglu, A., Pekdemir, T., Yildiz, E., Keskinler, B. and Akay, G. (2002), Drinking water denitrification by a membrane bio-reactor, *Wat. Res*., 36, pp. 1155-1166

Pillay, V.L. and Jacobs, E.P. (2003), The development and evaluation of a Reverse flow microfilter, *WRC Final Report* , K5/1232

Rothemund, C., Camper, A. And Wilderer, P.A. (1994), Biofilms growing on gas permeable membranes, *Wat. Sci. Tech.*, 29(10-11), pp. 447-454

Semmens, M. And Hanus, D. (1999), Studies of a membrane aerated bioreactor for wastewater treatment, MBR2 – Proc. 2nd Intl. Mtg. Membrane Bioreactors for Wastewater Treatment, Cranfield University, Cranfielfd, UK, 18 pp.

Shimizu, Y., Uryu, K., Okuno, Y. And Watanabe, A. (1996), Cross-flow Microfiltration of Activated Sludge Using Submerged Membrane with Air Bubbling, *Journal of Fermentation and Bioengineering*, 81(1), pp. 55-60

Stephenson, T., Judd, S., Jefferson, B. And Brindle, K. (2000), *Membrane Bioreactors for Wastewater Treatment*, IWA Publishing

Swart, A.F., Brouckaert, C.J. and Buckley, C.A. (1994), Criteria for selecting the operating regime of the crossflow microfilter or the tubular filter press for clarification of turbid waters, *Journal of Membrane Science,* vol 87, pp 57 – 69.

Tardieu, E., Grasmick, A., Geaugey, V. And Manem, J. (1998), Hydrodynamic control of bioparticle deposition in a MBR applied to wastewater treatment, *Journal of Membrane Science*, 147, pp. 1-12

Ueda, T., Hata, K. And Kikuoka, Y. (1996), Treatment of domestic sewage from rural settlements by a membrane bioreactor, *Wat. Sci. Technol*., 34, pp. 189-196

Ueda, T., Hata, K., Kikuoka, Y. And Seino, O. (1997), Effects of aeration on suction pressure in a submerged membrane bioreactor, *Wat. Res.*, 31(3), pp. 489-494

Wakeman, R.J. And Williams, C.J. (2002), Additional techniques to improve microfiltration, *Separation and Purification Technology*, 26, pp. 3-18

Wijmans, J.G., Baaij, J.P.B. and Smolders C.A. (1983) The mechanism of formation of micro-porous or skinned membranes produced by immersion precipitation. *J. Membrane Sci.*14: 263-274

Wisniewski, C., Grasmick, A. And Cruz, L. (2000), Critical particle size in membrane bioreactors. Case of a denitrifying bacterial suspension, *Journal of Membrane Science*, 178, pp. 141-150

Yeom, I., Nah, Y. And Ahn, K. (1999), Treatment of household wastewater using an intermittently aerated membrane bioreactor, *Desalination*, 124, pp. 193-204

Young, T.H., Chen, L.W. (1995) Pore formation mechanism of membrane from phase inversion process. *Desalination.* 103: 233-24

Zhang, B., Yamamoto, K., Ohgaki, S. And Kamiko, N. (1997), Floc Size Distribution and Bacterial Activities in Membrane Separation Activated Sludge Processes for Small-Scale Wastewater Treatment/Reclamation, *Wat. Sci. Technol.,* 35(6), pp. 37-44